B U L L E T I N

DE LA SOCIÉTÉ DES SCIENCES ET DES LETTRES DE ŁÓDŹ

SÉRIE: RECHERCHES SUR LES DÉFORMATIONS

Volume LXII, no. 1

ŁÓDŹ 2012

ŁÓDZKIE TOWARZYSTWO NAUKOWE
PL-90-505 Łódź, ul. M. Cuie-Skłodowskiej 11
tel. (42) 665 54 59, fax (42) 665 54 64
sprzedaż wydawnictw: tel. (42) 665 54 48
e-mail: ltn@ltn.lodz.pl

Wydano z pomocą finansową Ministerstwa Nauki i Szkolnictwa Wyższego

PL ISSN 0459–6854

Wydanie 1.
Nakład 250 egz.

Skład komputerowy: Zofia Fijarczyk

Druk i oprawa: *AnnGraf* s.c.
92-637 Łódź, ul. Rataja 54
tel. +48 601 24 10 83

INSTRUCTION AUX AUTEURS

1. La présente Série du Bulletin de la Société des Sciences et des Lettres de Łódź comprend des communications du domaine des mathématiques, de la physique ainsi que de leurs applications liées aux déformations au sense large.
2. Toute communications est présentée à la séance d'une Commission de la Société par un des membres (avec deux opinions de spécialistes designés par la Rédaction). Elle doit lui être adressée directement par l'auteur.
3. L'article doit être écrit en anglais, français, allemand ou russe et débuté par un résumé en anglais ou en langue de la communication présentée. Dans tous les travaux écrits par des auteurs étrangers le titre et le résumé en polonais seront préparés par la rédaction. Il faut fournir le texte original qui ne peut contenir plus de 15 pages (plus 2 copies).
4. Comme des articles seront reproduits par un procédé photographique, les auteurs sont priés de les préparer avec soin. Le texte tapé sur un ordinateur de la classe IBM PC avec l'utilisation d'une imprimante de laser, est absolument indispensable. Il doit être tapé préférablement en *AMS-TEX* ou, exceptionnellement, en *Plain-TEX* ou *LATEX*. Après l'acceptation de texte les auteurs sont priés d'envoyer les disquettes (PC). Quelle que soient les dimensions des feuilles de papier utilisées, le texte ne doit pas dépasser un cadre de frappe de 12.3×18.7 cm (0.9 cm pour la page courante y compris). Les deux marges doivent être de la même largeur.
5. Le nom de l'auteur (avec de prénom complet), écrit en italique sera placé à la 1ère page, 5.6 cm au dessous du bord supérieur du cadre de frappe; le titre de l'acticle, en majuscules d'orateur 14 points, 7.1 cm au dessous de même bord.
6. Le texte doit être tapé avec les caractères Times 10 points typographiques et l'interligne de 14 points hors de formules longues. Les résumés, les rénvois, la bibliographie et l'adresse de l'auteurs doivent être tapés avec les petites caractères 8 points typographiques et l'interligne de 12 points. Ne laissez pas de "blancs" inutiles pour respecter la densité du texte. En commençant le texte ou une formule par l'alinéa il faut taper 6 mm ou 2 cm de la marge gauche, respectivement.
7. Les texte des théorèmes, propositions, lemmes et corollaires doivent être écrits en italique.
8. Les articles cités seront rangés dans l'ordre alphabétique et précédés de leurs numéros placés entre crochets. Après les références, l'auteur indiquera son adress complète.
9. Envoi par la poste: protégez le manuscript à l'aide de cartons.
10. Les auteurs recevront 20 tirés à part à titre gratuit.

Adresse de la Rédaction de la Série:
Département d'Analyse complexe et Géométrie différentielle
de l'Institut de Mathématiques de l'Académie polonaise des Sciences
BANACHA 22, PL-90-238 ŁÓDŹ, POLOGNE

Name and surname of the authors

TITLE – INSTRUCTION FOR AUTHORS SUBMITTING THE PAPERS FOR BULLETIN

Summary

Abstract should be written in clear and concise way, and should present all the main points of the paper. In particular, new results obtained, new approaches or methods applied, scientific significance of the paper and conclusions should be emphasized.

1. General information

The paper for BULLETIN DE LA SOCIÉTÉ DES SCIENCES ET DES LETTRES DE ŁÓDŹ should be written in LaTeX, preferably in LaTeX 2e, using the style (the file **bull.cls**).

2. How to prepare a manuscript

To prepare the LaTeX 2e source file of your paper, copy the template file **instr.tex** with **Fig1.eps**, give the title of the paper, the authors with their affiliations/addresses, and go on with the body of the paper using all other means and commands of the standard class/style 'bull.cls'.

2.1. Example of a figure

Figures (including graphs and images) should be carefully prepared and submitted in electronic form (as separate files) in Encapsulated PostScript (EPS) format.

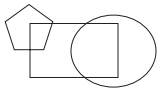

Fig. 1: The figure caption is located below the figure itself; it is automatically centered and should be typeset in small letters.

2.2. Example of a table

Tab. 1: The table caption is located above the table itself; it is automatically centered and should be typeset in small letters.

Description 1	Description 2	Description 3	Description 4
Row 1, Col 1	Row 1, Col 2	Row 1, Col 3	Row 1, Col 4
Row 2, Col 1	Row 2, Col 2	Row 2, Col 3	Row 2, Col 4

2.3. "Ghostwriting" and "guest authorship" are strictly forbiden

The printed version of an article is primary (comparing with the electronic version). Each contribution submitted is sent for evaluation to two independent referees before publishing.

3. How to submit a manuscript

Manuscripts have to be submitted in electronic form, preferably via e-mail as attachment files sent to the address **zofija@uni.lodz.pl**. If a whole manuscript exceeds 2 MB composed of more than one file, all parts of the manuscript, i.e. the text (including equations, tables, acknowledgements and references) and figures, should be ZIP-compressed to one file prior to transfer. If authors are unable to send their manuscript electronically, it should be provided on a disk (DOS format floppy or CD-ROM), containing the text and all electronic figures, and may be sent by regular mail to the address: **Department of Solid State Physics, University of Lodz, Bulletin de la Société des Sciences et des Lettres de Łódź, Pomorska 149/153, 90-236 Łódź, Poland**.

References

[1]

Affiliation/Address

TABLE DES MATIÈRES

Kyiv, 12 February 2012

Dear friends and colleagues,

I have grievous news. Professor Promarz Melikovich Tamrazov died yesterday 11 February 2012. A very good mathematician and very kind person died.

Sergey Plaksa

Professor Promarz Tamrazov, Member of the National Academy of Sciences of Ukraine, was a member of our Editional Board since 1995. His passing away is a considerable loss.

The Editors

PL ISSN 0459-6854

B U L L E T I N

DE LA SOCIÉTÉ DES SCIENCES ET DES LETTRES DE ŁÓDŹ

2012 Vol. LXII

Recherches sur les déformations no. 1

pp. 9–19

In memory of
Professor Roman Stanisław Ingarden

László Kozma and Lajos Tamássy

SOME QUESTIONS OF METRIC DIFFERENTIAL GEOMETRIES

Summary

We show that under mild conditions any general metric (distance) space determines a Finsler space, nevertheless there are many metric spaces, which determine the same Finsler space (Theorem 1). In the second part of the paper we obtain a necessary and sufficient condition in order that the indicatrices of a Finsler space be in affine relation. In this case the Finsler space is a generalized Berwald space (Theorem 2). Also certain isometries and motions of a Finsler space are discussed, and two theorems are obtained.

Introduction

In this paper we deal with two questions of Finsler geometry. Finsler geometry is built on the arc length of curves, and under certain very natural conditions it is the most general one among the metric differential geometries. In a Finsler geometry there exists the notion of the distance between two points, however the original notion is arc length, and distance is a deduced notion only. In contrary to this, in a general metric (distance) space the basic notion is distance, and arc length is no organic part of this geometry. What is the relation between the two types of metric geometries? When, and how can we define arc length of curves in a distance space? What is the relation between Finsler and distance spaces? These questions are investigated in Section 1.

The metric of the Euclidean space is defined by the unit sphere S. In a Finsler space metric is defined by the metric function $\mathcal{F}(p, y)$, which is equivalent to the indicatrix hypersurfaces $I_p \subset T_pM$. I_p plays the role of the unit sphere S. In a Riemann space these surfaces are ellipsoids. Affine deformatin is a regular linear transformation in the tangent spaces. Affine deformation seems to be a useful tool

for studying relations between different types of Finsler spaces, such as Euclidean, Riemann, Minkowski, Berwald, and generalized Berwald spaces, and also still at several other questions. Such affine deformations are studied in Section 2. Finally in Section 3 we discuss some questions related to isometries and motions of Finsler space.

1. Metric spaces

Arc length and distance are among the most important notions of any metric differential geometric spaces. Let M be a connected n-dimensional manifold, and $p(t)$, $t \in [0,1]$ a curve in it. Then the arc length of $p(t)$ is

$$s := \lim_{\Delta t \to 0} \sum |p(t+\Delta t) - p(t)| = \int_0^1 |\dot{p}(t)| dt, \tag{1}$$

where $|\cdot|$ means a norm of the vector $\dot{p}(t) \in T_{p(t)}M$. Thus the crucial tool in obtaining the arc length is the norm functional $\mathcal{F}(p,y) = |y|$, $p \in M$, $y \in T_pM$. Any arc length is founded locally, and based on a norm of the tangent vectors. Nevertheless there are some very natural requirements against the arc length. s should be positive. So $\mathcal{F}(p,y)$ must be positive except for $y = 0$. Furthermore it is natural to require that s be independent of any reparametrization of $p(t)$. In a differential geometric space it is also natural the condition that $\mathcal{F}$ is differentiable. These requirements are equivalent to the following conditions

(i) $\mathcal{F}(p,y) > 0$, and $\mathcal{F} \in C^\infty$ except of $y = 0$

(ii) $\mathcal{F}(p,\lambda y) = |\lambda| \mathcal{F}(p,y)$, $\lambda \in R$.

In most cases the triangle inequality

(iii) $|y_1 + y_2| \leq |y_1| + |y_2|$, $\forall\, y_1, y_2 \in T_pM$

is also required. The necessity of (iii) will be given later. (i)–(iii) mean that $\mathcal{F}(p,y)$ is a Banach norm on each T_pM, and conversely. A manifold with a Banach norm $\mathcal{F}(p,y)$ on each T_pM, which varies with $p \in M$ is a Finsler space $F^n = (M, \mathcal{F})$ [BCS]. They are the most general metric differential geometric spaces, which satisfy the aforementioned very natural requirements.

If the Banach norms $\mathcal{F}(p,y)$ are independent of the point $p \in M$, then F^n is a Minkowski space $\mathcal{M}^n$ or, in a special case a Euclidean space E^n. (iii) is equivalent to the property that in these spaces the shortest path between two points are represented by straight lines. If the Banach norms are Euclidean, but they vary with the point p, then F^n is a Riemann space V^n. If the norms are Euclidean, but they do not vary with the point, then we obtain the Euclidean space E^n.

$$z = \mathcal{F}(p_0, y) \subset T_{p_0}M \tag{2}$$

is a cone in $R^{n+1}(y^1, \ldots, y^n; z)$. This is not differentiable at $y = 0$. This is the reason why we had to exclude $y = 0$ in (i). The projection of the intersection of this cone

with the plane $z = 1$ is called indicatrix of the Finsler space $F^n = (M, \mathcal{F})$. It is given by

$$I(p_0) := \{y \in T_{p_0}M \mid \mathcal{F}(p_0, y) = 1\} \subset T_{p_0}M.$$

By (iii) this is a convex hypersurface of the tangent space, and by (ii) $I(p_0)$ is symmetric to the origin O of $T_{p_0}M$. (ii) can be weakened by requiring only

$$\text{(ii)}^* \qquad \mathcal{F}(p, \lambda y) = \lambda \mathcal{F}(p, y), \quad \lambda \in R^+.$$

This assures the independence of s from orientation preserving reparametrization only, and it allows not symmetric indicatrices too. In the first (more classical) case F^n is called reversible, while in the last case it is called irreversible, reflecting the fact that in an irreversible Finsler space the arc length on $p(t)$ from p_1 to p_2 may differ from the arc length from p_2 to p_1.

A notion more general than arc length is distance of two points. Let Γ be the collection of the curves $p(t)$ in a Finsler space F^n from p_1 to p_2. Then

$$\varrho^F(p_1, p_2) := \inf_{\Gamma} \int_0^1 \mathcal{F}(p(t), \dot{p}(t))dt \tag{3}$$

gives a distance function induced by the Finsler space F^n.

A metric space D^n is a manifold M equipped with a distance function

$$\varrho : M \times M \to R^+, \quad (p_1, p_2) \mapsto \varrho(p_1, p_2)$$

with the properties

(iv) $\varrho(p_1, p_2) > 0$ except $\varrho(p, p) = 0$ (positivity)

(v) $\varrho(p_1, p_2) = \varrho(p_2, p_1)$ (symmetry)

(vi) $\varrho(p_1, p_3) \leq \varrho(p_1, p_2) + \varrho(p_2, p_3)$ (triangle inequality).

A reversible Finsler space F^n determines by (3) a distance function ϱ^F with properties (iv)–(vi). If F^n is irreversible, then we lose the symmetry (v). In this case D^n is called quasi-metric [B]. In the sequel the symmetry of ϱ will not be required, nor excluded. The corresponding distance spaces D^n in this paper will be called metric. Dealing with differential geometric spaces the condition of the differentiability of the distance function

$$\varrho(p_1, p_2) \in C^\infty \quad \text{except at } (p, p)$$

is natural, and this will be assumed.

A Finsler space F^n determines a distance function $\varrho^F(p_1, p_2)$, and thus a metric space D^n. Does this ϱ^F uniquely determine the F^n, and in a broader sense does any ϱ determine an F^n? Similar questions were investigated in several places, among others in [SzT1] and [SzT2]. Our approach and results will be different from those. First we prove

Theorem 1. A) *Any metric space* $D^n = (M, \varrho)$ *determines a Finsler space* $F^n = (\mathcal{M}, \mathcal{F})$.

B) *The distance function* $\varrho^F(p_1, p_2)$ *deduced from a Finsler space* $F^n = (\mathcal{M}, \mathcal{F})$ *determines* F^n.

C) *There are many metric spaces* D^n *which determine the same Finler space* F^n.

Proof.

A) Let $D^n = (M, \varrho)$ be a metric space, and $y_0 \in T_{p_0}M$, $y = ty_0$. Then the directional derivative of the distance function $\varrho(p_0, p)$ at a fix p_0 in the direction of y depends on p_0 and $y = t\,y_0$ only:

$$[\nabla_{ty_0}\varrho(p_0, p)]_{p_0} = \varphi(p_0, t\,y_0). \tag{4}$$

The left hand side of (4) equals

$$t\,[\nabla_{y_0}\varrho(p_0, p)]_{p_0} = t\varphi(p_0, y_0).$$

Thus $\varphi(p_0, ty_0)$ is linear in t. It is defined on a line ty_0 of $T_{p_0}M(y^1, \ldots, y^n)$. Then $z = \varphi(ty_0)$ is a ray in $R^{n+1}(y^1, \ldots, y^n; z) = T_{p_0}M(y) \times R^1(z)$. These rays considered in every direction $y_0 \in T_{p_0}M$ form a cone $z = \varphi(p_0, y)$ like (2), which is convex because of (vi). Then

$$\mathcal{F}(p, y) := \varphi(p, y) \tag{5}$$

is a Finsler metric, and $F^n = (M, \mathcal{F})$ is determined by $D^n = (M, \varrho)$. The projection of the intersection of this cone with the plane $z = 1$ yields the indicatrix I_p at every $p \in M$. In this consideration we used $\varrho(p_0, p)$ in a small neighbourhood $\mathcal{N}_{p_0} \subset M$ of p_0 only. We call $\varrho(p_0, p)$ on $\mathcal{N}_{p_0}$ the germ of the function $\varrho(p_0, p)$.

B) Suppose that the distance function $\varrho^F(p_0, p)$ is deduced from a Finsler space $F^n = (M, \mathcal{F})$. Let $p(t)$ be a curve, such that $p(0) = p_0$, $\dot{p}(0) = y_0$. Then, by the definition (3) of $\varrho^F(p_0, p((t))$, the directional derivative of $\varrho^F(p_0, p(t))$ at p_0 is

$$\left[\nabla_{y_0}\varrho^F(p_0, p(t))\right]_{p_0} = \left[\frac{d}{dt}\int_{t_0}^{t}\mathcal{F}(p(\tau), \dot{p}(\tau))d\tau\right]_{t=0} = \mathcal{F}(p_0, y_0).$$

Then, by the proof of part A), the Finsler space induced by ϱ^F is just the starting $F^n = (M, \mathcal{F})$.

C) In part A) of the proof it was shown that by (4) and (5) any metric space $D^n = (M, \varrho)$ determines a Finsler space $F^n = (M, \mathcal{F})$. However at the proof we used only the germ of the distance function $\varrho(p_0, p)$ of D^n. So if $D^{*n} = (M, \varrho^*)$ is another metric space, whose distance functions $\varrho^*(p_0, p)$ equal with $\varrho(p_0, p)$ of D^n on each $\mathcal{N}_{p_0}$, but they are different outside of $\mathcal{N}_{p_0}$, then D^n and D^{*n} induce the same $\varrho^F(p_0, p)$, and the same $F^n = (M, \mathcal{F})$. Thus every $D^{*n} = (M, \varrho)$ with the property

$$\varrho^*(p_0, p) = \varrho(p_0, p), \quad p \in \mathcal{N}_{p_0}$$

and

$$\varrho^*(p_0,p) \neq \varrho(p_0,p), \quad p \notin \mathcal{N}_{p_0}$$

yields the same Finsler space.

We discuss still some consequences.

1. If we want to accept (1) as the definition of the arc length of a curve $p(t) \subset M$ in a metric space $D^n = (M,\varrho)$, then we have to give the meaning of the norm $|\cdot|$ appearing in (1). The most natural explanation for $|\dot{p}_0|$ is $\varphi(p_0,\dot{p}_0)$ of (4). However, by (5) this equals $\mathcal{F}(p_0,\dot{p}_0)$, where $\mathcal{F}$ is the Finsler metric of the Finsler space $F^n = (M,\mathcal{F})$ induced by D^n. Thus, by this natural explanation of the norm, we obtain for the arc length in D^n the arc length measured in the induced Finsler space. Then the arc length of $p(t)$ must be the same in all of those different metric spaces D^{*n} which induce the same Finsler space.

2. Furthermore, as it is known, a curve $p(t)$ is a geodesic in a metric space if

$$\varrho(p_0,p) + \varrho(p,p_1) = \varrho(p_0,p_1) \tag{6}$$

for $p_0 = p(t_0)$, $p_1 = p(t_1)$, and for any $p = p(t)$, $t_0 < t < t_1$. Such curves do not exist in a D^n in general. If such curves still exist in a D^n between any pair of points, then D^n is an F^n. Namely dividing the curve into small parts by $p(t)$, $p(t+\Delta t)$ etc., we obtain

$$\varrho(p,(t),p(t+\Delta t)) = \left[\nabla_{\dot{p}}\varrho(p(t_0),p(t))\right]_t \Delta t \overset{(4)}{=} \varphi(p,\dot{p})\Delta t = \mathcal{F}(p,\dot{p})\Delta t. \tag{7}$$

By summing of these expressions we obtain

$$\varrho(p_0,p_1) = \int_{t_0}^{t_1} \mathcal{F}(p(\tau),\dot{p}(\tau))d\tau = \varrho^F(p_0,p_1), \tag{8}$$

and then $D^n(M,\varrho) = F^n(M,\mathcal{F})$.

3. Finally we remark that arc length s^F of a curve $p(t)$ measured in the induced Finsler space is never smaller than the distance $\varrho(p_s,p_e)$ between the starting point p_s and the end point p_e of $p(t)$. This follows from the triangle inequality (vi)

$$\varrho(p_s,p_1) + \varrho(p_1,p_2) + \cdots + \varrho(p_n,p_e) \geq \varrho(p_s,p_e),$$

from (7) and from (8) putting in this last one $p_0 = p(t_0) = p_s$, $p_1 = p(t_0+\Delta t)$, etc.

This also means that if $p(t)$ is a geodesic in the induced Finsler space, then its Finsler arc length s^F is not smaller than any distance $\varrho^*(p_s,p_e)$ measured in those metric spaces D^{*n}, which induce F^n.

2. Affine deformation

In this part of the paper we investigate affine deformation of the Finsler metric, extending the works [KT], [SzT1] and [SzT2]. In a Finsler space $F^n = (M,\mathcal{F})$ the

Finsler metric $\mathcal{F}(p,y)$ determines an indicatrix

$$I_{p_0} := \{y \in T_{p_0}M \mid \mathcal{F}(p_0,y) = 1\}, \quad p_0 \in M$$

in each tangent space T_pM. By the homogeneity of $\mathcal{F}$ the indicatrix bundle I and the metric function $\mathcal{F}$ determine each other. So in place of $F^n = (M,\mathcal{F})$ we can write $F^n = (M,I)$. Indicatrices fit better to our investigations than metric function. Indicatrices of a Euclidean space E^n are spheres S. Indicatrices of a Riemann space V^n are ellipsoids Q_p, and those of a Minkowski space $\mathcal{M}^n$ are independent of p. So $E^n = (M,S)$, $V^n = (M,Q)$ and $F^n = (M,I)$. An affine deformation $\mathfrak{a}$ is an affine (i.e. regular, linear) transformation of the tangent spaces:

$$\mathfrak{a}_p : T_pM \to T_pM \qquad \text{or} \quad \mathfrak{a}_{p_1,p_2} : T_{p_1}M \to T_{p_2}M$$

$$y \mapsto \mathfrak{a}_p y \qquad\qquad y_1 \mapsto y_2$$

So the affine deformation of $E^n = (M,S)$ is a $V^n = (M,Q)$ denoted by $\mathfrak{a}E^n = V^n$, where

$$Q_p = \mathfrak{a}_p S.$$

Any V^n is an affine deformation of E^n (at least locally). Two V_1^n and V_2^n over the same base manifold M are affine deformation of each other: $V_2^n = \mathfrak{a}V_1^n$. The affine deformation of an $\mathcal{M}^n$ is a Finsler space $\mathfrak{a}\mathcal{M}^n(M,I_0) = F^n(M,I)$ with

$$\bar{I}_p = \mathfrak{a}_p I_0,$$

but conversely this is not true. The affine deformation of a Finsler space $F^n = (M,I)$ is an other Finsler space $\mathfrak{a}F^n(M,I) = \bar{F}^n(M,\bar{I})$, where $\bar{I}_p = \mathfrak{a}_p I_p$. However two Finsler spaces are no affine deformation of each other in general. It is a question, which properties of an F^n are inherited by an affine deformation $\bar{F}^n = \mathfrak{a}F^n$.

Given a Riemann space $V^n = (M,Q)$, among the tangent vectors $\xi \in TM$ there exist several metric linear connections with not vanishing torsion $T \neq 0$, and a single one, the Levi–Civita connection with vanishing torsion $T = 0$. Such connection exists also in the Minkowski spaces (the trivial connection, with identically vanishing coefficients $\Gamma_j{}^i{}_k = 0$), but such connections do not exist for Finsler spaces in general. There exist metric linear connections also in the Finsler spaces, but not among the tangent vectors $\xi_p \in T_pM$, but in the vertical subbundle VTM of TTM. These vectors $\xi(p,y)$ sit on the couple of a point p and a vector $y \in T_pM$. $((p,y)$ sometimes is called line element, for $\xi(p,y) = \xi(p,\lambda y)$, $\lambda \in R)$. We can say that F^n is a vector bundle Ψ endowed with a Riemann metric. The base manifold of Ψ is $TM = \{(p,y)\}$, the typical fiber is an n-dimensional vector space $\mathcal{V}^n$, each $\mathcal{V}^n(p,y)$ endowed with a Riemann metric $g(p,y)$. Finsler spaces with metric linear connections in TM and with not necessarily vanishing torsion are called generalized Berwald spaces denoted by $\mathcal{B}^n$. If the torsion vanishes: $T = 0$, then such a space is called Berwald space denoted here by B^n. Generalized Berwald spaces $\mathcal{B}^n$ are exactly the affine deformation of Minkowski spaces [SzT1]:

$$\mathcal{B}^n = \mathfrak{a}\mathcal{M}^n.$$

They can be characterized also by the property that the indicatrices of such a space are in affine relation relation. This means that a Finsler space $F^n = (M, I)$ is a generalized Berwald space if and only if for any pair p_1, p_2 there exists $\mathfrak{a}_{p_1,p_2}$, such that

$$\mathfrak{a}_{p_1,p_2} I_{P_1} = I_{p_2}.$$

So it seems to be an interesting question: when are the indicatrices of an F^n in affine relation. We want to give for this a necessary and sufficient condition. This will be also a necessary and sufficient condition in order that the Finsler space is a generalized Berwald space $\mathcal{B}^n$.

It is known that in a vector space $\mathcal{V}^n$, and then in any T_pM there exists a unique ellipsoid centered at the origin O of $\mathcal{V}^n$, which ellipsoid is contained in a given hypersutface, in our case in the indicatrix I_p, and which is of maximal volume (this is the Löwner ellipsoid, see e.g. [L] p. 180). Thus given a Finsler space $F^n = (M, I)$, we have in each I_p an ellipsoid Q_p centered at O and of maximal volume. These ellipsoids determine a Riemann space $V^n = (M, Q)$.

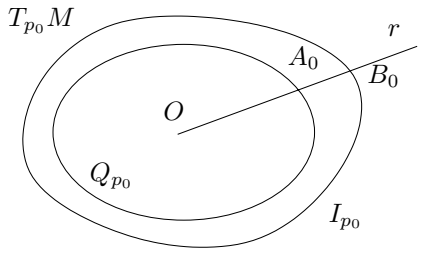

Fig. 1: Löwner ellipsoid vs. relation (9).

Now let $r(p_0, y_0)$ be a ray in $T_{p_0}M$ emanating from the origin O in the direction of the vector $y_0 \in T_{p_0}M$. Let A_0 be the intersection point of the ray and Q_{p_0} and let B_0 the intersection point of the ray and I_{p_0}. Let us equip the tangent space with a Euclidean metric, and let

$$\lambda(p_0, y_0) := \frac{|OB_0|}{|OA_0|}, \tag{9}$$

where $|\,.\,|$ means the Euclidean norm. Let $\mathfrak{a}^*_{p_0,p}$ be an affine transformation, such that

$$\mathfrak{a}^*_{p_0,p} : T_{p_0}M \to T_pM$$
$$Q_{p_0} \to Q_p.$$

We denote the corresponding objects and quantities in T_pM without the subscript $_0$. Then

$$\lambda(p, y) = \lambda(p_0, y_0), \quad \text{where } y = \mathfrak{a}^*_{p_0,p}\, y_0, \tag{10}$$

if and only if I_p is in affine relation to I_{p_0}.

Namely if F^n is a $\mathcal{B}^n$, then the indicatrices I_p of $\mathcal{B}^n$ are in affine relation: $I_{p_2} = \mathfrak{a}_{p_1,p_2} I_{p_1}$, and then also $Q_{p_2} = \mathfrak{a}_{p_1,p_2} Q_{p_1}$, for an affine transformation takes maximal ellipsoid into maximal ellipsoid. Thus, in this case the value of $\lambda(p_0, y_0)$ with $\mathfrak{a}^*_{p_0,p} = \mathfrak{a}_{p_0,p}$ is independent of p. Conversely, if $\lambda(p, y) = \lambda(p_0, y_0)$ then I_{p_0} and I_p are in the same affine relation as Q_{p_0} and Q_p, which yields that (9) is independent of the point p.

Theorem 2. *Indicatrices I_p of a Finsler space $F^n = (M, I)$ are in affine relation, and thus F^n is a generalized Berwald space $\mathcal{B}^n$ if and only if the affine proportions expressed by* (9) *are the same in each point $p \in M$.*

3. Isometries and motions

Remark 1. If a diffeomorphism $\varphi : M_1 \to M_2$ is an isometry between two Finsler spaces $F_1^n = (M_1, I_1)$ and $F_2^n = (M, I_2)$, then $d\varphi$ must be an affine relation between $I_1(p)$ and $I_2(\varphi p)$. So then there must exist a relation similar to (10), namely

$$\lambda(p, y) = \lambda(\varphi(p), (d\varphi)y).$$

This is a necessary, but not sufficient condition of the isometry between F_1^n and F_2^n.

The same holds if φ is a conformal mapping between F_1^n and F_2^n.

Remark 2. Affine relation between indicatrices is an equivalence relation. Then the maximal connected subsets M_α, $\alpha \in \mathcal{A}$ of M, where any I_{p_1} and I_{p_2}, $p_1, p_2 \in M_\alpha$ are in affine relation, form equivalence classes, and M decomposes to

$$M = \bigcup_{\lambda \in \mathcal{A}} M_\alpha. \tag{11}$$

Each M_α is closed (in the topology of M). Namely let $p_n \to p_0$, $p_n \in M_\alpha$. We know that $I_p \in C^\circ$ on M, and $I_{p_n} = \mathfrak{a}_{q_0,p_n} I_{q_0}$ for a $q_0 \in M_\alpha$. Then also $\mathfrak{a}_{q_0,p} \in C^\circ$ on M_α, and

$$I_{p_0} = \lim_{p_n \to p_0} I_{p_n} = \lim \mathfrak{a}_{q_0,p_n} I_{q_0} = \mathfrak{a}^* I_{q_0}$$

$$\mathfrak{a}^* := \lim_{p_n \to p_0} \mathfrak{a}_{q_0,p_n}.$$

Then also I_{p_0} is in affine relation to I_{q_0}, and hence $p_0 \in M_\alpha$. This has some consequences. For example if an M_1 is an n-dimensional closed domain, then to this M_1 can join no other n-dimensional M_2, for in this case $M_1 \cup M_2$ form a unique equivalence class.

Remark 3. Suppose that the base manifold M of the Finsler space $F^n = (M, I)$ decomposes according to (11). Then F^n restricted to M_α is a part of a generalized Berwald space: $\mathcal{B}^n_\alpha$

$$F^n \restriction M_\alpha = \mathcal{B}^n_\alpha \restriction M_\alpha.$$

In this sense any Finsler space F^n is put together from part of generalized Berwald spaces:

$$F^n = \bigcup_\alpha (\mathcal{B}^n_\alpha \restriction M_\alpha).$$

Nevertheless among the M_α may exist several ones consisting of a single point:

$$M_\alpha = \{p_\alpha\}.$$

Remark 4. Since a conformal or especially an isometric mapping $\varphi : M \to N$ between two Finsler spaces

$$F^n_1 = (M, I_1) \quad \text{and} \quad F^n_2 = (N, I_2)$$

generates an affine relation between the indicatrices $I_1(p)$ and $I_2(\varphi(p))$, we have $N_\alpha = \varphi(M_\alpha)$. Thus the structures $\{M_\alpha\}$ and $\{N_\alpha\}$ must be diffeomorphic.

Remark 5. Suppose that $F^n = (M, \mathcal{F})$ has a continuous 1-parameter group of motions. Let $p(t)$ be an orbit of a point $p \in M$. Then the indicatrices $I(p(t))$ are affine equivalent. Therefore any orbit must be contained in an M_α.

From this follows

Theorem 3. *If F^n admits a transitive group of motions, then any two indicatrices are in affine relation. Consequently F^n is a generalized Berwald space $\mathcal{B}^m$.*

Remark 6. Suppose that $\{M_\alpha\}$ contains an M_1 consisting from a single point: $M_1 = \{p_1\}$. Then p_1 is a fix point of any continuous group of motion.

Theorem 4. *If in the decomposition $M = \cup_\alpha M_\alpha$ of a reversible Finsler space $F^2 = (M, I)$ there exists exactly two M_1 and M_2 containing a single point: $M_1 = \{p_1\}$ and $M_2 = \{p_2\}$, F^2 admits a 1-parameter continuous group $\varphi(p, t)$ of motions different of the identity, and the injectivity radii $\iota(p_1)$ and $\iota(p_2)$ are such that $\iota(p_1) + \iota(p_2) \geq \varrho^F(p_1, p_2)$, then M is diffeomorphic to the sphere S^2.*

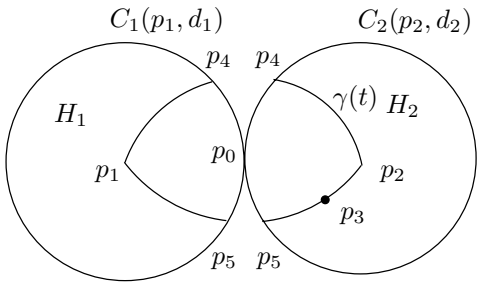

Fig. 2: Illustration to the proof of Theorem 4.

Proof. Let p_0 be a point of a geodesic arc connecting p_1 and p_2, such that

$$\varrho(p_1,p_0)<\iota(p_1) \quad \text{and} \quad \varrho(p_2,p_0)<\iota(p_2). \tag{12}$$

Such a p_0 exists because of our assumption. In consequence of (12) the exponential maps $\exp(p_1)$ and $\exp(p_2)$ to

$$H_1 := \{p \in M \mid \varrho(p_1,p) \le \varrho(p_1,p_0)\}$$

and

$$H_2 := \{p \in M \mid \varrho(p_2,p) \le \varrho(p_2,p_0)\}$$

are $1:1$. Thus through each point of H_1, resp. H_2 goes a single geodesic circle centered at p_1, resp. p_2. Therefore $H_1 \cup H_2$ can be mapped on a revolution surface Ψ of E^3 diffeomorphic to S^2 in such a way that geodesic circles are mapped on the parallel curves of Ψ, and the geodesics between p_1 and p_2 into meridians of Ψ, and that the maps on these families of curves are isometries.

Still we must show only that $H_1 \cup H_2 = M$. Suppose that there exists a point $p_3 \notin H_1 \cup H_2$. We know that any geodesics emanating from p_1 meet perpendicularly the geodesic circle $C(p_1,d_1)$ centered at p_1 and having the radius $d_1 = \varrho(p_1,p_0)$. But $C(p_1,d_1) = C(p_2,d_2)$, where $d_2 = \varrho(p_2,p_0)$. Therefore the geodesic $\gamma(t)$ from p_1 through p_3 meets at $p_4 \in C(p_1,d_1) = C(p_2,d_2)$ perpendicularly also $C(p_2,d_2)$, and thus $\gamma(t)$ goes through also the center p_2 of $C_2(p_2,d_2)$, and goes further meeting again $C(p_1,d_1) = C(p_2,d_2)$, and so on. Therefore $p_3 \in \gamma(t) \subset H_1 \cup H_2$.

We remark that if there exists a further M_3 consisting of a single point $q_0 \in H_1 \cup H_2$, then q_0 is a fixpoint, and it lies on a geodesic γ^* connecting p_1 and p_2. Since p_1, p_2, q_0 are fix points, γ^* is pointwise fix, and then $\varphi(p,t)$ is an isometry. If we have only one fix point, then M may be diffeomorphic to a rotation paraboloid, which is not diffeomorphic to S^2. So the number of the fix points in the theorem must be exactly two.

This theorem can be extended to irreversible F^2, and to F^n $(n>2)$ too. We do not know simple wording and proofs for these cases.

Remark 7. [to Theorem 4] Any geodesic $\gamma(t)$ starting from p_1 is closed. Namely $\gamma(t)$ meets $C(p_1,d_1) = C(p_2,d_2)$ perpendicularly at p_4, and passes through p_2. After this $\gamma(t)$ meets again the geodesic circle at a point p_5. However the points corresponding to p_4 and p_5 in $\exp^{-1}(p_1)$ and $\exp^{-1}(p_2)$ are diametrical points. Therefore leaving p_5 $\gamma(t)$ goes through p_1, meets again p_4, and so on.

Remark 8. [to Theorem 4] I_{p_1} and I_{p_2} must be ellipses. Namely

$$[d(\varphi(t_a))]_{p_i} I_{p_i} = I_{p_i}, \quad i=1,2$$

for infinitely many t_a, since $\varphi(t)$ are isometries. However if a curve (here I_{p_i}) of a vector space $\mathcal{V}^2$ (here of $T_{p_i}M$) is invariant against infinite many different linear transformations (here against $d\varphi(t)$), then it is an ellipse (see [Th, p. 83], or [G]).

References

[BCS] D. Bao, S. S. Chern, and Z. Shen, *An introduction to Riemann-Finsler geometry*, Springer Verlag, New York (2000).

[B] L. M. Blumenthal, *Theory and Application of Distance Geometry*, Clarendon Press, Oxford 1953.

[G] P. M. Gruber, *Minimal ellipsoids and their duals*, Rend. Circ. Math. Palermo **37** (1988), 35–64.

[KT] L. Kozma and L. Tamássy, *Finsler geometry without line elements faced to applications*, Rep. Math. Phys. **51** (2003), 233-250.

[L] D. Laugwitz, *Differential and Riemannian geometry*, Acad. Press, New York and London 1965.

[SzT1] J. Szilasi and L. Tamássy, *Affine deformation of Minkowski spaces*, Bull. Transilvania Univ. **4**(53), no. 2 (2011), 89–96.

[SzT2] J. Szilasi and L. Tamássy, *Generalized Berwald spaces as affine deformation of Minkowski spaces*, (*to appear*).

[T1] L. Tamássy, *Relation between metric spaces and Finsler spaces*, Diff. Geom. Appl. **26** (2008), 483–494.

[T2] L. Tamássy, *Distance functions of Finsler spaces and distance spaces*, Diff. Geom. Appl., Proc. Conf. Olomouc 2007 Aug., 559–570

[Th] A. G. Thompson, *Minkowski geometry*, Cambridge Univ. Press, Cambridge 1996.

Institute of Mathematics
University of Debrecen
4010 Debrecen, P. O. Box 12
Hungary
e-mail: laszlo.kozma@science.unideb.hu
e-mail: tamassy@science.unideb.hu

Presented by Julian Ławrynowicz at the Session of the Mathematical-Physical Commission of the Łódź Society of Sciences and Arts on December 15, 2011

O PEWNYCH ZAGADNIENIACH METRYCZNYCH GEOMETRII RÓŻNICZKOWEJ

S t r e s z c z e n i e

Wykazujemy, że przy umiarkowanych warunkach każda ogólna przestrzeń metryczna (z odległością) określa przestrzeń Finslera, istnieje jednak wiele przestrzeni metrycznych, które określają tę samą przestrzeń Finslera (twierdzenie 1). W drugiej części pracy otrzymujemy warunek konieczny i dostateczny na to, by indykatrysy danej przestrzeni Finslera były w relacji afiniczności. W tym przypadku przestrzeń Finslera jest uzgodnioną przestrzenią Berwalda (twierdzenie 2). Dyskutujemy również pewne izometrie i przemieszczenia (ruchy) przestrzeni Finslera, uzyskując dwa dalsze twierdzenia.

PL ISSN 0459-6854

B U L L E T I N

DE LA SOCIÉTÉ DES SCIENCES ET DES LETTRES DE ŁÓDŹ

2012 Vol. LXII

Recherches sur les déformations no. 1

pp. 21–26

In memory of
Professor Roman Stanisław Ingarden

Claude Surry and Leszek Wojtczak

HISTORICAL REMARKS ON FALK VARIATIONAL INEQUALITIES. FINITE ELEMENT SOLUTION ERROR

Summary

We present a version of the Lax-Stampacchia theorem on the minimizations of a functional on a closed convex K included in a Hilbert space H. We give an estimate of the error with a finite element method on an approximate closed convex $K_h \subset K \subset H$. This estimate has been obtained by Falk.

1. The Falk variational inequalities

We consider the Falk variational inequalities when applied to the finite element solution error estimate. We start with the presentation of one of the inequalities, namely,

Theorem 1. *$a(u, v)$ is a bilinear, continuous, coercive form on $H \times H$, H being a real Hilbert space*

$$\exists \Lambda \in R \quad \text{so that} \quad |a(u, v)| \leq \Lambda |u| \ |v|,$$

$$\exists \lambda \in R \quad \text{so that} \quad a(u, u) \geq \lambda |u|^2.$$

$|\ |$ is the norm in H as well the absolute value.

Define H' as the dual of H. Let $f \in H'$.

Let $K \neq \phi$ be a closed convex subset of H. For every $f \in H'$, $\exists$ is a unique solution leading to

$$\left\{ \begin{array}{l} a(u, v-u) \geq \langle f, v-u \rangle \quad \forall v \in K, \\ u \in K. \end{array} \right. \tag{1}$$

Proof. A convex set is a set in which

$$(u, v \in K) \Rightarrow (\alpha u + (1-\alpha)v \in K \quad \forall \alpha \in [0,1]), \tag{2}$$

$$a(u, v) = (u, v). \tag{3}$$

$(\bullet, \bullet)$ denotes the scalar product H.

Due to the Riesz representation theorem, there exists a unique $\tilde{f} \in H$ such that

$$\left(\tilde{f}, v\right) = \langle f, v\rangle \tag{4}$$

and (1) is written as

$$(u - \tilde{f}, v - u) \geq 0 \quad \forall v \in K, \qquad u \in K \tag{5}$$

and u is the projection of $\tilde{f}$ on K

$$u = P_K(\tilde{f}). \tag{6}$$

For $u \in H$ we introduce

$$w = S(u), \tag{7}$$

$$(w, v - w) \geq (u, v - w) - \rho\left\{a(u, v - w) - \langle f, v - w\rangle\right\}, \quad \forall v \in K, \quad w \in K. \tag{8}$$

The application

$$v \rightsquigarrow (u, v) - \{\rho a(u, v) - \langle f, v\rangle\} \tag{9}$$

is a continuous linear form on H.

The solution of (8) is unique and for some $\rho > 0$ $u \rightsquigarrow S(u) = w$ admits a fixed point; the fixed point being a solution of (1). By the Banach fixed point theorem, we must show that S is a contraction. Consider $u_1, u_2 \in H$ and $w_1 = S(u_1)$, $w_2 = S(u_2)$. By (8) we have

$$w_1 \in K(w_1, v - w_1) \geq (u_1, v - w_1) - \rho\left\{a(u_1, v - w_1) - \langle f, v - w_1\rangle\right\}, \ \forall v \in K,$$

$$w_2 \in K(w_2, v - w_2) \geq (u_2, v - w_2) - \rho\left\{a(u_2, v - w_2) - \langle f, v - w_2\rangle\right\}, \ \forall v \in K.$$

Take $v = w_2$ in the first inequality and $v = w_1$ in the second inequality. If we add the two inequalities we obtain

$$|w_1 - w_2|^2 \leq (u_1 - u_2, w_1 - w_2) - \rho a(u_1 - u_2, w_1 - w_2). \tag{10}$$

Consider the bilinear form

$$(u, v) - \rho a(u, v).$$

By the Riesz representation theorem, it exists $f_u \in H$ so that

$$a(u, v) = (f_u, v), \qquad \forall v \in H \tag{11}$$

with (1) hypothesis

$$|f_u|^2 = (f_u, f_u) = a(u, f_u) \leq \Lambda |u| \ |f_u|$$

and

$$|f_u| \leq \Lambda |u|.$$

With (11) we have

$$|(u,v) - \rho a(u,v)| = |(u - \rho f_u, v)| \leq |u - \rho f_u| \ |v|$$

with (1) hypothesis

$$\begin{aligned} |u - \rho f_u|^2 &= |u|^2 - 2\rho(f_u, u) + \rho^2 |f_u|^2 \\ &\leq |u|^2 - 2\rho\lambda(u,u) + \rho^2\Lambda^2 |u|^2 \\ &\leq (1 - 2\rho\lambda + \rho^2\Lambda^2)|u|^2 \end{aligned}$$

for

$$\rho \in \left[0, \frac{2\lambda}{\Lambda^2}\right].$$

Noting this number $\nu \in (0,1)$, we have

$$|(u,v) - \rho a(u,v)| < \nu |u| \ |v|.$$

By (10) we have:

$$|w_1 - w_2|^2 \leq \nu |u_1 - u_2| \ |w_1 - w_2|,$$

$$|w_1 - w_2| \leq \nu |u_1 - u_2|.$$

S is a contraction since $0 < \nu < 1$ and we have existence of u. By (1), for the uniqueness, we have if u_1 and u_2 are two solutions

$$\begin{aligned} a(u_1, u_2 - u_1) &\geq \langle f, u_2 - u_1 \rangle, \\ a(u_2, u_1 - u_2) &\geq \langle f, u_1 - u_2 \rangle. \end{aligned}$$

We add

$$\lambda |u_1 - u_2|^2 \leq a(u_1 - u_2, u_1 - u_2) \leq 0$$

and if $u_1 = u_2$ and the solution is unique.

Remark if a is symmetric $a(u,v) = a(v,u)$, $\forall u, v \in H$ we have the well known Lax-Milgram theorem. A rich literature is devoted to variational inequalities and we restrict the paper to the theory in

$$H_1(\Omega) \left\{ v / \int_\Omega \left[v^2 + \overrightarrow{\text{grad}} v)^2 \right] d\Omega < +\infty \right\},$$

$$\|v\|^2_{H^1(\Omega)} = \int_\Omega \left[v^2 + (\overrightarrow{\text{grad}} v)^2 \right] d\Omega \ [1] \ [2] \ [3],$$

$$|v|^2 = \int_\Omega v^2 d\Omega.$$

We give in the second section an example of variational inequality devoted to filtration in a porous medium.

2. Deviation of the Falk finite element errors estimate

The variational inequality in K which is an closed convex of $H^1(\Omega)$

$$\forall v \in K \cap V \quad a(u, v-u) \geq \langle f, v-u \rangle, \tag{12}$$

$$\forall v_h \in K_h \quad a(u_h, v_h - u_h) \geq \langle f, v_h - u_h \rangle. \tag{13}$$

K_h is a closed convex of a space of finite element V_h included on $H = H^1(\Omega)$.

Introduce $A \in L(H; H')$ defined by

$$Au(v) = a(u, v) \quad \forall (u, v) \in H.$$

Next, we can write a model problem in the form:

$$a(u, v) = \int_\Omega \frac{\partial u}{\partial x_i} \frac{\partial v}{\partial x_i} d\Omega, \tag{14}$$

$$\langle f, v \rangle = \int_\Omega f v d\Omega, \tag{15}$$

$$\forall v \in K \quad a(u, v-u) \geq \int_\Omega f(v-u) d\Omega, \tag{16}$$

$$H = \{v \in H^1(\Omega) \ / \ v = 0 \text{ on } d\Omega\} = H_0^1(\Omega),$$

$$K = \{v \in H_0^1(\Omega), \ v \geq 0 \text{ on } \Omega\}.$$

We see that if $\bar{\Omega}$ is a convex bounded subset with a boundary of class C^2 and $f \in L^2(\Omega)$, $|u|_{H^2(\Omega)}$ may be bounded a priori by $|f|_{L^2(\Omega)}$ and

$$\begin{cases} u \geq 0 \text{ on } \Omega \quad u = 0 \text{ on } \Gamma, \\ -\Delta u = f \quad u \geq 0 \quad -\Delta u - f \geq 0 \quad \text{on } \Omega, \\ u = 0 \quad \text{and} \quad \dfrac{\partial u}{\partial \nu} = 0 \quad \text{on} \quad \Gamma^* \quad \text{(free boundary)}. \end{cases} \tag{17}$$

Γ^* is the interface between the sets $u > 0$ and $u = 0$.

Theorem 2. *Let us introduce the relation*

$$K_h \subset V_h \subset V$$

and assume that $f \in H$, $Au \in H$. $\exists c > 0$ independent of the subspace V_h and the subspace $K_h \subset V_h \subset V = H$ such that

$$\|u - u_h\| \leq c \left\{ \inf_{v \in K_h} \left\{ \|u - v_h\|^2 + |u - v_h\| \right\} + \inf_{v \in K} |u_h - v|. \right\}^{\frac{1}{2}}. \tag{18}$$

Proof. By (12) and (13), we have $\langle f, v\rangle = f(v)$ and $\forall v \in K$

$$a(u,u) \le a(u,v) + f(u-v), \tag{19}$$

$$\forall v_h \in K_h \; a(u_h, v_h) \le a(u_h, v_h) + f(u_h - v_h) \tag{20}$$

and ($\forall v_h \in K_h$, $\forall v \in K$). Hence

$$\begin{aligned} \lambda\|u-u_h\|^2 &\le a(u, v-u_h) + a(u_h, v_h - u) + f(u-v) + f(u_h - v_h) \\ &= a(u, v-u_h) - f(v-u_h) + a(u, v_h - u) \\ &\quad -f(v_h - u) + a(u_h - u, v_h - u) \\ &= (f - Au, u - v_h) + (f - Au, u_h - v) + a(u-_h, v_h - u). \end{aligned} \tag{21}$$

We have used $K_h \subset V_h \subset v$ in the latter inequality

$$\|u-u_h\|^2 \le |f - Au|_{L^2(\Omega)} \, (|u - v_h| + |u_h - v|) + \Lambda\|u-u_h\| \; \|u - v_h\|$$

and

$$\|u-u_h\| \; \|u-v_h\| \le \frac{1}{2}\left\{\frac{\lambda}{\Lambda}\|u-u_h\|^2 + \frac{\Lambda}{\lambda}\|u-v\|^2\right\}. \tag{22}$$

Moreover,

$$\frac{\lambda}{2}\|u-u_h\|^2 \le |f - Au| \;\; [(u-v_h) + (u_h - v)] + \frac{\Lambda^2}{2\lambda}\|u-v_h\|^2 \tag{23}$$

and we get (18).

If $K = V \Rightarrow (f - Au) = 0$ we get the standard estimate.

References

[1] H. Brézis, G. Stampacchia, *Sur la régularité de la solution d'inéquations elliptiques*, Bull. Soc. Math. France **96** (1968), 153–180.

[2] R. S. Falk, *Approximation of an elliptic boundary value problem with unilateral constraints*, Revue Française d'Automatique, Informatique, Recherche Opérationnelle. Analyse Numérique **R-2** (1975), 5–12.

[3] R. S. Falk, *Error estimates for the approximation of a class of variational ineqalities*, Math. Comp. **28** (1974), 963–971.

Laboratoire Félix Trombe
Institut de Sciences et de Génie
de Matériaux et Procédes
Centre National de la Recherche Scientifique
B.P.5, Odeillo, F-66 125 Font Romeu Cédex
France

Presented by Claude Surry and Leszek Wojtczak at the Session of the Mathematical-Physical Commission of the Łódź Society of Sciences and Arts on July 5, 2012

HISTORYCZNE UWAGI O METODZIE WARIACYJNEJ FALKA. OSZACOWANIE BŁĘDU W METODZIE ELEMENTU SKOŃCZONEGO

S t r e s z c z e n i e

W niniejszej pracy przedstawiamy wersję twierdzenia Laxa-Stampacchii dotyczącego jego zastosowań w przypadku minimalizacji funkcjonału rozważanego na zamkniętym i wypukłym elemencie przestrzeni Hilberta. Oszacowanie błędu metodą elementu skończonego jest wtedy oszacowaniem zaproponowanym przez Falka w przypadku zamkniętych i wypukłych podprzestrzeni K w przestrzeni H spełniających relację $K_h \subset K \subset H$.

Z fizycznego punktu widzenia interpretacja metody może być zastosowana dla opisu penetracji kropli oliwy w warstwach przypowierzchniowych.

PL ISSN 0459-6854

B U L L E T I N

DE LA SOCIÉTÉ DES SCIENCES ET DES LETTRES DE ŁÓDŹ

2012 Vol. LXII

Recherches sur les déformations no. 1

pp. 27–31

In memory of
Professor Hans Grauert

Claude Surry and Leszek Wojtczak

HISTORICAL REMARKS ON THE FILTRATION PROBLEMS. BAIOCCHI-DUVAUT SOLUTIONS

Summary

We sum up the physical problem of a dam of porous medium, separated by two reservoirs. The flow is governed by the Darcy law. We modelize the problem, showing that we have a free boundary problem. We show that the solution is the solution of a variational inequality which can be solved by a penalization method. This filtration problem is found in surface science when a drop of oil penetrates the first layers.

1. The filtration problem

A dam of porous medium with parallel vertical walls, situated distance a apart, separates two reservoirs of water at levels $y = H$ and $y = h$. The variable y is the height parameter and the variable x represents the distance from the wall of the higher reservoir. The flow is stationary and we have the Darcy law

$$v = -k\nabla u; \tag{1}$$

v is the velocity of the fluid and

$$u(x, y) = y + p(x, y);$$

y is the gravity force with normalized unit and $p(x, y)$ is the inner pressure of the fluid. We have a bidimensional dam; this modelizes a three dimensional dam whose cross section $z = c$ does no vary with c. The function u is the piezometric head. The conservation law leads to

$$\operatorname{div}(k\nabla u) = 0$$

in the wet part of the dam. We assume the permeability constant

$$k(x, y) = 1.$$

We define the wet part by

$$W = \{(x, y); \quad 0 < x < a; \quad 0 < y < \varphi(x)\};$$

$y = \varphi(x)$ is the free boundary, separating the wet part from the dry part. The function u satisfies the equation

$$\Delta u = 0 \quad \text{in} \quad W, \tag{2}$$

$$\frac{\partial u}{\partial n} = 0 \quad \text{on} \quad \Gamma = y = \varphi(x), \qquad 0 < x < a, \tag{3}$$

where n is the outward normal. The flow is tangent to Γ. We have

$$\begin{aligned} u(0, y) &= H \quad \text{if} \quad 0 < y < H, \\ u(a, y) &= h \quad \text{if} \quad 0 < y < h, \\ u(a, y) &= y \quad \text{if} \quad h < y < \varphi(x), \end{aligned} \tag{4}$$

where $p(x, y) = H - y$ in the higher reservoir is the pressure.

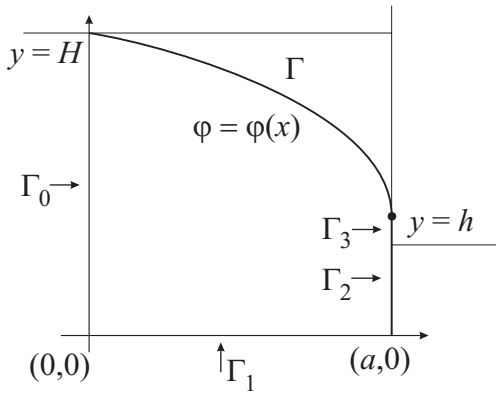

Fig. 1:

$p(x, y) = h(x, y) - y$ is the pressure in the lower reservoir, $p(x, y)$ is continuous

$$\text{on} \quad \Gamma = \{y = \varphi(x)\},$$

$$u(x, y) = y \quad \text{on} \quad \Gamma, \tag{5}$$

$$u_y(x, 0) = 0, \qquad 0 < x < a. \tag{6}$$

The bottom of the dam is impervious.

2. Modelization

The solution (2)–(6) exists. The function $p(x,y) = u(x,y) - y$ is positive in W (wet part), p is harmonic in W.

$$p = 0 \quad \text{on} \quad \Gamma \cup \Gamma_3 \, (\Gamma_3 = (a,y); \quad h < y < \varphi(x)) \,,$$

$$p > 0 \quad \text{on} \quad \Gamma_0 \cup \Gamma_2,$$

p cannot take the negative minimum on Γ_1,

$$p_y = u_y - 1 = -1 \quad \text{on} \quad \Gamma_1.$$

Using the maximum principle we have

$$p > 0 \quad \text{in} \quad W. \tag{7}$$

3. The variational inequality

We suppose $\varphi(x) \in C^1$, $u \in C^1(w \cup \Gamma) \cap (\overline{w})$. We set

$$\begin{cases} w(x,y) &= \displaystyle\int_y^{\varphi(x)} (u(x,t) - t)dt \quad \text{if} \quad 0 < y \leq \varphi(x), \\ &= 0 \qquad\qquad\qquad\qquad\quad \text{if} \quad \varphi(x) < y < H. \end{cases} \tag{8}$$

We calculate

$$w_y(x,y) = -u(x,y) + y, \tag{9}$$

$$w_x(x,y) = \int_y^{\varphi(x)} u_x(x,t)dt;$$

by (5)

$$w_{xx}(x,y) = \int_y^{\varphi(x)} u_{xx}(x,t)dt + \varphi'(x)u_x(x,\varphi(x)).$$

By (3), we have

$$-\varphi'(x)u_x + u_y = 0 \quad \text{on} \quad y = \varphi(x)$$

and

$$\int_y^{\varphi(x)} u_{xx}(x,t)dt = -\int_y^{\varphi(x)} u_{yy}(x,t)dt = -u_y(x,\varphi(y)) + u_y(x,y),$$

and we get

$$w_{xx} = u_y = -w_{yy} + 1 \quad \text{by (9)},$$

$$\Delta w = 1 \quad \text{in} \quad W, \tag{10}$$

$$w > 0 \quad \text{in} \quad W. \tag{11}$$

We define

$$\Omega = \{(x, y); \quad 0 < x < a, \quad 0 < y < H\}.$$

We have

$$w = 0 \quad \Delta w = 0 < 1 \quad \text{in} \quad \Omega/\overline{W}. \tag{12}$$

We check in the distributional sense $D'(\Omega)$:

$$\Delta w < 0$$

and we have

$$w = g \quad \text{in} \quad \partial\Omega; \tag{13}$$

g is defined by

$$g(0, y) = \frac{1}{2}(H - y)^2,$$

$$g(a, y) = \frac{1}{2}(h - y)^2 \quad \text{if} \quad 0 < y < h,$$

$$g_{xx}(x, 0) = 0 \quad \text{if} \quad 0 < x < a.$$

$$g(x, 0) = \frac{H^2}{2}\left(1 - \frac{x}{a}\right) + \frac{h^2}{2}\,\frac{x}{a}, \tag{14}$$

$g = 0$ elsewhere on $\partial\Omega$.

We define

$$K = \left\{v \in H^2(\Omega); \quad v = g \quad \text{on} \quad \partial\Omega, \quad v \geq 0 \quad \text{in} \quad \Omega\right\}. \tag{15}$$

w is a solution of the inequality

$$\forall v \in K$$

$$\int_\Omega \nabla w \; \nabla(v - w) d\Omega \geq -\int_\Omega (v - w) d\Omega. \tag{16}$$

Conversely, if w is a solution of (16), we obtain

$$W = \{(x, y) \in \Omega \quad w(x, y) > 0\},$$

$$0 < y < \varphi(x), \quad 0 < x < a, \quad \varphi(x) < H.$$

The function $u(x, y) = y - w(x, y)$, with φ, solving the physical problem (2)–(6) are such that φ and w are sufficiently regular.

References

[1] C. Baiocchi and A. Friedman, *A filtration problem in a porous medium with variable permeability*, Ann. Mat. Pura Appl. **114**, no. 4 (1977), 377–393.

[2] G. Duvaut and J. L. Lions, *Les inéquations en mécanique et physique*, Dunod, Paris 1972.

[3] M. Chipot, *Sur la régularité de la solution d'inéquations variationnelles elliptiques*, C. R. Acad. Sci. Paris, **288** (1979), 543–546.

[4] H. Brezis, D. Kinderlehrer, and G. Stampacchia, *Sur une nouvelle formulation du problème de lécoulement à travers une digue*, C. R. Acad. Sci. Paris, **287** (1978), 711–714.

[5] J. Bear, *Dynamics of Fluids in Porous Media*, Elsevier, New York 1972.

Laboratoire Félix Trombe
Institut de Sciences et de Génie
de Matériaux et Procédes
Centre National de la Recherche Scientifique
B.P.5, Odeillo, F-66 125 Font Romeu Cédex
France

Presented by Claude Surry and Leszek Wojtczak at the Session of the Mathematical-Physical Commission of the Łódź Society of Sciences and Arts on July 5, 2012

UWAGI HISTORYCZNE O PROBLEMACH FILTRACJI. ROZWIĄZANIA BAIOCCHIEGO I DUVAUTA

S t r e s z c z e n i e

Przedstawiamy problem fizyczny dla zachowań ośrodka porowatego rozdzielonego przez dwa rezerwuary o strumieniu określonym przez prawo Darcy'ego. Modelujemy w ten sposób problem o swobodnym charakterze brzegu.

Wskazujemy następnie na rozwiązania otrzymane na podstawie nierówności wariacyjnych znalezionych metodą penalizacji. Problem filtracji może być wtedy zinterpretowany przez zachowanie kropli oliwy, która penetruje pierwsze warstwy przypowierzchniowe.

PL ISSN 0459-6854

B U L L E T I N

DE LA SOCIÉTÉ DES SCIENCES ET DES LETTRES DE ŁÓDŹ

2012 Vol. LXII

Recherches sur les déformations no. 1

pp. 33–42

In memory of
Professor Roman Stanisław Ingarden

Julian Ławrynowicz, Kiyoharu Nôno, and Osamu Suzuki

BINARY AND TERNARY CLIFFORD ANALYSIS VS. NONCOMMUTATIVE GALOIS EXTENSIONS I

BASICS OF THE COMPARISON

Summary

A concept of noncommutative Galois extension is introduced and binary and ternary extensions are chosen. The ternary Clifford algebra is introduced with its Clifford analysis and the connection with the Galois extension is indicated. Then we can formulate the binary and ternary Hurwitz-type conditions and obtain the Dirac operator by these conditions. Hence the binary and ternary Dirac operators can be described in a unified manner.

In the first part of the paper we discuss binary and ternary Clifford algebras, noncommutative Galois extension and Clifford algebras, and noncommutative Galois structure on the nonion algebra.

Introduction

We can find several ternary phenomena around us. The most important phenomena are: 1) configurations of neighbouring atoms in a binary alloy with vacancies and in a ternary alloy [2, 6] (Fig. 1), 2) quark confinement [4, 5] (Fig. 2), 3) triplets in harmony of music (Fig. 3), 4) protein production mechanism (Fig. 4). We have enough mathematical methods for binary phenomena, for example, product of numbers and equivalence relation, but we have still not enough mathematics for ternary phenomena.

Ternary composition algebras were studied by Shaw [11]. Their need is already seen from Kikuchi's investigations of cooperative phenomena [6]. Shaw took into account that just as real 8-dimensional composition algebras, of signatures $(8,0)$ and $(4,4)$, can be constructed out of 4-dimansional complex spaces $\mathbb{C}(4,0)$ and $\mathbb{C}(2,2)$,

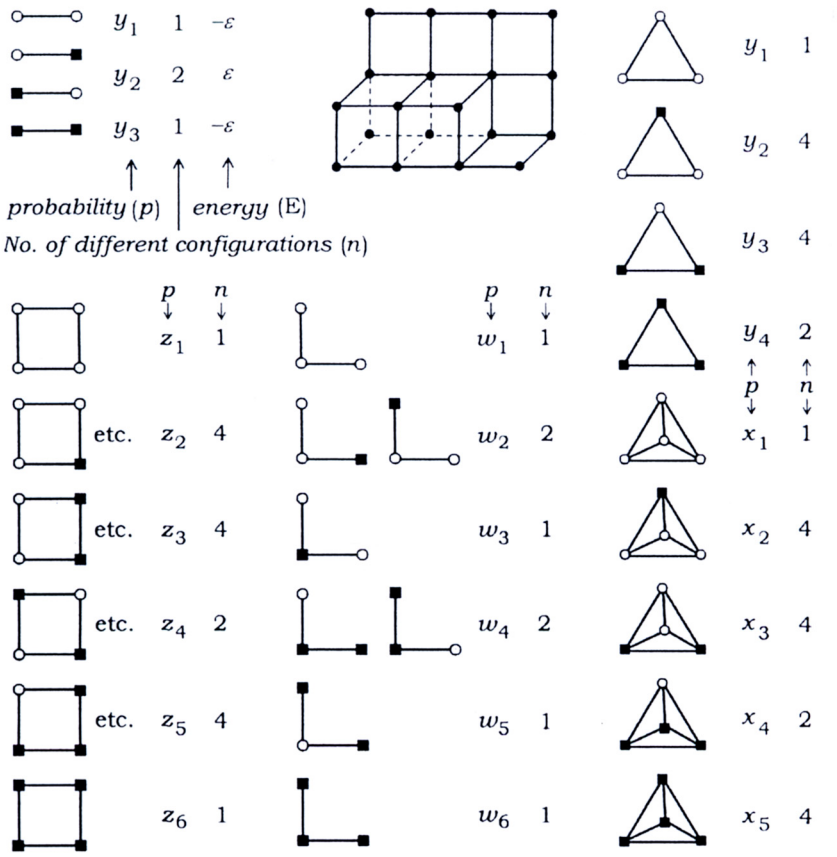

Fig. 1: Basic configurations of pairs, triples and quadruples of neighbouring atoms in a binary alloy according to R. Kikuchi.

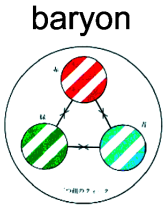

Fig. 2: Elementary particles construction by quarks.

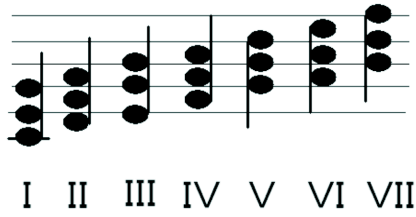

Fig. 3: Triplets in harmony of music.

1st base	2nd base				3rd base
	U	C	A	G	
U	UUU Phe	UCU Ser	UAU Tyr	UGU Cys	U
	UUC Phe	UCC Ser	UAC Tyr	UGC Cys	C
	UUA Leu	UCA Ser	UAA end	UGA end	A
	UUG Leu	UCG Ser	UAG end	UGG Trp	G
C	CUU Leu	CCU Pro	CAU His	CGU Arg	U
	CUC Leu	CCC Pro	CAC His	CGC Arg	C
	CUA Leu	CCA Pro	CAA Gln	CGA Arg	A
	CUG Leu	CCG Pro	CAG Gln	CGG Arg	G
A	AUU Ile	ACU Thr	AAU Asn	AGU Ser	U
	AUC Ile	ACC Thr	AAC Asn	AGC Ser	C
	AUA Ile	ACA Thr	AAA Lys	AGA Arg	A
	AUG Met	ACG Thr	AAG Lys	AGG Arg	G
G	GUU Val	GCU Ala	GAU Asp	GGU Gly	U
	GUC Val	GCC Ala	GAC Asp	GGC Gly	C
	GUA Val	GCA Ala	GAA Glu	GGA Gly	A
	GUG Val	GCG Ala	GAG Glu	GGG Gly	G

Fig. 4: Codon table.

complex 8-dimensional ternary composition algebras can be constructed out of a $\mathcal{K}$-module K^4, where $\mathcal{K}$ is a certain commutative algebra of dimension 4 over $\mathbb{R}$.

In [4], Kerner has introduced another concept of ternary algebra and gave trials to the quark confinement by this new method. He has also introduced a concept of ternary Clifford analysis and introduced ternary Dirac and Klein-Gordon operators. In this paper, we introduce concepts of binary and ternary Galois extensions and consider the Clifford analysis from that viewpoint. Also we introduce the concept of binary and ternary Hurwitz conditions and we observe intimate relationship between binary and ternary Clifford analysis. The present research is related with [9] and will be continued in [8].

1. Binary and ternary Clifford algebras and their analysis

We define concepts of the binary and ternary Clifford algebras [4] and make their Clifford analysis. We begin with the definition of Clifford algebras.

1.1. Definitions

Definition 1. 1) A pair $\{T_a, T_b\}$ of matrix elements constitute a basic *Clifford algebra* (of binary type), when it satisfies the following commutation relations:

$$\begin{cases} T_aT_b + T_bT_a = -2\eta^{ab}I_n, \\ \eta^{11} = \eta^{22} = 1, \quad \eta^{12} = i, \quad \eta^{21} = -i. \end{cases}$$

2) In an analogous manner, for the case of a triple of matrix elements $\{T_a, T_b, T_c\}$, we define a basic *ternary Clifford algebra*, when it satisfies the following conditions:

$$\begin{cases} T_aT_bT_c + T_bT_cT_a + T_cT_aT_b = 3\eta^{abc}I_n, \\ \eta^{abc} = \eta^{bca} = \eta^{cab}, \\ \eta^{111} = \eta^{222} = \eta^{333} = 1, \quad \eta^{123} = \eta^{231} = \eta^{321} = \mathrm{j}^2, \\ \eta^{321} = \eta^{213} = \eta^{132} = \mathrm{j}, \end{cases}$$

where I_n is the unit $n \times n$-matrix and j is a root of $z^3 - 1 = 0$.

3) For a general k-plet $\{T_1, T_2, \ldots, T_k\}$ of matrix elements of with k bigger than 2 (or 3), we define *general Clifford algebras* choosing 2 (resp. 3) elements from the k-plet respectively. The elements are called generators of the Clifford algebra.

Next we will make the Clifford analysis of Clifford algebras. We begin with the introduction of a concept of linear element of $\{T_1, T_2, \ldots, T_n\}$:

Definition 2. The following linear space of k-ple set $\{T_{i_1}, T_{i_2}, \ldots, T_{i_k}\}$ is called *linear element* of the system of the matrix elements $\{T_1, T_2, \ldots, T_n\}$:

$$\{\theta_{i_1}, \theta_{I_2}, \ldots, \theta_{i_k}\}_T = \{\theta_{i_1}T_{i_1} + \theta_{i_2}T_{i_2} + \ldots + \theta_{i_k}T_{i_k} | \theta_{i_j} \in K \ (j = 1, 2, \ldots, k)\}.$$

1.2. Quantization of a linear element

We introduce a concept of quantization: For a linear element $\{\theta_1, \theta_2, \ldots, \theta_M\}$, the following replacement for a polynomial $F(\theta_1, \theta_2, \ldots, \theta_M)$ is called *quantization*:

$$F(\theta_1, \theta_2, \ldots, \theta_M) \to F(\partial/\partial\theta_1, \ \partial/\partial\theta_2 \ldots, \partial/\partial\theta_M).$$

1.3. The binary Clifford analysis

We begin with a basic binary Clifford algebra with generators $\{T_1, T_2\}$. Making the quantization of a linear element $\theta_1T_1 + \theta_2T_2$, we introduce the following operators on the 2-dimensional Euclidean space:

$$D = T_1\frac{\partial}{\partial\theta_1} + T_2\frac{\partial}{\partial\theta_2}, \qquad D^* = T_1^*\frac{\partial}{\partial\theta_1} + T_2^*\frac{\partial}{\partial\theta_2}.$$

The operators are called *Dirac operator* and its *conjugate operator*. We notice that they satisfy the following condition:

$$\Delta = DD = D^*D^*, \quad \Delta := \left(\frac{\partial^2}{\partial\theta_1^2} + \frac{\partial^2}{\partial\theta_2^2}\right) \otimes 1_n.$$

The operator Δ is called *binary Laplace operator*. Choosing a system of generators $\{T_1, T_2, \ldots, T_n\}$ $(n = 2^m)$ of a general Clifford algebra, we can introduce the following operators on the n-dimensional Euclidean space:

$$D = T_1\frac{\partial}{\partial\theta_1} + T_2\frac{\partial}{\partial\theta_2} + \ldots + T_n\frac{\partial}{\partial\theta_n},$$

$$D^* = T_1^*\frac{\partial}{\partial\theta_1} + T_2^*\frac{\partial}{\partial\theta_2} + \ldots + T_n^*\frac{\partial}{\partial\theta_n}.$$

The operators are called *Dirac operator* and its *conjugate operator* when they satisfy the following condition:

$$\Delta = DD = D^*D^* \ \Delta = \left(\frac{\partial^2}{\partial\theta_1^2} + \frac{\partial^2}{\partial\theta_2^2} + \ldots + \frac{\partial^2}{\partial\theta_m^2} \right) \otimes 1_n.$$

The operator Δ is called *binary Laplace operator*.

1.4. The Clifford analysis of the ternary Clifford algebra

Next we proceed to the construction of Clifford analysis in the case of $k = 3$. We take a set of three elements and consider the ternary linear element:

$$\{\theta_1, \theta_2, \theta_3\}_Q = \{\theta_1 Q_1 + \theta_2 Q_2 + \theta_3 Q_3 | \theta_1, \theta_2, \theta_3 \in K\}, \quad Q = \{Q_1, Q_2, Q_3\}.$$

The following two elements associated to $\{\theta_1, \theta_2, \theta_3\}_Q$ are called conjugate elements:

$$\{\theta_1, \mathrm{j}\theta_2, \mathrm{j}^2\theta_3\}_Q, \quad \{\theta_1, \mathrm{j}^2, \mathrm{j}\theta_3\}_Q$$

which gives rise of an automorphism between linear elements (j is defined as in Sect. 1.1).

Next we proceed to the derivation of field operators. Choosing generators $\{T_1, T_2, T_3\}$ of a basic ternary Clifford algebra, we introduce the following three operators on the 3-dimensional Euclidean space:

$$\begin{aligned} D &= T_1 \frac{\partial}{\partial\theta_1} + T_2 \frac{\partial}{\partial\theta_2} + T_3 \frac{\partial}{\partial\theta_3}, \\ D^* &= T_1 \frac{\partial}{\partial\theta_1} + \mathrm{j}^2 T_2 \frac{\partial}{\partial\theta_2} + \mathrm{j} T_3 \frac{\partial}{\partial\theta_3}, \\ D^{**} &= T_1 \frac{\partial}{\partial\theta_1} + \mathrm{j} T_2 \frac{\partial}{\partial\theta_2} + \mathrm{j}^2 T_3 \frac{\partial}{\partial\theta_3}. \end{aligned}$$

The operators are called *Dirac operator* and its *conjugate operators* when they satisfy the following condition:

$$\Delta = D^3 = (D^*)^3 = (D^{**})^3,$$

$$\Delta = \left(\frac{\partial^3}{\partial\theta_1^3} + \frac{\partial^3}{\partial\theta_2^3} + \frac{\partial^3}{\partial\theta_3^3} - 3\frac{\partial^3}{\partial\theta_1\partial\theta_2\partial\theta_3} \right) \otimes 1_3.$$

The operator Δ is called the *ternary Klein-Gordon* operator.

Choosing a system of generators $\{T_1^{(\alpha)}, T_2^{(\alpha)}, T_3^{(\alpha)} : \alpha = 1, 2, \ldots, M\}$, we make their linear elements. Then we obtain the total set of ternary Dirac operators as follows:

$$\begin{aligned} D^{(\alpha)} &= T_1^{(\alpha)} \frac{\partial}{\partial\theta_1} + T_2^{(\alpha)} \frac{\partial}{\partial\theta_2} + T_3^{(\alpha)} \frac{\partial}{\partial\theta_3}, \\ D^{(\alpha)*} &= T_1^{(\alpha)} \frac{\partial}{\partial\theta_1} + \mathrm{j}^2 T_2^{(\alpha)} \frac{\partial}{\partial\theta_2} + \mathrm{j} T_3^{(\alpha)} \frac{\partial}{\partial\theta_3}, \\ D^{(\alpha)**} &= T_1^{(\alpha)} \frac{\partial}{\partial\theta_1} + \mathrm{j} T_2^{(\alpha)} \frac{\partial}{\partial\theta_2} + \mathrm{j}^2 T_3^{(\alpha)} \frac{\partial}{\partial\theta_3}. \end{aligned}$$

$$\Delta^{(\alpha)} = (D^{(\alpha)})^3 = (D^{(\alpha)*})^3 = (D^{(\alpha)**})^3,$$

$$\Delta^{(\alpha)} = \left(\frac{\partial^3}{\partial\theta_1^3} + \frac{\partial^3}{\partial\theta_2^3} + \frac{\partial^3}{\partial\theta_3^3} - 3\frac{\partial^3}{\partial\theta_1\partial\theta_2\partial\theta_3} \right)^{(\alpha)} \otimes 1_n.$$

The typical examples of ternary Clifford algebras with generators bigger than 3 can be obtained for the nonion algebra (see Sect. 3).

2. Non commutative Galois extension and Clifford algebras

In this section we introduce concepts of noncommutative Galois extension of binary type and ternary type, and discuss the relationship between Galois extension of binary and ternary type, and their Clifford algebras.

2.1. Noncommutative binary Galois extension

We can introduce a binary noncommutative Galois extension. Let A be a matrix algebra and A' be its subalgebra.

Definition 3. We take an element $\tau \in A$ with the condition $\tau^k = \pm 1$. Then the subalgebra $\sqrt[k]{\pm 1_n}[A']$ of of the following form is called a *noncommutative Galois extension of k-nary type* [7, 10]:

$$\sqrt[k]{\pm 1_n}[A'] = \left\{ \sum_{\rho=0}^{k-1} \theta_\upsilon \tau^\rho | \theta_\rho \in A' \ (\rho = 0, 1, \ldots, k-1) \right\}.$$

The extension is called proper when $\tau^\rho \notin A'$ $(\rho = 1, 2, \ldots, k-1)$.

We notice that we can obtain binary and ternary Clifford algebras from the Galois extensions $\sqrt[2]{-1}[A']$, $\sqrt[3]{1}[A'[]$, respectively.

2.2. Examples

We give two examples: The first one is the complex number $\sqrt{-1}[R]$ and the second one is the cubic root number $\sqrt[3]{1}[R]$:

$$\sqrt{-1}[R] = \{\theta_1 1 + \theta_2\sqrt{-1} | \theta_1,\ \theta_2 \in R\} = \left\{ \begin{pmatrix} \theta_1 & \theta_2 \\ -\theta_2 & \theta_1 \end{pmatrix} \middle| \theta_1,\ \theta_2 \in R \right\}$$

$$R[\sqrt{1}] = \{\theta_1 1 + \theta_2 j + \theta_3 j^2 | \theta_1, \theta_2, \theta_3 \in R\} = \left\{ \begin{pmatrix} \theta_1 & \theta_2 & \theta_3 \\ \theta_3 & \theta_1 & \theta_2 \\ \theta_2 & \theta_3 & \theta_1 \end{pmatrix} \middle| \theta_1, \theta_2 \in R \right\}.$$

2.3. Clifford algebras generated by binary Galois extensions

From these extensions we can introduce the binary Clifford algebras. We state the following well known theorem:

Theorem 1. *We can obtain any binary negative definite Clifford algebra from the Galois extensions of binary type. Namely there exists a sequence of noncommutative Galois extensions which generate the Clifford algebra:*

$$A^{(l)} = \sqrt[2]{-1}[A^{(l-1)}] \quad (l = 1, 2, 3, \dots, m).$$

Proof. The proof can be given by a well known construction of Clifford algebras:

$$\sqrt[2]{-1}[A^{(l)}] = \left\{ \begin{pmatrix} \theta_1 & \theta_2 \\ -\theta_2 & \theta_1 \end{pmatrix} \middle| \theta_1, \theta_2^* \in A^{(l-1)} \right\}.$$

In the next section we consider the structure of Galois extensions in the nonion algebra and make its Clifford analysis.

3. Noncommutative Galois structure on the nonion algebra

We introduce a concept of the nonion algebra N state some basic facts on the algebra, and consider the Galois extension structures on it.

3.1. Definition and notation

Definition 4. 1) The matrix algebra which is generated by the following 3 matrices is called *nonion algebra* N:

$$Q_1 = \begin{pmatrix} 0 & \mathrm{j} & 0 \\ 0 & 0 & \mathrm{j}^2 \\ 1 & 0 & 0 \end{pmatrix}, \quad Q_2 = \begin{pmatrix} 0 & \mathrm{j}^2 & 0 \\ 0 & 0 & \mathrm{j} \\ 1 & 0 & 0 \end{pmatrix}, \quad Q_3 = \begin{pmatrix} 0 & 1 & 0 \\ 0 & 0 & 1 \\ 1 & 0 & 0 \end{pmatrix}.$$

with j as in ( ).

2) The matrix algebra which is generated by the following 3 matrices over $\mathbb{R}$ is called *basic algebra* B:

$$T_4 = \begin{pmatrix} 0 & 0 & 1 \\ 0 & 1 & 0 \\ 1 & 0 & 0 \end{pmatrix}, \quad T_5 = \begin{pmatrix} 0 & 1 & 0 \\ 1 & 0 & 0 \\ 0 & 0 & 1 \end{pmatrix}, \quad T_6 = \begin{pmatrix} 1 & 0 & 0 \\ 0 & 0 & 1 \\ 0 & 1 & 0 \end{pmatrix}.$$

3) The algebra generated by $\{T_2, T_3\}$ is denoted by B':

$$T_2 = \begin{pmatrix} 0 & 1 & 0 \\ 0 & 0 & 1 \\ 1 & 0 & 0 \end{pmatrix}, \quad T_3 = \begin{pmatrix} 0 & 0 & 1 \\ 1 & 0 & 0 \\ 0 & 1 & 0 \end{pmatrix}.$$

3.2. Bases of N, B, and B'

Then we can prove the following the proposition:

Proposition 1. 1) *The following 9 elements constitute linear basis of the nonion algebra:*

$$Q_1 = \begin{pmatrix} 0 & \mathrm{j} & 0 \\ 0 & 0 & \mathrm{j}^2 \\ 1 & 0 & 0 \end{pmatrix}, \quad Q_2 = \begin{pmatrix} 0 & \mathrm{j}^2 & 0 \\ 0 & 0 & \mathrm{j} \\ 1 & 0 & 0 \end{pmatrix}, \quad Q_3 = \begin{pmatrix} 0 & 1 & 0 \\ 0 & 0 & 1 \\ 1 & 0 & 0 \end{pmatrix},$$

$$\overline{Q}_1 = \begin{pmatrix} 0 & 0 & 1 \\ \mathrm{j}^2 & 0 & 0 \\ 0 & \mathrm{j} & 0 \end{pmatrix}, \quad \overline{Q}_2 = \begin{pmatrix} 0 & 0 & 1 \\ \mathrm{j} & 0 & 0 \\ 0 & \mathrm{j}^2 & 0 \end{pmatrix}, \quad \overline{Q}_3 = \begin{pmatrix} 0 & 0 & 1 \\ 1 & 0 & 0 \\ 0 & 1 & 0 \end{pmatrix},$$

$$R_1 = \begin{pmatrix} 1 & 0 & 0 \\ 0 & 1 & 0 \\ 0 & 0 & 1 \end{pmatrix}, \quad R_2 = \begin{pmatrix} 1 & 0 & 0 \\ 0 & \mathrm{j} & 0 \\ 0 & 0 & \mathrm{j}^2 \end{pmatrix}, \quad R_3 = \begin{pmatrix} 1 & 0 & 0 \\ 0 & \mathrm{j}^2 & 0 \\ 0 & 0 & \mathrm{j} \end{pmatrix}.$$

2) *The following 6 elements are linear basis of B:*

$$T_1 = \begin{pmatrix} 1 & 0 & 0 \\ 0 & 1 & 0 \\ 0 & 0 & 1 \end{pmatrix}, \quad T_2 = \begin{pmatrix} 0 & 1 & 0 \\ 0 & 0 & 1 \\ 1 & 0 & 0 \end{pmatrix}, \quad T_3 = \begin{pmatrix} 0 & 0 & 1 \\ 1 & 0 & 0 \\ 0 & 1 & 0 \end{pmatrix},$$

$$T_4 = \begin{pmatrix} 0 & 0 & 1 \\ 0 & 1 & 0 \\ 1 & 0 & 0 \end{pmatrix}, \quad T_5 = \begin{pmatrix} 0 & 1 & 0 \\ 1 & 0 & 0 \\ 0 & 0 & 1 \end{pmatrix}, \quad T_6 = \begin{pmatrix} 1 & 0 & 0 \\ 0 & 0 & 1 \\ 0 & 1 & 0 \end{pmatrix}.$$

3) *The following 3 elements are linear basis of B':*

$$T_1 = \begin{pmatrix} 1 & 0 & 0 \\ 0 & 1 & 0 \\ 0 & 0 & 1 \end{pmatrix}, \quad T_2 = \begin{pmatrix} 0 & 1 & 0 \\ 0 & 0 & 1 \\ 1 & 0 & 0 \end{pmatrix}, \quad T_3 = \begin{pmatrix} 0 & 0 & 1 \\ 1 & 0 & 0 \\ 0 & 1 & 0 \end{pmatrix}.$$

4) *B and B' are subalgebras of N.*

Proof. [7].

3.3. The ternary Galois extension structure of the nonion algebra

We can give the following Galois extension structure of the nonion algebra. Namely we can prove

Theorem 2. 1) *The nonion algebra N is the ternary Galois extension of the space algebra B': $N = \sqrt[3]{1_3}[B']$.*

2) *The binary Galois extension*

$$\tilde{N} = \sqrt[2]{1_3}[N]$$

can be expressed as $\tilde{N} = \sqrt[3]{1_3}[B]$.

Proof. Ad 1). We notice that B' is the commutative Galois extension of real numbers

$$\mathbb{R} : B' = \sqrt[3]{1}[R].$$

Choosing $\tau = R_2$, we make the Galois extension $\sqrt[2]{1_3}[B']$. Then we can see that it is identical with N.

Ad 2). At first we notice that B is the noncommutative binary Galois extension of B': $B = \sqrt[3]{1_3}[B']$ with respect to $\tau = T_4$. Choosing $\tau = R_2$, we make the Galois extension $\sqrt[2]{1_3}[B]$. Then we can see that it is this is identical with $\tilde{N}$.

By this theorem we can introduce the Dirac operators and the Klein-Gordon operator. Namely we can prove

Theorem 3. *Let N be the nonion algebra and let*

$$\{\theta_1, \theta_2, \theta_3\}_X (X = Q, \overline{Q}, R)$$

be a linear element. Then by use of the quantization $\theta_1 \to \partial/\partial\theta_i$ $(i = 1, 2, 3)$, we have the Dirac operator and its conjugate Dirac operators:

$$\begin{cases} D = \{\partial/\partial\theta_1, \partial/\partial\theta_2, \partial/\partial\theta_3\}_X, \\ \\ D^* = \{\partial/\partial\theta_1, \mathrm{j}\partial/\partial\theta_2, \mathrm{j}^2\partial/\partial\theta_3\}_X \quad (X = Q, \overline{Q}, R), \\ \\ D^{**} = \{\partial/\partial\theta_1, \mathrm{j}^2\partial/\partial\theta_2, \mathrm{j}\partial/\partial\theta_3\}_X. \end{cases}$$

The quantization gives the Klein-Gordon operator:

$$\begin{aligned} \rho(\partial/\partial\theta) \otimes I_3 &= \det\{\partial/\partial\theta_1, \partial/\partial\theta_2, \partial/\partial\theta_3\}_X \otimes I_3 \\ &= \left(\partial^3/\partial\theta_1^3 + \partial^3/\partial\theta_2^3 + \partial^3/\partial\theta_3^3 - 3\partial^3/\partial\theta_1\partial\theta_2\partial\theta_3\right) \otimes I_3 \\ &= D^3 (= D^{*3} = D^{**3}). \end{aligned}$$

References

[1] V. Abramov, R. Kerner, and B. Le Roy, J. Math. Phys. **38** (1997), 1650–1669.

[2] F. L. Castillo Alvarado, J. Ławrynowicz, and Małgorzta Nowak-Kępczyk, *Fractal modelling of alloy thin films. Temperatures characteristic for local phase transitions*, in: Applied Complex and Quaternionic Approximation. Ed. by R. K. Kovacheva, J. Ławrynowicz, and S. Mariachafava, Ediz. "Nuova Cultura", Roma 2009, pp. 207–234.

[3] S. Kanemaki, *Hurwitz pair and Octonion*, Deformation of mathematical structures, (1989), 215–223.

[4] R. Kerner, Journ. Math. Phys. **33** (1997), 403–411.

[5] R. Kerner, Class And Quantum Gravity **14** (2002), A203–A225.

[6] R. Kikuchi, *A thery of cooperative phenomena*, Phys. Rev. **81** (1951), 988–1003.

[7] J. Ławrynowicz, K. Nôno, D. Nagayama, and O. Suzuki, *A method of noncommutative Galois theory for binary and ternary Clifford analysis*, Proc. of the ICNPAA Conference Wien 2012, American Inst. of Phys. Press, Woodbury, NY 2013, 8 pp., to appear.

[8] —, —, and O. Suzuki, *Binary and ternary analysis vs. noncommutative Galois extensions II. The corresponence between ternary and binary field operations*, Bull. Soc. Sci. Lettres Łódź Sér. Rech. Déform. **62**, no. 2 (2012) 10 pp., to appear.

[9] — and J. Rembieliński, *Hurwitz pairs equipped with complex structure*, Lecture Notes in Math. (Springer) **1165** (1985), 184–195.

[10] F. de Meyer and E. Ingram, *Separable Algebras over Commutative Rings* (Lecture Notes in Math. 181), Springer-Verlag, Berlin-Heidelberg-New York-Tokyo 1971.

[11] R. Shaw, *Ternary composition algebras:* 8 *dimensions out of* 4*?*, Il Nuovo Cimento **104 B**, no. 2 (1989), 161–183.

Institute of Physics
Univeristy of Łódź
Pomorska 149/153, PL-90-236 Łódź
Institute of Mathematics
Polish Academy of Sciences
Łódź Branch, Banacha 22, PL-90-238 Łódź
Poland
e-mail: jlawryno@uni.lodz.pl

Department of Mathematics
Fukuoka University
of Education Munakata-shi
Fukuoka
Japan
e-mail: nounoi@fukuoka-edu.ac.jp

Department of Computer and System Analysis
College of Humanities and Sciences
Nihon University
156 Setagaya,Tokyo
Japan
e-mail: osuzuki@cssa.chs.nihon-u.ac.jp

Presented by Julian Ławrynowicz at the Session of the Mathematical-Physical Commission of the Łódź Society of Sciences and Arts on 15 December, 2011

BINARNA I TERNARNA ANALIZA CLIFFORDA A NIEPRZEMIENNE ROZSZERZENIA GALOIS I

PODSTAWY PORÓWNANIA

S t r e s z c z e n i e

Wprowadzono pomysł nieprzemiennego rozszerzenia Galois przy wyborze rozszerzeń binarnych i ternarnych. Wprowadzono ternarną algebrę Clifforda oraz naszkicowano odpowiednią analizę Clifforda i związek z rozszerzeniem Galois. W konsekwencji potrafimy sformułować binarne i ternarne warunki typu Hurwitza i uzyskać z tych warunków operator Diraca. Tak więc operatory Diraca, binarny i ternarny, dadzą się jednolicie scharakteryzować.

W pierwszej części pracy omawiamy binarne i ternarne algebry Clifforda, nieprzemienne rozszerzenia Galois w kontekście algebr Clifforda i nieprzemienne struktury Galois na algebrze nonionowej.

PL ISSN 0459-6854

B U L L E T I N

DE LA SOCIÉTÉ DES SCIENCES ET DES LETTRES DE ŁÓDŹ

2012 Vol. LXII

Recherches sur les déformations no. 1

pp. 43–53

In memory of
Professor Roman Stanisław Ingarden

S. Marchiafava

TWISTOR THEORY FOR CR QUATERNIONIC MANIFOLDS: A REPORT

Summary

We report about the recent introduction of the notion of CR quaternionic manifolds in a general, non metrical, context and some first general results on their twistor theory ([M-O-P], [M-P1], [M-P2].

Keywords and phrases: quaternionic geometry, CR-geometry, twistor theory.

Introduction

Recently an increasing interest on quaternionic like structures has led to some developments on this subject concerning related notions of CR structures, see [Al-K], [Be-Fa], [Bi]. Here we report on further new developments dealing, in a non metrical context, with the introduction of a general notion of *CR quaternionic structure* and a related *twistor theory for CR quaternionic manifolds*, together with some first basic results and applications to submanifolds of quaternionic manifolds (research worked out in collaboration with Radu Pantilie and Liviu Ornea ([M-O-P], [M-P1] [M-P2]).

It is well known that the simplest situation to consider for quaternionic structures occurs in real dimension 4, with the identification $\mathbb{R}^4 \equiv \mathbb{H}$, where $\mathbb{H}$ is the skew-field of quaternions. Correspondingly, the basic case for CR quaternionic structures takes place in real dimension 3, with the identification $\mathbb{R}^3 \equiv \mathrm{Im}\mathbb{H}$.

The idea of the definition of CR quaternionic structures bases on the fact that a linear quaternionic structure on a real vector space E has an associated 2-sphere $\mathcal{Z}$ of

admissible linear complex structures on E (the left multiplications by unit imaginary quaternions) and for each of them there are corresponding (partially complex) CR structures.

We show that in the lowest dimension CR quaternionic geometry is a natural framework to encode a Lebrun construction of the *twistor manifold of a 3-dimensional conformal manifold* ([L]) and also we indicate how to extend it to the general quaternionic case ([M-O-P]).

It is interesting to note that it is defined also a dual notion of Co-CR quaternionic manifold, [M-P2]. The simplest example of Co-CR quaternionic manifold is provided by a 3-dimensional Einstein-Weyl space, endowed with a twistorial structure defined by N. Hitchin, [H].

1. CR and Co-CR structures

1.1. CR and Co-CR structures in a vector space

We recall briefly the following equivalent definitions.

A **complex structure on a real vector space** V^{2n} is:

1) an $\mathbb{R}$-isomorphism $\varphi : V \to \mathbb{C}^n$
2) $J \in \mathrm{End}V, \quad J^2 = -\mathrm{Id} \qquad (J\mathbf{v} = \varphi^{-1}(i\varphi\mathbf{v}))$
3) a subspace $C \subset V^{\mathbb{C}} = \mathbb{C} \otimes V,\ V^{\mathbb{C}} = C \oplus \overline{C} \quad \cong \quad \begin{cases} C \cap \bar{C} & = 0 \\ C + \bar{C} & = V^{\mathbb{C}} \end{cases}$
   $\big(C = (V^{\mathbb{C}})^{0,1} = \mathrm{Ker}(J + i)\big)$

Let V, V' be complex vector spaces and φ, φ', J, J' and C, C' be respectively the corresponding maps, endomorphisms and subspaces following the given definitions.

An ($\mathbb{R}$- linear) map $t : V \to V'$ is a **complex** (or **holomorphic**) map if, equivalently,

$$\varphi' \circ t \circ \varphi^{-1} \in \mathrm{Hom}_{\mathbb{C}}(\mathbb{C}^n) \quad \Leftrightarrow \quad t \circ J = J' \circ t \quad \Leftrightarrow \quad t(C) \subset C'$$

$$(\text{if} \quad t(C) \subset C' \quad \text{and} \quad \mathbf{v} \in C, \quad \text{i. e.} \quad (J + i)\mathbf{v} = 0, \Longrightarrow (J' + i)t\mathbf{v} = 0)\,.$$

There are two ways to weaken the definition of a complex structure, giving rise to the following corresponding definitions.

A **CR (partially complex) structure** C **on a** k**-dimensional real vector space** U is:

I) a subspace $C \subset U^{\mathbb{C}}, \qquad C \cap \bar{C} = \mathbf{0}$

II) an injective $\mathbb{R}$-linear map $\iota : U \to (E, J)$ in a complex vector space (E, J), such that

$$\mathrm{Im}\iota + J(\mathrm{Im}\iota) = E$$

[then $C = \iota^{-1}\big(\mathrm{Ker}(J + i)\big), \quad E \cong U^{\mathbb{C}}/C$].

Let $(U, C), (U', C')$ be CR vector spaces. Then the $\mathbb{R}$-linear map $t : U \to U'$ is a **CR map** if $t(C) \subset C'$.

One has also the following dual notion.

A **Co-CR (complex) structure** C **on a real vector space** U is:

I) A subspace $C \subset U^{\mathbb{C}}$, $\quad C + \bar{C} = U^{\mathbb{C}}$

II) A surjective map $\rho : (E, J) \to U$ such that $\mathrm{Ker}\rho \cap J(\mathrm{Ker}\rho) = \mathbf{0}$ [then $C = \rho\big(\mathrm{Ker}(J + i)\big)$, $\quad E \cong \bar{C}$].

(U, C) is a CR vector space if and only if $(U^*, C^0 = \mathrm{Ann}(C))$ is a Co-CR vector space.

Let $(U, C), (U', C')$ be Co-CR vector spaces. Then the $\mathbb{R}$-linear map $t : U \to U'$ is a **Co-CR map** if $t(C) \subset C'$.

1.2. CR and Co-CR structures on manifolds

Let's recall also that passing from the linear situation to the case of manifolds one has the following notions.

An **almost CR (partially complex) structure** (respectively, **almost Co-CR structure**) on a manifold M is a differentiable field $C = \{C_x\}_{x \in M}$ of subspaces of $T^{\mathbb{C}}M$, i.e. a complex distribution of $T^{\mathbb{C}}M$, such that (T_xM, C_x) is a CR structure (respectively, Co-CR structure) for any $x \in M$.

An almost CR (partially complex) structure (respectively, almost Co-CR (complex) structure) C on a manifold M is an **integrable almost CR (respectively, Co-CR) structure** if the distribution C is involutive, i.e.

$$[C, C] \subset C$$

An integrable almost CR (respectively, Co-CR) structure is called a **CR** (respectively, **Co-CR**) **structure**.

A typical example of almost CR manifold is given by an **embedded CR manifold** consisting in a generic submanifold M^{m+n}, $n < m$, of an m-dimensional complex manifold N.

Of course, almost complex and complex manifolds make part of the class of almost CR and CR (respectively Co-CR) manifolds.

2. CR and Co-CR quaternionic structures

Quaternionic structures are geometric structures where *families of complex structures* are naturally defined.

2.1. Quaternionic linear structures

Quaternionic linear structures as a quaternionic vector spaces together with their family of compatible complex structures (left multiplications by imaginary unitary quaternions).

$n = 1$

Let $\mathbb{H}$ be the algebra of quaternions. There exists a (normal) basis (i, j, k) verifying the well known multiplication table

$$i^2 = j^2 = k^2 = -1,$$
$$ij = -ji = k, \qquad jk = -kj = i, \qquad ki = -ik = j$$

such that the quaternions are written as

$$q = q^0 + q^1 i + q^2 j + q^3 k \in \mathbb{H}, \qquad\qquad q^i \in \mathbb{R} \quad (i = 0, 1, 2, 3).$$

Hence one has an identification of real vector spaces

$$\mathbb{H} \equiv \mathbb{R}^4.$$

It defines a **quaternionic structure** Q on $\mathbb{R}^4$ where $Q \cong \mathrm{Im}\mathbb{H}$ is the subalgebra of (left) multiplications by imaginary quaternions, $Q \subset \mathrm{End}(\mathbb{R}^4)$.

A left (respectively, right) multiplication by an imaginary unitary quaternion is a complex structure in $\mathbb{R}^4$: for example

$$\mathcal{I} = i\cdot, \qquad\qquad \mathcal{J} = j\cdot, \qquad\qquad \mathcal{K} = k\cdot,$$

$$\big(\mathcal{I}' = \cdot i, \qquad\qquad \mathcal{J}' = \cdot j, \qquad\qquad \mathcal{K}' = \cdot k\big).$$

The multiplications on the left (respectively, on the right) by imaginary unitary quaternions

$$q = q^1 i + q^2 j + q^3 k \qquad , \qquad (q^1)^2 + (q^2)^2 + (q^3)^2 = 1,$$

or, equivalently (to prove this statement let write $q = q^0 + pu$ where

$$p = \sqrt{(q^1)^2 + (q^2)^2 + (q^3)^2} \in \mathbb{R}$$

and

$$u = \frac{q^1 i + q^2 + q^3 k}{\sqrt{(q^1)^2 + (q^2)^2 + (q^3)^2}};$$

then since $q^2 = (q^0)^2 - p^2 + 2q^0 pu$, easily it follows that $q^2 = -1 \Leftrightarrow q = \pm u$), quaternions q such that $q^2 = -1$, form a sphere S^2 of **positive** (respectively, **negative**) **compatible complex structures**.

Let remark that *the sphere* S^2 *of (left) complex structures does not depend on the normal basis* (i, j, k). It can be seen as follows.

Let recall the quaternionic form of rotations groups in 3- and 4-dimensional euclidean spaces.

With respect to the identification $\mathbb{H} \equiv \mathbb{R}^4$ the orientation preserving isometries of $\mathbb{R}^4$ coincide with transformations of the form $T = T_{a,q}$,

$$T_{a,q} : \qquad \xi' = q\xi a \qquad\qquad \xi, \xi' \in \mathbb{H} \equiv \mathbb{R}^4$$

where $a, q \in Sp(1) \equiv S^3$ are unitary quaternions. Hence one has the isomorphism

$$SO(4) \cong Sp(1) \cdot Sp(1) \equiv \frac{Sp(1) \times Sp(1)}{\mathbb{Z}_2}\,.$$

If one drops the condition for quaternions q, a to be unitary one gets the (orientation preserving) conformal transformations of $\mathbb{R}^4$,

$$CO^+(4) \cong Sp(1) \cdot GL_1(\mathbb{H})\,.$$

With respect to the identification

$$\mathrm{Im}\mathbb{H} \equiv \mathbb{R}^3$$

the orientation preserving isometries of $\mathbb{R}^3$ are of the form $T = T_q$,

$$T_q : \qquad \xi' = q\xi\bar{q}$$

where $q \in Sp(1)$, hence

$$SO(3) \cong \frac{Sp(1)}{\mathbb{Z}_2}$$

(note that $\frac{Sp(1)}{\mathbb{Z}_2} \cong \mathbb{R}P^3$).

Moreover, by dropping the condition for q to be unitary one gets the (orientation preserving) conformal transformations of $\mathbb{R}^3$ and

$$CO^+(3) \cong \frac{GL_1(\mathbb{H})}{\mathbb{Z}_2}\,.$$

Note that a basic conformal invariant in dimension 3 is the *isotropic cone*

$$(z^1)^2 + (z^2)^2 + (z^3)^2 = 0$$

in the complexified $\mathbb{C}^3$ of the euclidean 3-dimensional space $\mathbb{R}^3$ and the *isotropic lines* form a Riemann sphere $\mathbb{C}P^1$.

The groups $SO(3), SO(4)$ (resp. $CO^+(3), CO^+(4)$) are the (generic) holonomy groups of 3-, 4-dimensional oriented Riemannian (resp. conformal) manifolds.

In the following considerations one could refer to the prototype given by the spaces and morphisms

$$\iota : \mathbb{R}^3 \equiv \mathrm{Im}\mathbb{H} \to \mathbb{R}^4 \equiv \mathbb{H} \equiv \mathbb{R} \oplus \mathrm{Im}\mathbb{H}\,.$$

Let U be an oriented 3-dimensional real vector space endowed with a conformal structure $c = \{g\}$ represented by an euclidean scalar product g, which extends to the complexified $U^{\mathbb{C}}$.

A non trivial CR structure C of U is 1-dimensional.

Correspondingly, *a non trivial Co-CR structure C is 2-dimensional.* To see this, let's take into account that with respect to the identification

$$g : U \to U^* \qquad \mathbf{v} \mapsto g(\mathbf{v}) = g(\mathbf{v}, \cdot)$$

the annihilator C^0 of a subspace $C \subset U$, formed by the 1-forms $\theta \in U^*$ s.t. $\theta_{|_C} = 0$, is identified with the orthogonal $C^\perp$.

Let $(\mathbf{u}, \mathbf{v}, \mathbf{w})$ be a g-orthonormal positively oriented basis of U. Then

- $C(\mathbf{u}) = \mathrm{Span}_{\mathbb{C}}\{\mathbf{v} + \mathbf{i}\mathbf{w}\}$ is a CR structure or, equivalently, an *isotropic line*
- $C(\mathbf{u})^\perp = \mathrm{Span}_{\mathbb{C}}\{\mathbf{u}, \mathbf{v} + \mathbf{i}\mathbf{w}\}$ is a Co-CR structure or, equivalently, a *coisotropic plane.*

The bijective correspondences

$$\mathbf{u} \in \mathbf{S^2} \subset \mathbf{U} \quad \longleftrightarrow \quad \mathbf{C(u)} \subset \mathbf{U}^{\mathbb{C}} \quad \longleftrightarrow \quad \mathbf{C(u)}^{\perp} \subset \mathbf{U}^{\mathbb{C}}$$

give identifications between the unit sphere S^2, the space of (1-dimensional) CR structures, the space of (2-dimensional) Co-CR structures of (U, g).

Passing to the conformal structure $c = \{g\}$ one gets the *identifications of the spaces of non trivial CR, respectively Co-CR structures, of* (U, c) *with the complex projective line* $\mathbb{C}P^1$.

Let notice that one has also the *conformal isomorphisms between* $(U^{\mathbb{C}}, \{g_{\mathbb{C}}\})$ and $(U^{*\mathbb{C}}, \{g_{\mathbb{C}}^{-1}\})$.

Let $E = \mathbb{R} \oplus U$ be the 4-dimensional euclidean space endowed with the metric $g_E = g_0 \oplus g$, where g_0 is the canonical metric of $\mathbb{R}$, and corresponding conformal structure $\{g_E\}$.

E carries a natural quaternionic structure Q, which will be identified with the conformal structure $\{g_E\}$, defined as follows.

With respect to g one has an identification isomorphism $\sigma : E \to \mathbb{H}$ for any choice of an orthonormal oriented basis $(\mathbf{u}, \mathbf{v}, \mathbf{w})$ of U, by linearly extending the correspondence

$$(\mathbf{e} \equiv \mathbf{1}, \mathbf{u}, \mathbf{v}, \mathbf{w}) \mapsto (\mathbf{1}, \mathbf{i}, \mathbf{j}, \mathbf{k})$$

where (i, j, k) is the fixed normal base of $\mathbb{H}$.

A change of the orthonormal basis or a conformal change of the metric g will correspond to the composition of σ with an inner automorphism of $\mathbb{H}$. Hence *the quaternionic structure* Q *is well defined by the oriented conformal structure* $c = \{g\}$.

Let's remark also that through the injection ι of U in E there is a bijection between the CR structures $C(\mathbf{u})$ of U and the admissible complex structures $J_{\mathbf{u}}$ of (E, Q) such that $\mathrm{Span}\{\mathbf{e} + i\mathbf{u}\} \oplus C(\mathbf{u}) = \mathrm{Ker}(\mathbf{J_u} + i)$, which gives a basic example of a *CR quaternionic structure*: in fact, for any compatible complex structure $J \in Q$ the triple (ι, E, J) is a linear CR structure, that is $C(J) = \iota^{-1}(E^J) \subset U^{\mathbb{C}}$ where $E^J = \mathrm{Ker}(J + i)$ is the eigenspace of J corresponding to $-i$, is a CR structure of U.

The typical situation is just $\iota : U \equiv \mathrm{Im}\mathbb{H} \to E \equiv \mathbb{H}$.

The recalled facts are basic tools for the following construction of C. Lebrun ([L]) in the case of a 3-manifold.

If $(M^3, \{g\})$ is a conformal oriented 3-manifold LeBrun constructed a CR 5-manifold N, called the *twistor CR manifold of* $(M^3, \{g\})$ which naturally fibers on M with fiber $\mathbb{C}P^1$,

$$\begin{array}{ccc} \mathbb{C}P^1 & \hookrightarrow & N \\ & & \downarrow \\ & & M \end{array} .$$

In a first definition of Lebrun N is the manifold of null directions of the cotangent bundle $\mathbb{C}T^*M$, then he observes that $N \to M$ may be identified with the sphere bundle $SM \to M$ with respect to a representative g of the conformal class. In our language N is the manifold of CR structures in the tangent spaces of M. Moreover

LeBrun introduces an almost CR structure on N and here below we will see how his construction fits into a general one.

Let first recall some more definitions.

$n \geq 1$

An interesting generalization of an oriented, conformal 4-dimensional manifold is obtained by considering as structural group the **generalized quaternionic group** $G = Sp(1) \cdot GL_n(\mathbb{H})$, formed by the automorphisms of $\mathbb{H}^n \equiv \mathbb{R}^{4n}$ of the form

$$T = T_{q,A} : \qquad \xi' = q\xi A \qquad \xi, \xi' \in \mathbb{H}^n$$

where $q \in Sp(1)$, $A \in GL_n(\mathbb{H})$.

Note that this group of transformations leaves invariant the space $Q \subset \mathrm{End}\mathbb{R}^{4n}$ of left multiplications by imaginary quaternions: if $L_\lambda = \lambda\cdot, \lambda \in \mathbb{H}$ then

$$T \circ L_\lambda = L_{\lambda'} \circ T \qquad , \quad \lambda' = q\lambda\bar{q}$$

$(T(\lambda\xi) = q\lambda\xi A = (q\lambda\bar{q})q\xi A = \lambda' T\xi)$.

In particular, G leaves invariant the sphere $\mathcal{Z} = S^2(Q)$ of left multiplications by unitary imaginary quaternions, that is the sphere of **compatible complex structures**.

An **almost quaternionic manifold** (M, Q) is a manifold M^{4n} together with a $Sp(1) \cdot GL_n(\mathbb{H})$-structure $Q \subset \mathrm{End}TM$ on the tangent bundle, locally spanned by a triple of field of endomorphisms (I, J, K) verifying the Hamilton multiplicative table

$$I^2 = J^2 = K^2 = -Id \quad ;$$
$$IJ = -JI = K\,,\; JK = -KJ = I\,,\; KI = -IK = J\,.$$

defined on an open set $U \subset M$. An **almost quaternionic connection** ∇ on TM is a connection **compatible with** Q, i.e. it leaves Q invariant.

The **n-dimensional quaternionic projective space** $\mathbb{H}P^n$ with the standard atlas of quaternionic (non homogeneous) projective coordinates carries a generalized quaternionic structure (see [Bo], [Ma]) and it is the main example of a 4n-dimensional "*quaternionic manifold*".

A **quaternionic manifold** is an almost quaternionic manifold which admits a compatible torsionless connection, i.e. a **quaternionic connection** ∇.

Note that in the 1-dimensional case a quaternionic manifold (M^4, Q) equipped with a quaternionic connection ∇ is the same as a *Weyl space*, that is a conformal manifold (M^4, c) together with a Weyl connection (i.e. a torsion free conformal connection) $D \equiv \nabla$.

A basic link between quaternionic geometry and complex geometry is provided by the following twistorial construction.

Let (M^{4n}, Q) be a quaternionic manifold and ∇ a quaternionic connection. The **twistor bundle** $\mathcal{Z} \to M^{4n}$ of (M^{4n}, Q) is the bundle whose fiber at a point $x \in M^{4n}$ is the sphere $S^2_x = S^2(Q_x)$ of compatible complex structures J_x of T_xM with respect to the quaternionic structure Q_x. Due to the canonical identification $\mathbb{C}P^1 \equiv S^2$, the

vertical bundle $\mathcal{V}$ of the twistor bundle is a complex bundle. **The twistor space $\mathcal{Z}$ carries a natural complex structure** $\mathcal{I}$ which extends the complex structure of $\mathcal{V}$ as follows. Let $T_J\mathcal{Z}$ be the tangent space at a point $J \in \mathcal{Z}$; then it decomposes as $T_J\mathcal{Z} = \mathcal{V}_J \oplus \mathcal{H}_J$ where V_J is the vertical space of the fibration and $\mathcal{H}_J$ is the horizontal space with respect to the quaternionic connection ∇. The differential $d\pi(J)$ at J restricted to $\mathcal{H}_J$ is an isomorphism

$$d\pi(J)\Big|_{\mathcal{H}_J} : \mathcal{H}_J \to T_xM$$

and it can be used to pull-back the complex structure J to a complex structure on $\mathcal{H}_J$. Then $\mathcal{I}$ is the "sum" of the complex structures of $\mathcal{V}_J$ and $\mathcal{H}_J$.

In [A-M-P] an almost complex structure for the twistor space of any almost quaternionic manifold was defined.

In the following we will limit ourselves to the CR structures, by omitting to mention the dual Co-CR structures.

2.2. Linear CR quaternionic structures

Let U be a (real) vector space and (E, Q) a quaternionic vector space.

Let $\iota : U \to E$ be an injective linear map. (E, ι) is a **linear CR quaternionic structure on** U if (ι, J) induces a linear CR structure on U, $\forall J \in \mathcal{Z}$.

CR quaternionic linear maps

Let $(U, E, \iota), (U', E', \iota')$ be CR quaternionic vector spaces and $t : U \to U'$, $T : \mathcal{Z} \to \mathcal{Z}'$ be maps. Then $t : (U, E, \iota) \to (U', E', \iota')$ is a **CR quaternionic linear map w.r.t.** T if t is linear and there exists a quaternionic map $\widetilde{t} : E \to E'$ w.r.t. T and $\iota' \circ t = \widetilde{t} \circ \iota'$.

Proposition 1. *Let $(U, E, \iota), (U', E', \iota')$ be CR quaternionic vector spaces, $t : U \to U'$ a non zero linear map, $T : \mathcal{Z} \to \mathcal{Z}'$ be a map. Then the following assertions are equivalent:*

(i) *t is CR quaternionic, with respect to T.*

(ii) *T is a holomorphic diffeomorphism and, for any $J \in \mathcal{Z}$, we have*

$$t(U^J) \subset (U')^{T(J)} .$$

Furthermore, if assertion (i) or (ii) holds then there exists a unique linear map $\widetilde{t} : E \to E'$ which is quaternionic, with respect to T and such that $\iota' \circ t = \widetilde{t} \circ \iota$.

2.3. CR quaternionic manifolds

Definition. Let $E \to M$ be a quaternionic vector bundle on a manifold M^{4m} and $\iota : TM \to E$ un injective morphism of vector bundles. (E, ι) is an **almost CR quaternionic structure on** M if (E_x, ι_x) is a linear CR quaternionic structure on T_xM, $\forall x \in M$.

Examples

Main source of *examples of almost CR quaternionic manifolds* is provided by the submanifolds of an almost quaternionic manifold N (including N itself of course) : an hypersurface or, more generally, an open neighbourhood of a poinf x of a submanifold $M \subset N$ such that (T_xM, E_x, ι_x) is a CR quaternionic vector space, where ι is the inclusion $TM \to E \equiv TN_{|N}$, is an almost CR quaternionic manifold.

Let (M, E, ι) be an almost CR quaternionic manifold. An **almost quaternionic connection** of (M, E, i) is a connection ∇ on E which preserves the quaternionic structure Q. A **quaternionic connection** is a torsion free, i.e. $d^{\nabla}\iota = 0$, almost quaternionic connection.

2.4. Definition of (integrable almost) CR quaternionic structure on M

Let (M, E, ι) be an almost CR quaternionic manifold. Then for any (local) section J of $\mathcal{Z} = \mathcal{Z}(E)$ the complex distribution $\mathcal{C} = \iota^{-1}(E^J)$ is a (local) almost CR structure on M, called *admissible (local) almost CR structure on* (M, E, i).

Almost twistorial structure of an almost CR quaternionic manifold (M, E, ι) **with respect to** ∇, almost quaternionic connection on E.

For any $J \in \mathcal{Z}$, let $\mathcal{H}^{0,1}_J \subset T^{\mathbb{C}}_J\mathcal{Z}$ be the ∇-horizontal lift of $\iota^{-1}(E^J)$, being E^J the $-i$-eigenspace of J. Define

$$\mathcal{C}^{\nabla}_J = \mathcal{H}^{0,1}_J \oplus (\mathrm{Ker} d\pi)^{0,1}_J \qquad (J \in \mathcal{Z})$$

$(\mathcal{Z}, \pi, \mathcal{C})$ is the **almost twistorial structure of** (M, E, i, ∇). It was proved in [M-O-P] that the integrability conditions for such a structure are

$$T^{\nabla}(\bigwedge^2(T^JM)) \subset E^J, \qquad R^{\nabla}(\bigwedge^2(T^JM)) \subset E^J\,.$$

Proposition 2. *Let M be endowed with an almost CR quaternionic structure (E, i), $\mathrm{rank}\, E = 4k, \dim(M) = 4k-\ell$, $(0 \leq \ell \leq 2k-1)$. Let ∇ be a quaternionic connection on (M, E, ι).*

If $2k - \ell \neq 2$ then the almost twistorial structure of (M, E, i, ∇) is integrable.

Definitions. Let $(M, \mathcal{C})$ be a CR manifold.

1) $(M, \mathcal{C})$ is **realizable** if M is an embedded submanifold, of codimension ℓ, of a complex manifold N such that $\mathcal{C} = T^{\mathbb{C}}M \cap (T^{0,1}N_{|_M})$.

2) $(M, \mathcal{C})$ is **locally realizable** if each point of M has an open neighbourhood U such that $(U, \mathcal{C}_{|_U})$ is realizable.

As a main result of [L], LeBrun proved that *if N is the twistor CR manifold of a smooth conformal Riemannian 3-manifold $(M, c \equiv \{g\})$, then N is embeddable iff M admits a real-analytic atlas for which $c \equiv \{g\}$ is represented by a real analytic metric.* In [M-O-P] a generalization of the LeBrun result to CR quaternionic manifolds was given. Let's first consider the following definition.

Definition. Let $(M, \mathcal{C})$ be a CR manifold, $\dim M = 2k - \ell, \operatorname{rank} \mathcal{C} = k - \ell$. Suppose, further, that $(M, \mathcal{C})$ is endowed with a *conjugation* τ; that is, τ is an involutive CR diffeomorphism from $(M, \mathcal{C})$ onto $(M, \overline{\mathcal{C}})$. We say that $(M, \mathcal{C}, \tau)$ is *realizable* if $(M, \mathcal{C})$ is realizable and τ is the restriction of a conjugation on the corresponding complex manifold.

The following extension of the notion of realizability holds.

Definition. Let (M, E, i, ∇) be a CR quaternionic manifold and let $(\mathcal{Z}, \mathcal{C})$ be its twistor space. Then (M, E, i, ∇) is **realizable** if M is an embedded submanifold of a quaternionic manifold N such that $E = TN_{|_M}$, as quaternionic vector bundles, and $\mathcal{C} = T^{\mathbb{C}}\mathcal{Z} \cap (T^{0,1}\mathcal{Z}_N)_{|_M}$, where $\mathcal{Z}_N$ is the twistor space of N.

Proposition 3. *Let (M, E, i, ∇) be a CR quaternionic manifold and $(\mathcal{Z}, \mathcal{C}, \tau)$ be its twistor space, endowed with the conjugation given, on the fibres of Z, by the antipodal map.*

Then the following assertions are equivalent:

(i) *(M, E, i, ∇) is realizable.*

(ii) *$(\mathcal{Z}, \mathcal{C}, \tau)$ is realizable.*

As corollaries one has the following propositions.

Proposition 4. *Any real analytic CR quaternionic manifold (M, E, i, ∇) is realizable. Moreover the corresponding embedding into a quaternionic manifold is germ unique.*

If (M, E, i, ∇) is a real analytic CR quaternionic manifold one call the corresponding quaternionic manifold the *heaven space* of (M, E, i, ∇).

Proposition 5. *Let (M, E, i, ∇) be a CR quaternionic manifold and let $(\mathcal{Z}, \mathcal{C}, \tau)$ be its twistor space, endowed with the conjugation given, on the fibres of $\mathcal{Z}$, by the antipodal map. If $(\mathcal{Z}, \mathcal{C}, \tau)$ is realizable then (M, E, ι) admits quaternionic connections ∇' such that the twistor space of (M, E, i, ∇') is equal to $(\mathcal{Z}, \mathcal{C})$.*

Acknowledgment

Article corresponding to a talk given at Hypercomplex Seminar 2011, Będlewo. Work done under the programme of G.N.S.A.G.A.-INDAM of C.N.R. and PRIN07 "Geometria Riemanniana e struture differenziabili" of M.I.U.R. (Italy).

References

[Al-K] D. V. Alekseevsky and Y. Kamishima, *Pseudo-conformal quaternionic CR structure on $(4n+3)$-dimensional manifolds*, Ann. Mat. Pura Appl. **187**, (4) (2008), 487–529.

[A-M-P] D. V. Alekseevsky, S. Marchiafava, and M. Pontecorvo, *Compatible complex structures on almost quaternionic manifolds*, Trans. Amer. Math. Soc. **351** (1999), 997–1014.

[Be-Fa] A. Bejancu and H. R. Farran, *On totally umbilical QR-submanifolds of quaternion Kaehlerian manifolds*, Bull. Austral. Math. Soc. **62** (2000), 95–103.

[Bi] O. Biquard, *Métriques d'Einstein asymptotiquement symétriques*, Astérisque **265** (2000), vi+109.

[Bo] E. Bonan, *Sur les G-structures de type quaternionien*, Cahiers Topologie Géom. Différentielle **9** (1967), 389–461.

[I-M-P-O] S. Ianus, S. Marchiafava, R. Pantilie, and L. Ornea, *Twistorial maps between quaternionic manifolds*, Ann. SNS Pisa **IX**, s. V (2010), 47–67.

[H] N.J. Hitchin, *Complex manifolds and Einstein equations*, in: Twistor geometry and non linear systems (Primorsko, 1980), Lecture Notes in Math., Springer Verlag, Berlin 1982, 970.

[L] C. R. LeBrun, *CR manifolds and three-dimensional conformal geometry*, Trans. AMS **284**, no. 2 (1984), 601–616.

[M-O-P] S. Marchiafava, R. Pantilie, and L. Ornea, *Twistor theory for CR quaternionic manifolds and related structures*, Monatsh. Math. (2011) (in print).

[M-P1] S. Marchiafava and R. Pantilie *A note on CR quaternionic manifolds and related structures*, Advances in Geometry (2012), to appear; arXiv:[math.DG] 30Sep2011.

[M-P2] S. Marchiafava and R. Pantilie, *Twistor theory for Co-CR quaternionic manifolds and related structures*, Israel Math. J. (2011), to appear; arXiv:[math.DG] 27Jun2011.

[Ma] E. Martinelli, *Variétés à structure quaternionienne généralisé*, Rev. Roumaine Math. Pures Appl. **10** (1965), 915–922.

[Sal] S. Salamon, *Differential geometry of quaternionic manifolds*, Ann. Sci. École Norm. Sup. **19**, no. 4 (1986), 31–55.

Dipartimento di Matematica
Università di Roma "La Sapienza"
Piazzale A. Moro 2, I-00185 Roma
Italy
e-mail: marchiaf@mat.uniroma1.it

Presented by Julian Ławrynowicz at the Session of the Mathematical-Physical Commission of the Łódź Society of Sciences and Arts on November 24, 2011

TEORIA TWISTORÓW DLA ROZMAITOŚCI CR-KWATERNIONOWYCH: KRYTYCZNY PRZEGLĄD

S t r e s z c z e n i e

Dokonujemy krytycznego przeglądu ostatnich sposobów wprowadzenia pojęcia rozmaitości kwaternionowych ogólności, w kontekście nie-metrycznym oraz pewnych ogólnych wyników podstawowych w ramach odpowiadającej im teorii twistorów ([M-O-P], [M-P1], [MP2]).

PL ISSN 0459-6854

B U L L E T I N

DE LA SOCIÉTÉ DES SCIENCES ET DES LETTRES DE ŁÓDŹ

2012 Vol. LXII

Recherches sur les déformations no. 1

pp. 55–64

In memory of
Professor Roman Stanisław Ingarden

Dimitra Georgakaki and Hariton M. Polatoglou

STUDY AND USE OF NOISE FOR THE AFM CANTILEVER RESPONSE IN TIME AND FREQUENCY DOMAIN

Summary

Many modern nanometrological applications that make use of the Atomic Force Microscope (AFM), demand quantitative force measurements ranging from 1 pN to 100 nN. The main obstacle in the production of traceable nanoforce measurements lies in the various difficulties that arise from the cantilever's spring constant (or stiffness) calibration, at an accuracy that is compatible to each application. In this paper we present a simulation study of the performance of two very common dynamic calibration techniques, the thermal noise method and the Sader's method. The virtual "experimental" data are created from the numerical solution of the equations that describe the AFM system and the vibrating cantilever dynamics, under the approximation of "lumped parameters". As regards the thermal noise method, with the Power Spectral Density of the harmonic oscillator, the parameters $(f, Q,)$ are determined and the stiffness k that corresponds to the lowest frequency, is calculated. Sader's method uses the oscillator's dimensions and behavior in a liquid environment with known properties (density ρ and viscosity η) to calculate k. An attempt is made to compare the performance of the above methods as well as the assumptions that regard the geometry, uniformity and dimensions of the cantilever and the liquid properties. With this study, the role of noise in the cantilever response is stated and carefully investigated.

1. Introduction

In a typical Atomic Force Microscope (AFM) there exist static and dynamic operational modes, according to the behavior of the nanotip attached to the AFM microcantilever. As static operational mode we refer to contact mode, where the tip is placed at a close distance from the sample. The dynamic modes of operation are divided to three different categories according to the distance of the nanotip from

the sample's surface: i) near-contact mode, ii) tapping / intermittent mode and iii) non-contact mode (Mironov 2004). The dynamic modes are used for measurements that demand larger signal to noise ratio and consequently they give better atomical resolution. Technically, dynamic modes treat measurements at a higher frequency level where the $1/f$ noise level becomes weaker (Cook et al. 2006).

Measurements of the nanoforces that are developed between the nanotip and the sample surface, suggest a value of the cantilever elastic constant k, as accurate as possible. Initially, the metrologists were making use of the nominal value of the cantilever stiffness, provided by the manufacturer's specifications of the corresponding commercial cantilever. Unfortunately, this methodology often led to wrong results, as the specifications range was rather broad. Soon, a lot of methodologies have been applied in order to better calibrate the cantilever spring constant.

The dimensional methods (Neumeister and Ducker 1994) are based on the estimation of the geometrical properties of the microcantilever as well as the sample properties. These methodologies provide very good results for rectangular cantilevers but they are not so reliable for V-cantilevers. In the latter case the results can be combined with Finite Element Analysis for better accuracy (Choi and Gethin 2009), but the mathematical problem becomes more complicated. Amongst the static experimental methods we mention here the method of the Reference Cantilever, the method of the Inverted Loaded Cantilever and the Pendulum Method. Detailed studies present the most popular static methods that are used in today's calibration procedures (Palacio and Bhushan 2010, Kim et al 2010). As regards the dynamic methods the most popular ones are: Cleveland method (Cleveland et al 1992), Sader method (Sader 1998) and thermal noise method (Hutter and Bechhoefer 1993).

In this paper we study and compare Sader's method and thermal noise method on virtual mathematical data that we have produced by solving a nonlinear dynamic model. These methods are chosen for inter-comparison because: 1) they both represent non-destructive techniques, 2) they can be applied to all kinds of cantilevers independent of material or coating, 3) they demand minimum infrastructure and 4) they are easy to implement for the user of the Atomic Force Microscope as they do not demand any special training. We also examine how does thermal noise affect the cantilever response.

2. Mathematical methods

2.1. Cantilever's equation

In order to create a time-series of virtual experimental data we must solve the equation of the forced harmonic oscillator with dumping (Sarid 2007)

$$\ddot{x}(t) + \frac{\omega_c}{Q}\dot{x}(t) + \omega_c^2 x(t) = \frac{F_{\text{th}}}{m_{\text{eff}}} \tag{1}$$

where ω_c is the oscillation frequency of the cantilever, Q is the quality factor of the oscillation, F_{th} is the force induced by the thermal oscillations of the cantilever

(thermal noise) and m_{eff} is the cantilever's effective mass. It should be noted here that F_{th} is a parameter that we introduce to the AFM system and we choose it according to the thermal noise strength that we wish to impose to the system. Some F_{th} values are presented in the Results Section of this paper and their effect on the AFM system is analyzed. By applying a Fourier Transform on the time-series $x(t)$ we get the Power Spectral Density (PSD). In this theoretical spectrum we will try to fit the mathematical model of the thermal noise and calculate the free parameters ω_c and Q. The final goal is to calculate the spring constant k and compare this value with that estimated from Sader's method.

2.2. Thermal noise

The thermal noise method (Hutter and Bechhoefer 1993), is based on the equipartition energy theorem. According to this theorem, for each general coordinate X which stores energy according to the relation $E_x \sim X^2$, we have that $\widehat{E_x} = \frac{1}{2}k_BT$. In our case as X we have the cantilever displacement x under the thermal force, which stores energy $\frac{1}{2}k\left\langle x^2\right\rangle$, where $\left\langle x^2\right\rangle$ represents the mean value of the cantilever displacement in the time interval that we study the system's motion. Consequently we have for the elastic constant k

$$k = k_BT/\left\langle x^2\right\rangle. \tag{2}$$

The thermal noise theory is based on three assumptions: (1) The dimension l of the cantilever's nanotip is much smaller than the dimension L of the cantilever, (2) the cantilever is treated as a homogeneous medium, (3) the cantilever's motion is examined in vacuum or air. In order to formulate a mathematical model for the calculation of the cantilever's displacement as a function of frequency we follow a certain procedure: Initially we consider the displacement as a time-series $x(t)$ and we apply a Fourier transform to equation (1) in order to reformulate the problem to the frequency domain:

$$|x(\omega)|^2 = \frac{|F_{\text{th}}(\omega)|^2}{m_{\text{eff}}^2((\omega_c^2-\omega^2)^2+(\frac{\omega_c}{Q})^2\omega^2)}. \tag{3}$$

Then we calculate the Power Spectral Density $\text{PSD}(x,w)$ and by combining the result with equation (2) we conclude to a mathematical model that relates the response of the system in time with the response in frequency domain

$$PSD(x,\omega) = \frac{2k_BT}{\pi m_{\text{eff}}}\frac{\omega_c/\text{Q}}{(\omega_c^2-\omega^2)^2+(\frac{\omega_c}{Q})^2\omega^2} \tag{4}$$

$$PSD(x,\text{f}) = \frac{2k_BT}{\pi m_{\text{eff}}}\frac{\frac{2\pi f_c}{16Q\pi^4}}{(f_c^2-f^2)^2+(\frac{f_c}{Q})^2f^2} \tag{5}$$

Our final expression is simplified to the following form

$$PSD(x,\text{f}) = \text{norm}\frac{A_{\text{factor}}}{(B_{\text{factor}}^2-f^2)^2+A_{\text{factor}}^2f^2} \tag{6}$$

with A_{factor}, B_{factor}, norm the free parameters for the fitting of the model to the virtual data created in section 2.1 by solving cantilever's equation.

2.3. Sader's method

The Sader method (Sader 1995, 1998) is based on the general theory of a cantilever that is immersed to a viscous fluid and is excited by an external driving force. In order to formulate a mathematical model that describes the dynamical behavior of the cantilever we make the following assumptions: (1) The cross section of the cantilever is uniform, (2) the length L of the cantilever is much larger than its width b, (3) the cantilever is an isotropic elastic medium thus the phenomena of the internal viscosity are neglected, (4) the oscillation amplitude is much smaller than any geometrical dimension (length L, width b, thickness h).

Considering our system as a continuous medium we can observe two different forces that act on the cantilever: the hydrodynamic force F_{hydro} arising from the motion of the fluid around the cantilever (in our case the fluid is the air) and the driving force F_{drive} which excites the cantilever. For the estimation of F_{hydro}, Sader introduced the hydrodynamic function $\Gamma(\omega)$ which he later used as a correction factor for the estimation of the elastic constant k. We must therefore find analytical expressions for the hydrodynamic functions of cantilevers with circular and rectangular cross sections. For a cylindrical cantilever the function $\Gamma(\omega)$ is well defined in literature and is given by the following equations

$$\Gamma_{\text{circ}}(\omega) = 1 + \frac{4iK_1(-i\sqrt{i\text{Re}})}{\sqrt{i\text{Re}}K_0(-i\sqrt{i\text{Re}})} \tag{7}$$

where Re is Reynolds number, ϱ the fluid density, η the fluid viscosity and the functions K_0, K_1 represent modified Bessel functions of third kind.

As regards the rectangular cantilever, Sader suggested a correction function $\Omega(\omega)$ (Sader 1995, 1998), such as $\Gamma_{\text{rect}}(\omega) = \Omega(\omega)\Gamma_{\text{circ}}(\omega)$. The function $\Omega(\omega)$ is complex and the real as well as the imaginary part is a sum of polynomial terms in the power of τ, where τ=logRe. Analytical expressions are given by Sader (Sadder 1998). Having now estimated the hydrodynamic function $\Gamma_{\text{rect}}(\omega)$, we must come to an expression for the elastic constant, which will include the corrections for the calibration, due to the transition of the cantilever properties from vacuum to air.

More specifically the relation of the cantilever oscillation in vacuum with the oscillation in air is given by the following equations

$$\omega_{\text{vacuum}} = \omega_{\text{air}}(1 + \frac{\pi\rho_{\text{air}}b}{4\rho_{\text{cant}}h})Real[\Gamma(\omega_{\text{air}})], \tag{8}$$

$$\rho_{\text{cant}}h = \frac{\pi\rho_{\text{air}}b}{4}(Q_{\text{air}}\Im[\Gamma(\omega_{\text{air}})]. - Real[\Gamma(\omega_{\text{air}})]). \tag{9}$$

Combining equations (9) and (10) with the general equation

$$k = m_{\text{eff}}\rho_{\text{cant}}hbL\omega^2_{\text{vacuum}}$$

we have the final equation for the calibration of the constant k

$$k = 0.1906\rho_{\text{air}} b^2 L Q_{\text{air}} \omega_{\text{air}}^2 Im[\Gamma(\omega_{\text{air}})]. \tag{10}$$

3. Results

The cantilever that is about to be calibrated is a RTESPA-CP model with serial code MPP-11123-10. It is made of silicon with n-type doping of antimony. It also has a coating of 50 nm thickness. The cantilever's dimensions are: length $L = 125\,\mu$m, width $b = 35\,\mu$m and thickness $h = 3.75\,\mu$m. The Bruker company gives nominal value ranges for the oscillation frequency as well as the elastic constant of the cantilever which are $f_0 = 305 - 349\,$KHz and $k = 20 - 80\,$N/m respectively. The parameters used in the simulation are presented in Table I.

Table I. All the parameters used in the numerical procedure.

Cantilever parameters	Air parameters	Secondary parameters
$L = 125\ \mu$m	$\eta = 1.8610^{-5}$kg/ms	$I = bh^3/12$
$b = 35\ \mu$m	$\rho_{\text{air}} = 1.18\,\text{kg/m}^3$	$k = 3EI/L^3$
$h = 3.75\ \mu$m		$m_{\text{eff}} = 0.2427Lbh\varrho$
$\rho_{\text{cant}} = 2330$ kg/m3		$f_0 = \sqrt{(k/m_{\text{eff}})}$
$E = 169.5{\cdot}10^9$ Pa		$\omega_0 = 2\pi f_0$
		$\text{Re} = \rho_{\text{air}}\omega b^2/4\eta$

The steps of the algorithmic procedure that we use in order to estimate the elastic constant k are presented in Fig. 1:

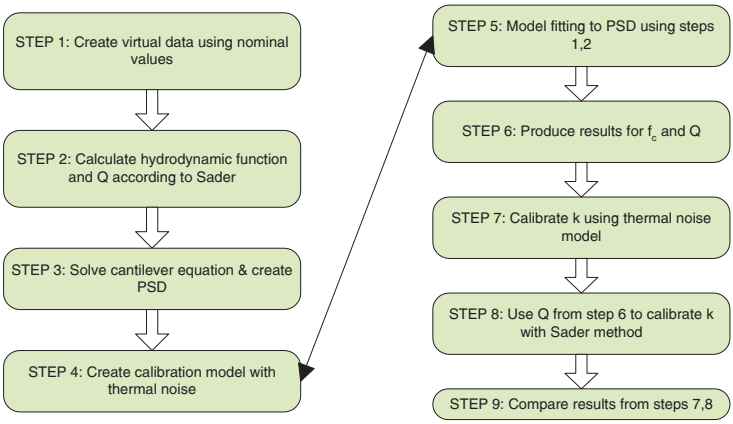

Fig. 1: Steps of the calibration procedure.

The theoretical value for k is calculated from the relation $k = \frac{3EI}{L^3}$ and for the given parameters from Table I we have $k = 40.04\,\mathrm{N/m}$. The theoretical value for the oscillation frequency is given from

$$f_0 = \sqrt{\frac{k}{m_{\mathrm{eff}}}}$$

and thus $f_0 = 330\,\mathrm{KHz}$. It is observed from the above that the values of elastic constant and oscillation frequency are between the nominal ranges provided by the specifications. As regards the quality factor Q we can use the equation provided by Sader and find that $Q = Q_{\mathrm{air}} = 143.494$:

$$Q = \frac{(4m_{\mathrm{eff}}/\pi\rho_{\mathrm{air}}b^2) + Real[\Gamma(\omega_0)]}{\Im[\Gamma(\omega_0)]}. \tag{11}$$

For the numerical solution of the cantilever equation of motion we must be very careful about the initial conditions that we will choose because of the nonlinearity of the problem. According to Hutter (Hutter 1993) the thermal fluctuations of the cantilever are some Angstroms at room temperature so for that reason we expect changes at that order of magnitude at the graphs of displacement vs time.

In the following figures we can observe various cases of time series of displacement and power spectral densities for different levels of thermal noise at a logarithmic rate. The noise levels are chosen such as $kx(t) \geqq F_{\mathrm{th}}$ from Eq. 1:

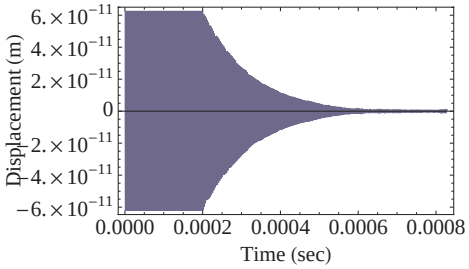

Fig. 2: Time series with $F_{\mathrm{th}} = 10^{-8}N$.

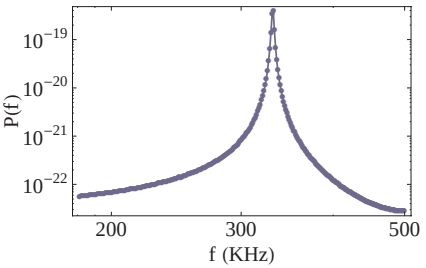

Fig. 3: Power spectrum with $F_{\mathrm{th}} = 10^{-8}N$.

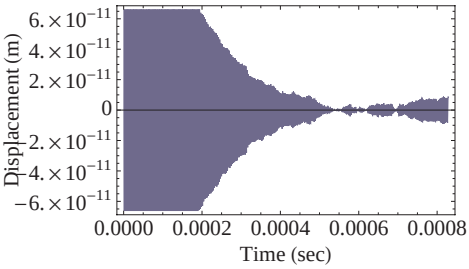

Fig. 4: Time series with $F_{\mathrm{th}} = 10^{-7}N$.

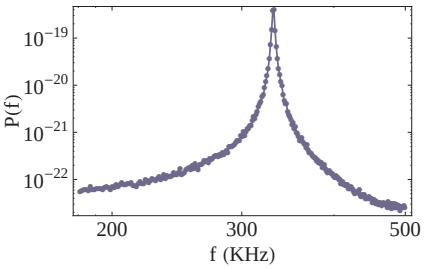

Fig. 5: Power spectrum with $F_{\mathrm{th}} = 10^{-7}N$.

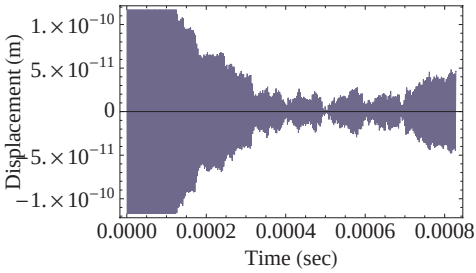

Fig. 6: Time series with $F_{\text{th}} = 510^{-7}N$.

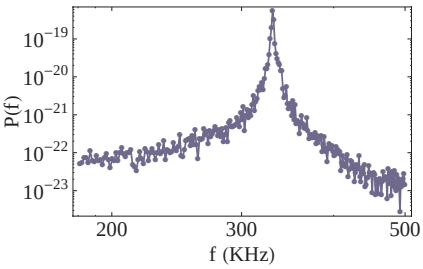

Fig. 7: Power spectrum with $F_{\text{th}} = 510^{-7}N$.

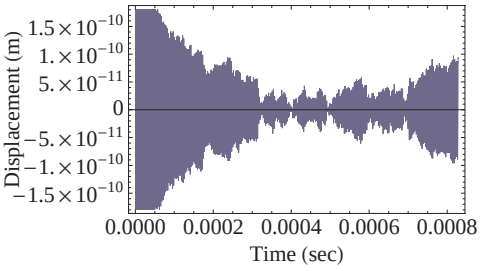

Fig. 8: Time series with $F_{\text{th}} = 10^{-6}N$.

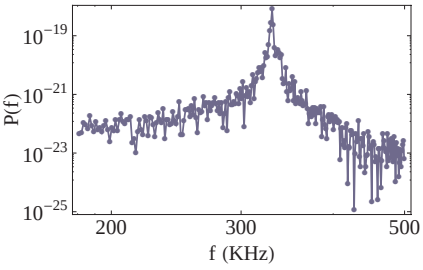

Fig. 9: Power spectrum with $F_{\text{th}} = 10^{-6}N$.

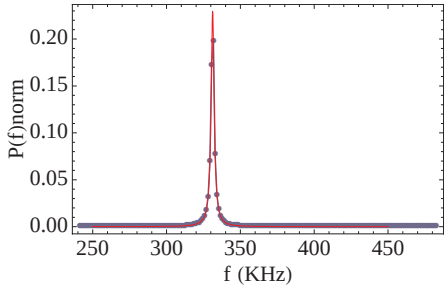

Fig. 10: Fitting with $F_{\text{th}} = 10^{-8}N$.

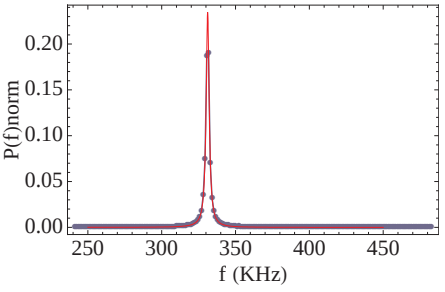

Fig. 11: Fitting with $F_{\text{th}} = 10^{-7}N$.

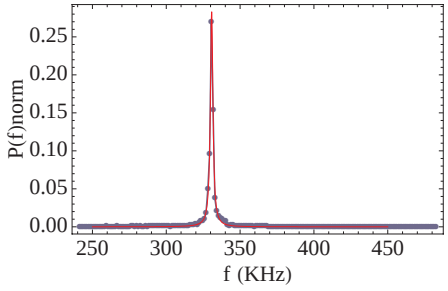

Fig. 12: Fitting with $F_{\text{th}} = 510^{-7}N$.

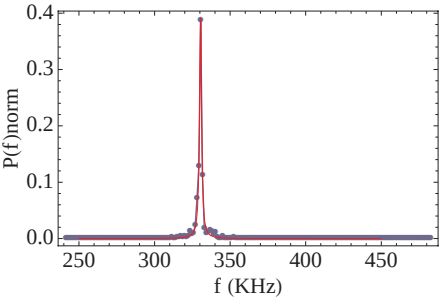

Fig. 13: Fitting with $F_{\text{th}} = 10^{-6}N$.

We observe that for even strong noise levels the peak that corresponds to the natural cantilever frequency can easily be distinguished. For every noise level we well proceed similarly and try to fit the models produced form equations 5, 6 to the PSDs that we have created earlier. The results of these fittings are presented in the following figures and the results for the fitting parameters are shown in Table II:

Table II. Parameters estimation with the thermal noise method and comparison with theory.

$F_{\rm th}$	$f_{\rm theor}$	$Q_{\rm theor}$	$k_{\rm theor}$	f_0	Q	$k_{\rm thermal}$
10^{-8}	330	143.494	40.04	331.229	134.511	31.9
10^{-7}	330	143.494	40.04	331.13	136.556	31.6565
510^{-7}	330	143.494	40.04	330.748	159.973	30.7272
10^{-6}	330	143.494	40.04	330.435	202.989	28.209

It is worth mentioning that for strong noise levels more points appear to the spectrum and that results to an overestimation of the quality factor Q and a simultaneous underestimation of the elastic constant k. Having estimated with this nonlinear fittings presented in figures $10-13$ the parameters Q and ω_0 and knowing the dimensions of the cantilever, we apply equations $8-10$ and calculate $k_{\rm Sader}$. The results from both methods are summarized in Table III and are compared with the theoretical ones. We observe that when we calculate the elastic constant using the parameters directly from thermal noise method we must also be very careful with the noise level as we may be led to an overestimation of k with Sader method. The difference% between these methodologies is given from (Cook 2006) as $\delta\% = 100(k_{\rm th} - k_{\rm Sader})/0.5(k_{\rm th} + k_{\rm Sader})$. It should be noted that in the final case of Table III, the noise level causes a difference of about 50% between $k_{\rm Sader}$ and $k_{\rm th}$ and therefore the calibration results are not to be trusted in that region.

Table III. Stiffness estimation with Sader method, comparison with thermal noise and theory.

$F_{\rm th}$	$k_{\rm th}$	$k_{\rm Sader}$ (before th. noise fit)	$k_{\rm Sader}$ (after th. noise fit)	$k_{\rm theor}$	$\delta\%$
10^{-8}	31.9	31.6437	29.8679	40.04	6.58
10^{-7}	31.6565	31.6437	30.3052	40.04	4.36
510^{-7}	30.7272	31.6437	35.4261	40.04	-14.2
10^{-6}	28.209	31.6437	44.8733	40.04	-45.6

4. Conclusions

The main purpose of this work is the presentation and comparative study of two very popular methods that we encounter in mechanical metrology of a calibration of an Atomic Force Cantilever. With the thermal noise method we have produced

a mathematical model with the aid of which we can obtain the lowest oscillation frequency and the oscillation quality factor. Then these parameters were used for the calculation of k_{th} and k_{Sader}. The results were compared with each other as well as with the results provided by literature for this specific type of cantilever. It has been shown that if we do not choose the noise level properly we can be driven to an underestimation or overestimation of the k constant. In a real AFM experiment this noise level is determined from the vertical position of the cantilever tip above the sample surface. In every other case with a proper noise level these two methods give corresponding results.

Acknowledgment

This research has been co-financed by the European Union (European Social Fund – ESF) and Greek national funds through the Operational Program "Education and Lifelong Learning" of the National Strategic Reference Framework (NSRF) – Research Funding Program: Heracleitus II. Investing in knowledge society through the European Social Fund.

References

[1] V. L. Mironov, *Fundamentals of Scanning Probe Microscopy*, Nizhniy Novgorod 2004.

[2] S. M. Cook, et al., *Practical implementation of dynamic methods for measuring atomic force microscope cantilever spring constants*, Nanotechnology **17** (2006), 2135–2145.

[3] J. M. Neumeister and W. A. Ducker, *Lateral, normal, and longitudinal spring constants of atomic force microscopy cantilevers*, Rev. Sci. Instrum. **65**, no. 8 (1994), 2527–2531.

[4] J. L. Choi and D. T. Gethin, *Simulation of atomic force microscopy operation via three-dimensional finite element modeling*, Nanotechnology **20** (2009), 14.

[5] M. L. Palacio and B. Bhushan, *Normal and Lateral Force Calibration Techniques for AFM Cantilevers*, Critical Reviews in Solid State and Materials Sciences **35** (2010), 73–104.

[6] M.-S. Kim, et al, *Accurate determination of spring constant of atomic force microscope cantilevers and comparison with other methods*, Measurement **43** (2010), 520–526.

[7] J. P. Cleveland and S. Manne, *A nondestructive method for determining the spring constant of cantilevers for scanning force microscopy*, Rev. Sci. Instrum. **64**, no. 2 (1993), 403–405.

[8] J. E. Sader, *Frequency response of cantilever beams immersed in viscous fluids with applications to the atomic force microscope*, Journal of Applied Physics **84**, no. 1 (1998), 64–73.

[9] J. L. Hutter and J. Bechhoefer, *Calibration of atomic-force microscope tips*, Rev. Sci. Instrum. **64** no. 7 (1993) 1868–1873.

[10] D. Sarid, *Exploring Scanning Probe Microscopy with Mathematica*, Wiley, 2007.

[11] J. E. Sader, et al, *Method for the calibration of atomic force microscope cantilevers*, Rev. Sci. Instrum. **66** no. 7 (1995), 3789–3798.

[12] J. E. Sader, *Calibration of rectangular atomic force microscope cantilevers*, Review of Scientific Instruments **70** no. 10 (1999), 3967–3969.

Physics Department
Solid State Physics Section
Aristotle University of Thessaloniki
Gr-54124 Thessaloniki
Greece

Presented by Ilona Zasada at the Session of the Mathematical-Physical Commission of the Łódź Society of Sciences and Arts on October 27, 2012

STUDIUM I OPIS ZASTOSOWANIA SZMERÓW W REAKCJACH WSPORNIKÓW MIKROSKOPU SIŁ ATOMOWYCH (AFM) W OBSZARZE CZASU I CZĘSTOŚCI

S t r e s z c z e n i e

Szereg nowoczesnych zastosowań nanometrologicznych związanych z użyciem mikroskopu sił atomowych wymaga pomiarów ilościowych siły w zakresie od 1 pN do 100 nN. Główną trudnością w prowadzeniu pomiarów nanosił są problemy powstające w związku z kalibracją stałej wygięcia wspornika (tj. sztywności) z dokładnością zadawalającą w danym zastosowaniu. W pracy przedstawiamy symulacje dwóch powszechnie używanych technik kalibracji: metody termicznego szmeru i metody Sadera. Zbiór danych "eksperymentalnych" utworzony jest z rozwiązań numerycznych układów równań opisujących układ mikroskopu sił atomowych i dynamikę drgań wspornika w przybliżeniu "parametrów scalonych". W modelu termicznego szmeru z gęstością mocy widmowej oscylatora harmonicznego, wyznaczone są parametry (f, Q) i obliczona sztywność k odpowiadająca najniższej częstości. Metoda Sadera uwzględnia wymiary oscylatora i jego zachowanie się w otoczeniu cieczy o znanych własnościach (gęstości ρ i lepkości η) do obliczenia sztywności k. Przedstawiono próbę porównania wydajności powyższych metod oraz założeń dotyczących geometrii, jednorodności i wymiarów wspornika jak i własności cieczy. Na podstawie przedstawionych badań sformułowano i starnnie zbadano rolę szumu w reakcji wspornika mikroskopu.

PL ISSN 0459-6854

B U L L E T I N

DE LA SOCIÉTÉ DES SCIENCES ET DES LETTRES DE ŁÓDŹ

2012 Vol. LXII

Recherches sur les déformations no. 1

pp. 65–78

In memory of
Professor Hans Grauert

Stanisław Bednarek

NEW CONSTRUCTIONS OF MAGNETOHYDRODYNAMIC DRIVES WITH INTERNAL POWER SOURCES

Summary

This article refers to magnetohydrodynamic drives which create electric current necessary for their operation on themselves. It happens thanks to transformation of the electrodes chemical energy and the electrolyte into electric energy. There are two models of rotational drives of such a type described. In one of them the electrolyte rotates and, besides, in the second one there are also electrodes rotating in a reverse direction. There are three models of linear induction motors presented with moving electrolyte. These are engines comprising: electrodes that are permanently joined with magnets, changeable sets of electrodes and a series of bars instead of magnets. There are technical clues presented that refer to the construction of those engines and a detailed explanation of their operation. Every engine described in this article is an original solution of the author. At the end, there is a short discussion about possibilities of practical application of such engines.

1. Introduction

In literature, regarding experiments with physics, there is a following experiment described. Round glass vessel with a flat bottom and low walls, so called crystallizer, is placed on a graphic display unit. There are two copper electrodes placed in the vessel, which are coaxial towards each other and towards themselves. Electrolyte-water solution of copper sulfate – was poured into the vessel filling the space between the electrodes. There was also a flat ring winding that surrounded the vessel placed on the graphical display unit. The electrodes and coil tips were attached to the sources of direct current. In the presented scheme, the electric current flows through the electrolyte in a radial direction, and this electrolyte is in magnetic field created

by a coil. Electric displacement of this field is vertical, i.e. perpendicular towards the direction of the current flow. In the presented situation, electrodynamics force, directed horizontally and contacting the electrodes, influences the electrolyte. This force gives a moment regarding the vessel's axis, which triggers a rotary movement of the electrolyte. If we increase the current intensity, flowing through the coil or the electrolyte, there will be an increase in the rotary movement speed [1, 2].

The described system is a demo model of magnetohydrodynamic drive. (Magnetohydrodynamics is a branch of physics researching influence of magnetic fields on liquids or gases placed inside them, which conduct electric current). It is a rotational engine because the liquid rotates. This engine is supplied from the external power sources. In the well-known American physics magazine, there are descriptions of magnetohydrodynamic drives prepared by the author of this article. Those drives do not demand electric power supply from the external sources [3]. Electrodes created from two different metals, with different positions within electrochemical series, immersed in the electrolyte with a chemical composition adequately adjusted to the electrodes' material, were used in case of those engines. As a result there is a electromotor force created between those electrodes, which causes a flow of electric current necessary for operation of these engines. Power source is in this case placed inside the drive, which is why they are called drives with the external power source. Aim of this presentation is to present a construction and operation of several models of magnetohydrodynamic drives, using the mentioned idea.

2. Rotational drive with immovable electrodes

A set of coaxial, cylindrical electrodes was put into a glass, cylindrical, opened from the top vessel 1, with a diameter of 10 cm an a height of 5 cm, Fig. 1. This set comprises an external electrode 2, created from a 1 mm copper sheet and an internal galvanized electrode 3. The galvanized electrode should be prepared from a 2–3 mm galvanized sheet or from a galvanized bar. Diameter of the copper electrode is slightly smaller from the vessel's diameter, and the galvanized electrode's diameter should be 4 times smaller than that of the copper electrode. Both electrodes are connected with a ring cut out from a 2 mm copper or brazen sheet which provides their good electric contact.

The upper part of the ring, between the electrodes, and the external surface of the copper electrode, as well as the lower and side surface of the ring are covered with an electro insulating coating, resistant to caustics, e.g. covered with a previously melted paraffin. This coating prevents from stray currents flowing. The space between the electrodes is filled with water solution 5 of sulfurous acid of 10 % concentration or with saturated solution of domestic salt in water. The described vessel was placed on the upper part of a cylindrical neodymium magnet 6 with a diameter similar to that of the vessel's diameter and height of 6 cm. Induction value of the field generated by this magnet in half of the electrolyte column in the vessel should be around 0.15 T or

more. A system of several, radially located thick bars, made from non-ferromagnetic metal, favorably from copper, can be used instead the ring to join the electrodes. Such a drive is presented in Photo 1.

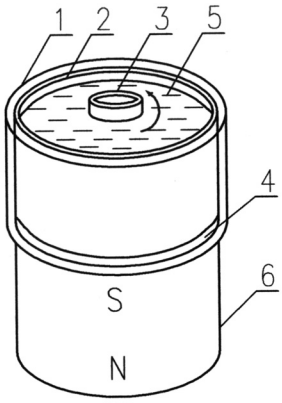

Fig. 1: Structure of a rotary drive with immovable electrodes; 1 – glass vessel, 2 – external electrode, 3 – internal electrode, 4 – a ring comprising the electrodes, 5 – electrolyte, 6 – neodymium magnet.

Photo 1: Plan of the rotary drive, where electrodes are joined with magnets.

The system of electrodes together with acid or salt solution creates a galvanic cell. In case of sulfurous acid solution it is a Volta cell giving an electromotor force of about 1 V. This cell was connected from the bottom with a metal ring, and under the influence of electromotor power, current flows through that ring, and through the electrolyte in a radial direction, Fig. 2. Copper electrode has a higher potential than the galvanized one which is why the conventional direction of current flow through the electrolyte is from zinc to copper, i.e. reversed than in the case of the ring comprising the electrodes, which creates an external circuit of the cell. The electrolyte is in the electromagnetic field, whose electric displacement is approximately vertical. As a result, an electrodynamics power influences the electrolyte. It contacts with electrodes' surface causing a rotary movement of the electrolyte.

If the density of the current intensity in the electrolyte is j, and value of the component of the vertical electric displacement of the magnetic field equals B, density of the electrodynamics force f (i.e. a force influencing the element of electrolyte volume) is expressed by the following formula

$$f = jB. \tag{1}$$

Reversing the magnet, causing its poles to swap, results in reversing the rotation direction of the electrolyte. With the given parameters of the system, sped of the rotation is so big that the surface of the electrolyte becomes a paraboloid and

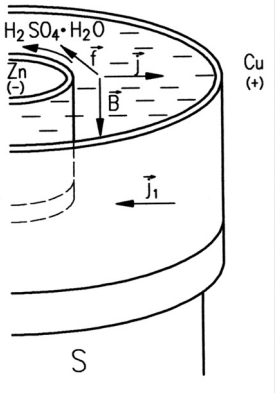

Fig. 2: Explanation of the cause of a rotary movement of the electrolyte in the rotary drive; **j** – current density in electrolyte, **B** – vertical component of magnetic displacement, **f** – density of electrodynamics force, $\mathbf{j}_1$ – current density In a ring comprising the electrodes.

movement is greatly visible. Rotation speed becomes higher when water solution of sulfate acid is used as electrolyte. With a smaller value of field induction, e.g. when we use a ferrite magnet, rotation speed will be lower, and in order to enhance its visibility, the electrolyte surface can be sprinkled with cork filling or ground pepper.

It is also possible to use an external galvanized electrode and an internal copper electrode which causes reversal of current direction within electrolyte. However, it need to be remembered that the electrode should be made of thicker sheet, as it is melted during the drive operation. Good results were also obtained with other materials of electrodes and electrolyte. Among others. The internal electrode was made from a carbon bar, coming from a battery or from an electrode coming from an arc lamp, and the external electrode from a galvanized sheet and water solution of ammonium chloride (salt ammoniac) was used as electrolyte. In the electrodes system copper-zinc, 5 % water solution of acetic acid, i.e. vinegar, was used as electrolyte.

It is also possible to place the magnet in a different position. Instead of a thick, cylindrical magnet laying under the vessel, relatively thin cylindrical magnet was used. It was put into the internal electrode, which was shaped cylindrically with an adequate diameter. Engine of such a construction is presented in Photo 2. Another construction of a drive where electrolyte rotates in reverse directions in different spaces between the electrodes, is shown in the Photo 3. In this drive, a flat, glass vessel was used, so called Petri dish, filled with electrolyte. Two low, coaxial electrodes were immersed in the electrolyte – a zinc and a copper one, connected along the diameter with an insulated copper belt. The vessel was placed on a ring magnet, with diameters allowing to divide the electrolyte into three sections. First is the middle area above the magnet. There are also two side sections – one between the external surface of the magnet and the external electrode, and the second one between the internal surface of the magnet and the internal electrode.

Photo 2: Look of the magnetohydrodynamic drive with a magnet placed in an external electrode.

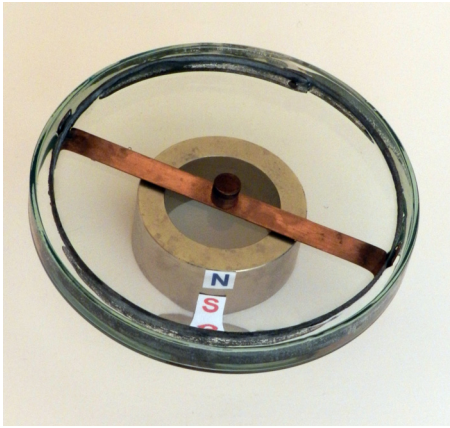

Photo 3: General view of the magnetohydrodynamic drive with electrolyte rotating in opposite directions.

Electrodynamics force, driving the electrolyte, is created in this engine, similarly to the previous case. However, as a result of the fact that a sense of magnetic induction in side areas is reversed towards the middle area, the electrolyte in the middle area rotates in the reversed direction towards the remaining sections. Operation of this engine allows to make a conclusion about a space distribution of magnetic field's lines, around the ring magnet.

3. A drive with rotating electrodes

On the bottom of a glass vessel 1, similar to that of the previous experiment, but with the height of 10 cm, there is a stand 2, made from non-ferromagnetic and electro insulating material, Fig. 3. In the middle of the stand there is a vertical axle 3, tipped with a blade. A conical bearing mounting 4 in a shape of a flat cylinder is placed on the blade. This bearing was placed coaxially in a hub 5, with a shape of a disk. Axle, bearing and the hub are made from non-ferromagnetic materials, where the hub is also an electric insulator. In the created model, the axle and the bearing are made from brass, and the hub is made from textolite. The axle was 9 cm long, and the hub's diameter was 1.8 cm.

Two pairs of electrodes 6, 7 are fixed to the hub on the opposite sides, in the shape of belts that are 1.5 cm wide, bent at 90 degrees, made from zinc and copper. The galvanized electrodes 6 are placed on the axle's side, and copper electrodes 7 are placed on the external side. Vertical sections of the electrodes are 8 cm long, and horizontal ones' length is 4 cm. The exact length of the horizontal sections needs to be adjusted to the internal diameter of the vessel. Thickness of the copper electrodes is 1 mm, and thickness of the copper ones should be higher. The vertical sections of

the electrodes were cleaned to metallic gloss, pressed together, fixed to the hub with small screws made from non-ferromagnetic material.

Both pairs of electrodes consisting of the zinc and copper belt are insulated from each other by the hub's material. Surfaces of the electrodes, turned externally, are covered with electro insulating coating, resistant to caustics, e.g. covered with earlier melted paraffin. Similarly with the previous experiment, the vessel is filled with electrolyte 8, favorably 10 % water solution of sulfurous acid. The described vessel was placed on a flat surface of the cylindrical neodymium magnet 9, creating, in the half of the electrolyte column height, field with induction of about 0.15 T or higher.

Electrode pairs made from different metals immersed in electrolyte are galvanic cells. Because of the electromotor forces created by them, the current flows in radial direction, Fig. 4. In the space between the electrodes, this flow takes place from zinc to copper, and in vertical electrodes sections connected with each other this flow is reversed. Both electrolyte between the electrodes and vertical sections of the electrodes are placed within a magnetic field, whose electric displacement is approximately turned vertically, i.e. perpendicularly towards the direction of the current flow. As a result, the electrolyte and the vertical sections of the electrodes are influenced by electrodynamics forces, turned in the opposite directions and creating pairs of forces. Moment of these forces influencing the electrodes causes their rotation in one direction, and forces influencing the electrolyte turn it in the opposite side.

Similarly to the previously described drive, swapping the magnet poles changes the directions of electrodes and electrolyte movements into the opposite ones. It is also possible to place zinc electrodes on the external side, and the copper ones on

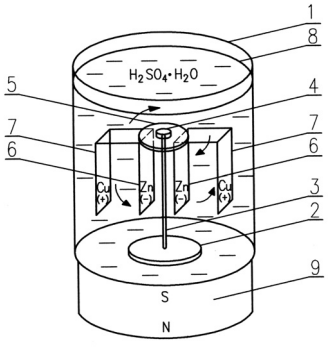

Fig. 3: Structure of a drive with rotating electrodes; 1 – glass vessel, 2 – stand, 3 – axle, 4 – bearing, 5 – hub, 6 – internal electrode, 7 – external electrode, 8 – electrolyte, 9 – neodymium magnet.

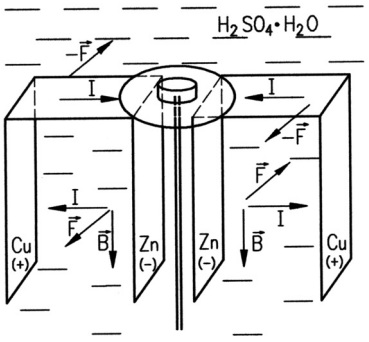

Fig. 4: Explanation of a principle of the drive with rotating electrodes operation; I – current density, **B** – vertical component of induction of a magnetic field; **F**– electrodynamics force.

the internal side. The same remarks as previously are connected with using different materials for electrodes, and different electrolytes. Photo 4 shows an example of the constructed magnetohydrodynamic drive with rotating electrodes.

In this case the electrodes are joined in the upper part. Photo 5 presents a rotor of this engine. It is also possible to construct a similar drive whose electrodes are joined in its lower part. Photo 6 presents a general structure of this drive, and Photo 7 shows a structure of a rotor used in this engine.

Photo 4: View from the magnetohydrodynamic drive with rotating electrodes, joined in the upper part.

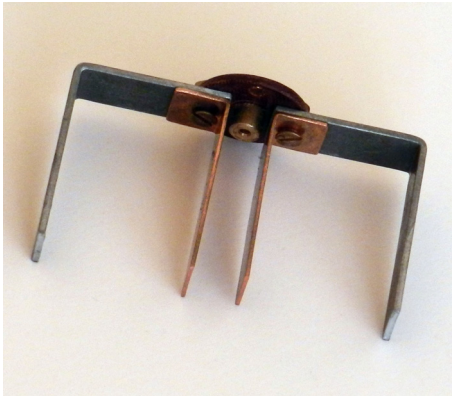

Photo 5: Rotor of the magnetohydrodynamic drive with electrodes joined in the upper part.

Photo 6: View from the magnetohydrodynamic drive with rotating electrodes, joined in the lower part.

Photo 7: Rotor of the magnetohydrodynamic drive with electrodes joined in the lower part.

4. Linear drive with magnets

Dimensions of the two rectangular electrodes 1 and 2 are 8×5 cm. They are placed perpendicularly towards each other in vertical planes, Fig. 5. The distance between them is 2 cm. electrode 1 is made from 2 mm zinc sheet, and electrode 2 from 1 mm copper sheet. At bottom edges, the electrodes are soldered with armature in the shape of a 2 mm copper belt 3 placed between them, which provides good electric contact. At their top edges, there is an insulating spacing board 4 with the same dimensions as those of the armature placed between them. A thin insulating separator 5 is glued to this board, slightly wider than it, thanks to which the board covers the upper edges of the electrodes. Two cuboidal neodymium magnets 6, 7 are glued to the armature and the board, facing each other with opposite poles. Their magnetization direction is vertical, and value of the induction of the field created in the half of height of the area between the electrodes is 0.15 T.

Cyanoacrylate glue was used for all glued connections of the drive elements. Except the internal surfaces of electrodes facing each other, all other surfaces of the drive were covered with electro insulating coating, resistant to caustics. The described system of electrodes was put into a glass, cylindrical vessel with 20 cm in diameter and 8 cm of height – so called crystallizer. Distances of the electrodes from the vessel's wall should be approximately the same. The same electrolyte as in the case of the previously presented drives was poured to the vessel. The upper surface of the electrolyte is placed several mm below the upper edge of the electrodes.

Similarly to the previously described drives, electromotor force is created between the electrodes. It causes the electric current to flow through the armature and the electrolyte placed between the electrodes, Fig. 6. Direction of the current flow in the electrolyte is perpendicular towards the surface of the electrodes, and the current flows from the zinc to the copper electrode. The electrolyte is placed in almost homogenous magnetic fields, generated by a system of magnets. Magnetic displacement of this field has a vertical direction. As a result, an electrodynamics force influences the electrolyte, directed horizontally, along the electrodes. This force cause the flow of the electrolyte from one side of the area between the electrodes. In order to make the electrolyte movement more visible, its surface may be sprinkled with cork filling or ground pepper.

Together with electrodynamics force, there is a reaction force influencing the system of electrodes and magnets. If those elements were fixed to a water craft, the engine would serve as a drive, under the condition that the reaction force was able to fight the resistance to motion. Regarding the fact that the magnets are glued permanently to the system of electrodes, the electrolyte flow will always happen from the same side. In case of this engine there is also no possibility to exchange the zinc plate which melts with the flow of time. The speed of the electrolyte flow can be enhanced by putting additional magnets on the previously glued ones. It needs to be remembered about keeping the same orientation of the added magnets' poles. Increasing the electrodes' surface and decreasing the distance between them also cause

a faster movement of electrolyte. Linear magnetohydrodynamic drive constructed according to the described concept, placed vertically in a vessel is presented in the Photo 8.

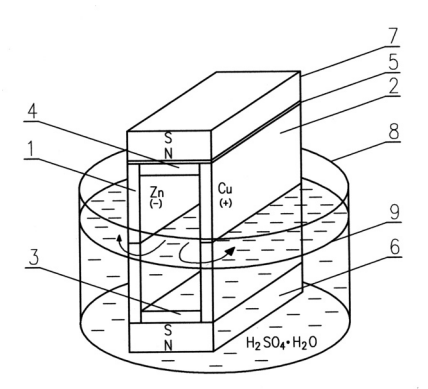

Fig. 5: Structure of a linear drive with magnets; 1 – zinc electrode, 2 – copper electrode, 3 – armature, 4 – spacing board, 5 – insulating separator, 6, 7 – neodymium magnets, 8 – glass vessel, 9 – electrolyte.

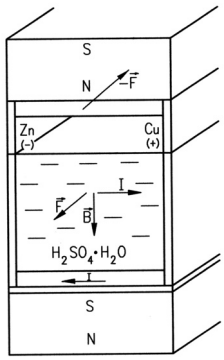

Fig. 6: Explanation of a principle of operation of the linear drive with magnets; I – current intensity, **B** – magnetic field induction, **F** – electro dynamic force, **F** – reaction force.

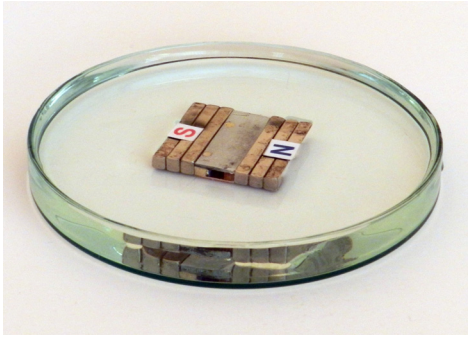

Photo 8: An example of structure of a magnetohydrodynamic linear drive.

5. Linear drive with exchangeable electrodes

Removal of the limitations present in the previously described model is enabled by the a drive with exchangeable electrodes, whose construction, from the electrolyte flow angle is shown in the Fig. 7. Zinc 1 and copper 2 electrodes have the same dimensions as in the case of linear drive, and the distance between them is also the same. There are two identical sets of electrodes, turned with the electrodes

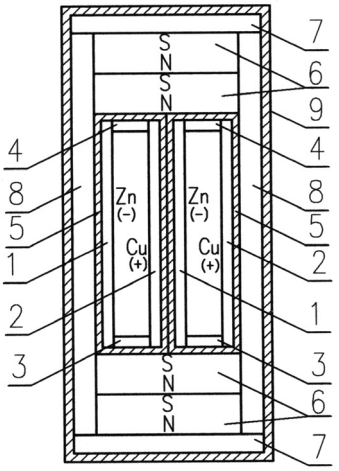

Fig. 7: Structure of a linear drive with exchangeable electrodes; 1 – zinc electrode, 2 – copper electrode, 3 – armature, 4 – spacing board, 5 – electro insulating layer of the electrodes, 6 – neodymium magnet, 7 – plates covering the magnets, 8 – plates joining the magnets, 9 – electro insulating layer of the magnetic core.

of the same material in the same direction which causes an increase in this drive power. It is also a possibility to use a bigger number of identically turned sets of electrodes. Electrodes in each set are joined by armatures 3 soldered from the bottom, mad from copper sheet. From the upper part, the electrodes are separated with spacing boards 4 with electro insulating properties, glued with cyanoacrylate glue. The external surfaces of each set are covered with an electro insulating layer 5, resistant to caustics, and made from heat-shrinkable film. External dimensions of both sets of the electrodes makes it able to tightly put it into the magnetic core.

Sources of the magnetic field in the above mentioned magnetic core are cuboidal neodymium magnets 6. They are magnetized along the shorter side, i.e. along their thickness, and turned in the same direction with the same poles. For an increase in the value of the magnetic field induction, two magnets on the upper side and two magnets on the lower side were used, and turned with their poles in the above mentioned way. There is also a possibility to use a higher number of magnets but an increase of the field induction will not be proportional to the magnets number. Length and width of the magnets equal the length and width of the electrode sets put together.

In order to limit the dispersion of the magnetic stream outside the drive, and additionally increase the induction of the magnetic field between the electrodes, a magnetic coat was used. It consisted of rectangular steel plates, made from the magnetically soft ferromagnetic with a high level of magnetic permeability. The coat

comprises two plates 7, coating the magnets from the upper part and from the bottom part, and two plates 8, joining the magnets from the sides. The connections of the plates with magnets were done with a cyanoacrylate glue. External surfaces of the magnetic core are covered with an electro insulating layer 9, resistant to caustics in the form of earlier melted paraffin or heat-shrinkable film.

Assets of the described model comprise a possibility to exchange a set of electrodes after a zinc electrode is melted, and change of the electrodes orientation towards magnetic poles, which allows to show a reversal of electrolyte flow direction and a sense of the drive force. It can be easily achieved through removing a set of electrodes from the magnetic core and putting a new, or previously used one, after rotating it for 180 degrees towards its lengthwise axis. Using a magnetic core prevents the dispersion of the magnetic stream outside the drive and enhances the value of the magnetic field induction in a space between the electrodes. It causes an increase in the speed of electrolyte flow and in the engine power. Even bigger increase in power can be achieved through using a bigger number of electrodes sets, e.g. placed in a smaller distance towards each other, in a way that allows to put them in the same hole of the magnetic core. Photo 9 shows a linear magnetohydrodynamic drive, with a one exchangeable set of electrodes in a magnetic core, placed vertically in a vessel with electrolyte. Photo 10 present an engine of that type with two exchangeable sets of electrodes, in a common magnetic core, placed vertically in a vessel with electrolyte.

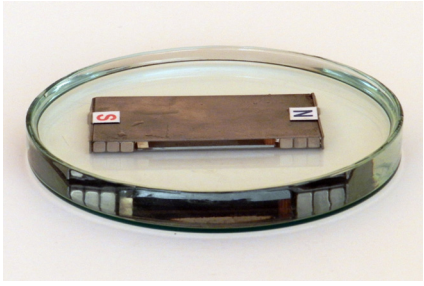

Photo 9: Linear magnetohydrodynamic drive with one exchangeable sets of electrodes.

Photo 10: Linear magnetohydrodynamic drive with two exchangeable sets of electrodes.

6. Linear drive without magnets

This model has a simple construction, presented in Fig. 8. In a glass vessel 1 with a diameter of 20 cm and height of 25 cm, e.g. in a big beaker, there is a set of two vertical, perpendicular electrodes. Their distances from a wall of the vessel should be approximately the same. One of these electrodes 2 is made from 2 mm or more zinc sheet, and the second electrode 3 is made from 1 mm copper sheet. The electrodes are 12 cm long and 20 cm high, and a distance between them is 3.5 cm. nearby one

of the vertical edges of each electrode, there is a series of holes with tips of the copper bars 4 with 3 cm in diameter, short-circuiting the electrodes. What is more, the connections of the electrodes with plates have been soldered. Distance between the neighboring bars axes is 12 mm. external surfaces of the electrodes and surfaces of the bars have been covered with an electro insulating layer, resistant to caustics. Electrolyte 5–10 % water solution of sulfurous acid – was poured into the vessel, in the amount allowing to completely cover the electrodes set.

In the described drive, we can observe a slow flow of the electrolyte among the electrodes, from the bars towards the open end of the electrodes. This effect is explained in the following manner. Electrodes made from copper and zinc, and covered by water solution of sulfurous acid become Volta cells, Fig. 9. Electromotor power generated by them cause the current flow through the electrolyte comprised within the space between the electrodes, from the zinc to copper plate, and further through bars, short-circuiting the electrodes in the opposite direction. These currents flow vertically. Electro insulating layer secures against the stray currents outside the electrodes and bars, and enhances the intensity of the current flowing among the electrodes. Currents flowing through the bars generate a magnetic field, which in the area among the electrodes has an approximately vertical direction. Because of that, electrodynamics power influences the electrolyte comprised within this area. This power is turned vertically towards the open end of the electrodes. At the same time, the electrodes set is influenced by the opposite reaction force, which could be a driving force in a case of attaching the described engine to a water craft.

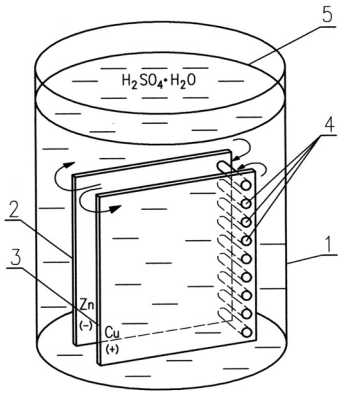

Fig. 8: Structure of a linear drive without magnets; 1 – glass vessel, 2 – zinc electrode, 3 – copper electrode, 4 – short-circuiting bars, 5 – electrolyte.

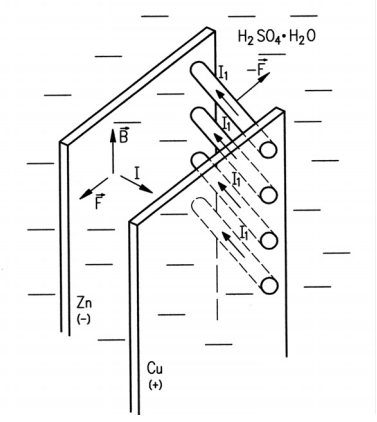

Fig. 9: Explanation of a principle of operation of the linear drive without magnets; I – current intensity in electrolyte, I_1 – current intensity in a bar, **B** – magnetic field induction, **F** – electrodynamics force, **F** – reaction force.

Reversing the location of electrodes around the lengthwise horizontal axis does not change the direction of electrolyte flow, which always happens towards the open end of the electrodes. It happens because their current flow direction between the electrodes is simultaneously reversed as well as the direction of magnetic field induction generated by the bars. This fact proves also that a decisive role in the engine operation is played by a magnetic field generated by the bars, and not the magnetic field of the Earth. If the magnetic field of Earth was decisive, then the sense of their induction vector would be permanent and the direction of the electrolyte flow would be changed into the reversed one after reversing the electrodes. The fastest electrolyte movement in this engine was observed while using 10 % water solution of sulfurous acid. In order to make the electrolyte movement more visible, we can put several little crystals of potassium tetraoxomanganate nearby the electrodes' tips. They will slowly drop in the electrolyte and dissolve leaving a colorful, vertical trail, which will be then moved as a result of electrolyte movement.

7. Summary

The described models of magnetohydrodynamic drives with external power sources transform internal energy, comprised within the electrodes and the electrolyte into electric power necessary for their operation. It happens as a result of external-energetic electrochemical reactions. It is obvious that resources of energy that can be processed is limited and after a while such drives stop working. If we use the electrodes made from copper and zinc, and electrolyte in a form of water solution of sulfurous acid, the zinc electrode will melt, which makes the engine stop working. The concept of using the energy comprised within materials of elements of the magnetohydrodynamic engine for the power feed is very interesting. When those drives are used for experiments, they allow to create an interesting problematic situation, regarding explanation of the principles of their operation by pupils or students, which bring obvious educational advantages.

Magnetohydrodynamic drives can be also used in the field of technology, among others as a drive for water crafts, especially submarines. Advantages of such a drive comprise a simple structure and reliability, and first of all a very quiet operation, during which there are no disturbances of water or sound effects. Thanks to that, crafts with such drives cannot be detected with known methods of echolocation. It is significant for military units – especially submarines. There is one more advantage of using magnetohydrodynamic engines with internal power supply in case of submarines, as such drives are capable of using the energy comprised within the salty water, filing seas and oceans. Because of the fact that volume of this water is enormous ($10^{17}\,\mathrm{m}^3$), there would be enough energy for a very long time, and units using this free energy would be totally independent from any kinds of fuels. Problems connected with realization of this concept comprise small power of draught generated by those engines and changes in the sea ecosystem caused by the products

of electrochemical reactions taking place during the drives' operation. The time will show whether this kind of drive triggers interest and the mentioned problems are defeated.

References

[1] T. Dryński, *Demonstration experiments in physics*, Polish Scientific Edition, Warsaw 1966.

[2] G. Gębura and R. Subieta, *Methods of physical experiments*, Polish Scientific Edition, Warsaw 1978.

[3] S. Bednarek, *Self-powered magnetohydrodynamic motors*, Am. Jour. Phys. **64** (1996), 90–92.

Chair of Modelling the Teaching and Learning Processes
University of Łódź
Pomorska 149/153, PL-90-236 Łódź
Poland
e-mail: bedastan@uni.lodz.pl

Presented by Leszek Wojtczak at the Session of the Mathematical-Physical Commission of the Łódź Society of Sciences and Arts on July 5, 2012

NOWE KONSTRUKCJE SILNIKÓW MAGNETOHYDRODYNAMICZNYCH Z WEWNĘTRZNYM ZASILANIEM

S t r e s z c z e n i e

Artykuł dotyczy siników magnetohydrodynamicznych, które same wytwarzają przepływ prądu elektrycznego, niezbędny do ich działania. Odbywa się to dzięki przemianie energii chemicznej elektrod i zawartego między nimi elektrolitu na energię elektryczną. Opisane zostały dwa modele rotacyjnych silników tego typu. W jednym z nich wiruje elektrolit, a w drugim poruszają się również elektrody w kierunku przeciwnym do elektrolitu. Przedstawiono też trzy modele silników liniowych, w których porusza się elektrolit. Są to silniki mające elektrody połączone na stałe z magnesami, wymienne zespoły elektrod oraz szereg prętów zamiast magnesów. Podane zostały wskazówki techniczne, dotyczące budowy tych silników oraz szczegółowe wyjaśnienie zasady ich działania. Wszystkie opisane silniki są oryginalnymi rozwiązaniami autora artykułu. Na zakończenie zamieszczono krótką dyskusję możliwości praktycznego zastosowania tych silników.

PL ISSN 0459-6854

B U L L E T I N

DE LA SOCIÉTÉ DES SCIENCES ET DES LETTRES DE ŁÓDŹ

2012 Vol. LXII

Recherches sur les déformations no. 1

pp. 79–92

In memory of
Professor Hans Grauert

Małgorzata Nowak-Kępczyk

SURFACE SEGREGATION IN BINARY ALLOYS THIN FILMS IN VALENTA-SUKIENNICKI MODEL VS. THE EXPERIMENTAL DATA IN Cu_xNi_{1-x} ALLOYS

Summary

The study of thin films has been very intense during the last decades. It is observed, both theoretically and experimentally that in thin alloy films the concentrations of atoms differ between inner and outer layers in broad range of temperature. This effect, called surface segregation is chosen and discussed in the article. Other classical surface phenomena: relaxation, adsorption and reconstruction are also mentioned.

We apply, one of many, the so called Valenta-Sukiennicki model, originally used only for stoichiometric alloys [13], considering the pairwise interactions between atoms. Based on our previous considerations [40, 41] we decide to use the extended version of this model, which describes binary alloys of arbitrary concentrations of atoms. In the study we shall consider Cu_xNi_{1-x} fcc alloys. We present the calculations concerning the segregation effect in ultra thin film, containing merely between 6 and 10 layers. We also discuss the sample size-effect influencing the segregation and compare the calculations with those obtained by other authors [67].

1. Introduction

It is observed, both theoretically and experimentally that in thin alloy films the concentrations of atoms differ between inner and outer layers in broad range of temperatures. This effect, called surface segregation is considered to be one of the classical surface phenomena. The other often considered phenomena are: relaxation – meaning the change of interlayers' distances between the outer layers, meaning usually their contraction, adsorption of other atoms to the surface, and reconstruc-

tion – meaning the change of ordering pattern in the surface layer(s) compared to the internal ones.

It is easy, within the Valenta-Sukiennicki model to include the effect of relaxation, but the contraction between layers distance is about a couple of percent for most atoms [21], therefore it seems that the effect is relatively weak and it might be neglected. The investigation of the reconstruction and adsorption effects within the model are still an awaiting challenge.

Cu-Ni alloys are, for various reasons, under special interest of researchers. Not only because of their wide practical applications, due to the catalytic properties, good seawater corrosion resistance, fabricability, etc.; Cu and Ni have very similar atom sizes, which makes them interesting from the point of view of many theoretical models including the Valenta-Sukiennicki model.

2. Description of the Valenta-Sukiennicki model

Let A_pB_q denote a binary alloy containing A an B atoms with concentrations $p/(p+q)$ and $q/(p+q)$ in the sample, respectively. In particular, in this paper we shall consider a binary A_xB_{1-x} alloy of fcc lattice and (111) surface orientation. We divide the system into n monoatomic layers parallel to the surface. Each layer consists of N atoms and the number N is big enough to assume the surface of the layer is infinite. The lattice of the alloy consists of two sublattices, α and β. The relative number of α sites (β sites) is equal to F_α (F_β). We have $F_\alpha + F_\beta = 1$. Let us assume the alloy is stoichiometric and thus

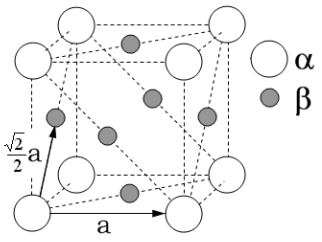

Fig. 1: AB_3 alloy with fcc lattice and (111) orientation of the surface

$$x = F_\alpha \quad \text{and} \quad 1 - x = F_\beta. \tag{1}$$

Denote by $p_X^\sigma(i)$ the probability that the site σ in i-th layer is occupied by atom X, $\sigma \in \{\alpha, \beta\}$, $X \in \{A, B\}$, $i = 1, 2, \ldots, n$. In a completely disordered state we have:

$$p_A^\alpha(i) = p_A^\beta(i), \quad p_B^\alpha(i) = p_B^\beta(i), \quad ; i = 1, 2, \ldots, n.$$

We always have

$$p_A^\alpha(i) + p_B^\alpha(i) = 1 \quad \text{and} \quad p_A^\beta(i) + p_B^\beta(i) = 1. \tag{2}$$

The concentration of A atoms (B atoms) in i-th layer is given by:

$$z_A(i) = F_\alpha p_A^\alpha(i) + F_\beta p_A^\beta(i) \quad \left(z_B(i) = F_\alpha p_B^\alpha(i) + F_\beta p_B^\beta(i)\right).$$

Obviously,

$$\sum_{i=1}^{n} z_A(i) = nF_\alpha \quad \text{and} \quad \sum_{i=1}^{n} z_B(i) = nF_\beta. \tag{3}$$

and

$$z_A(i) = 1 - z_B(i), \quad i = 1, 2, \ldots, n.$$

We define a long-range order parameter $t(i)$ as

$$t_i = \frac{p_A^\alpha(i) - z_A(i)}{1 - F_\alpha}, \quad i = 1, 2, \ldots, n. \tag{4}$$

In a completely disordered state $t(i) = 0$, while in a completely ordered state $t(i) = 1$ for $i = 1, 2, \ldots, n$.

The free energy of the system is given by:

$$F = U - TS, \tag{5}$$

where U denotes the internal energy of the system, T absolute temperature, S entropy. The equilibrium of the system is attained when the free energy of the system is minimized.

Internal energy. In Bragg-Williams approximation the internal energy is given as an average over the energies corresponding to given long-range order.

Let R_1 (R_2) denote the smallest (the second smallest, respectively) distance between atoms in the lattice. The atoms situated in the lattice sites at the distance of R_1 (or R_2) from the given atom will be called its first neighbours (second neighbours, respectively). The number of pairs of first neighbours X and Y, and such that X is in i-th layer, Y is in j-th layer ($j = i, i \pm 1, i \pm 2$) equals [39, 62, 65]

$$\langle XY \rangle_{R_1}^{ij} = \frac{1}{2} N \left(F_\alpha \left(p_X^\alpha(i) r_{\alpha\alpha}^{R_1} p_Y^\alpha(j) + p_X^\alpha(i) r_{\alpha\beta}^{R_1} p_Y^\beta(j) \right) \right.$$

$$\left. + F_\beta \left(p_X^\beta(i) r_{\beta\alpha}^{R_1} p_Y^\alpha(j) + p_X^\beta(i) r_{\beta\beta}^{R_1} p_Y^\beta(j) \right) \right), \tag{6}$$

for $X, Y \in \{A, B\}$, $i = 1, 2, \ldots, n$, where $r_{\sigma\tau}^{R_1}$ denotes coefficients characteristic for the lattice of the alloy, namely the number of neighbours of an atom occupying a σ site in i-th layer which are situated in τ site in $i + j$-th layer if X and Y are first neighbours R_1. (Similar formula holds for the second neighbours, including the R_2 sub- and superscripts). We have shown that in case of binary fcc alloys including only the first neighbours gives a good enough approximation of the internal energy of the system [39, 43]. We shall, however also include second neighbours because of small sizes of the samples considered.

Denoting the interaction energies between atoms X and Y situated at the distance R_k, $k = 1, 2$, as $-v_{XY}(R_k)$, the internal energy coming from first and second neighbours interactions in the film consisting of n layers is given by

$$U = -\sum_{\substack{i,j=1,2,\dots,n \\ X,Y\in\{A,B\}}} \langle XY\rangle_{R_1}^{ij}\, v_{XY}(R_1) - \sum_{\substack{i,j=1,2,\dots,n \\ X,Y\in\{A,B\}}} \langle XY\rangle_{R_2}^{ij}\, v_{XY}(R_2). \tag{7}$$

Entropy. Entropy of binary alloy film is calculated according to the formula

$$S_{\mathrm{B}} = k_{\mathrm{B}} \ln g, \tag{8}$$

where k_{B} denotes Boltzmann constant, and g denotes the number of configurations of a given state for atoms concentrations in layers and long-range order parameters [13, 39]. Thus we have

$$S_{\mathrm{B}} = k_{\mathrm{B}} \ln \prod_{i=1}^{n} g(i) == k_{\mathrm{B}} \ln \prod_{i=1}^{n} \begin{pmatrix} NF_\alpha \\ NF_\alpha p_A^\alpha \end{pmatrix} \begin{pmatrix} NF_\beta \\ NF_\beta p_B^\beta \end{pmatrix}$$

$$= k_{\mathrm{B}} \ln \prod_{i=1}^{n} \frac{(NF_\alpha)!(NF_\beta)!}{(NF_\alpha p_A^\alpha)!(NF_\alpha p_B^\alpha)!(NF_\beta p_A^\beta)!NF_\beta p_B^\beta)!}. \tag{9}$$

where $\begin{pmatrix} n \\ k \end{pmatrix}$ denotes Newton symbol.

2.1. Non-stoichiometric alloys

For practical reasons non-stoichiometric alloys are more interesting than the stoichiometric ones [49].

Non-stoichiometric alloys cannot be described by Valenta-Sukiennicki automatically, because we no longer have equality between the number of atoms and the number of the corresponding lattice sites, which makes formula (6) invalid. In order to overcome this problem we assume that some kind of order exists in the alloy [24], although we do not know it. Therefore, we may accept the equalities (1) if we define the α sites (β sites, respectively) as those occupied by A atoms (atoms B, respectively) in the ordered state. This allows us to calculate the mean approximate value of the coefficients $r_{\sigma\tau}^{R_s}$ in (6) as in [42] and the formula for entropy (9) remains valid.

3. Problems with experimental data

As our aim is to obtain numerical results which could be compared with the experimental data a couple of remarks should be made before.

Conjecture on local minima. Many models, including the Valenta-Sukiennicki model assume that the system stabilizes at the lowest level of free energy. Some experimental data show, however, that in case of alloys of gold there are problems in obtaining the state of minimal energy despite annealing [46]. It has also been experimentally observed that surface segregation might also depend on annealing temperature: in Pt-Rh alloys the enrichment of Pt at the top surface layer on annealing

at 700°C (1000 K) was observed, while on annealing below 600°C Rh enrichment at the first surface has been observed [55]. This leads us to formulate a conjecture that in the experiment the system may attain not the lowest state of free energy but one of the states which constitute local minima of the free energy function.

There is strong consensus that in Cu-Ni alloys Cu has tendency to segregate to the surface in broad range of temperatures and at all concentrations of Cu in the bulk. There are, however, reports about Ni atoms gathered in the several top layers of the film when the Ni concentration in the alloy is less than 16 % [56]. This might perhaps be explained by the local minima conjecture stated above.

Segregation profile. Another interesting question is the shape of the profile of the segregation – it might be oscillatory or monotonic, say, exponential [61]. Some authors claim that the segregation might occur only on the first one or two layers of the alloys [54]. It is also observed that the clean equilibrated surfaces of the Cu-rich polycrystalline alloys consist almost entirely of Cu atoms [11].

There are controversies and uncertainties concerning the reliability of the experimental data themselves [53, 56]. One of the reasons is difficulty in obtaining reliable experimental data, the other is the possibility of applying simplifying assumptions which in effect lead to unreliable results. For example, some researchers even assume the monotonic segregation profile in order to interpret the results of their experiments [63].

Non-stoichiometry. Another problem is stoichiometry and its connection with surface segregation. It has been observed that even tiny deviations from stoichiometry in the bulk composition of the NiPt-L1(0) ordered alloy have a great impact on the atomic configuration of the (111) surface [4, 47].

Size effect. There is a possibility, that ultra thin layers, namely consisting of less than 20 layers, have different segregation profile than the so called thin layers, which although have never been strictly defined, are to consist of between 20 and 200 layers [64]. The problem has recently been investigated by Yan and Wang [67] who have shown based on Darken model that it is expected that in the samples of thickness 1 nm–10 nm a special size effect is observed. The justification of this fact comes from observation that an exteremely thin film can simply not possess enough atoms of a particular kind to fill the external layers. We are going to investigate segregation profiles between samples consisting of different, and very small numbers of layers.

4. Theoretical and experimental data for Cu_xNi_{1-x} alloys

Cu_xNi_{1-x} alloys have fcc lattice. We assume the interactions between Cu and Ni atoms can be modelled by Lennard-Jones potential:

$$V(r) = 4\varepsilon \left(\left(\frac{\sigma}{r} \right)^{12} - \left(\frac{\sigma}{r} \right)^{6} \right), \tag{10}$$

where r denotes the distance between the molecules, σ denotes the distance at which the potential equals zero, ε denotes the potential well depth. Based on available Lennard-Jones potential coefficients for Cu and Ni atoms we may assume

$$\varepsilon_{\mathrm{Cu}} = 0.4092\mathrm{eV}, \quad \sigma_{\mathrm{Cu}} = 0.2338\mathrm{nm}, \quad \varepsilon_{\mathrm{Ni}} = 0.5195\mathrm{eV}, \quad \sigma_{\mathrm{Ni}} = 0.2282\mathrm{nm}, \tag{11}$$

and according to the Lorentz-Berthelot mixing rules commonly used in molecular dynamics numerical programms [1] we have

$$\varepsilon_{\mathrm{Cu-Ni}} = \sqrt{\varepsilon_{\mathrm{Cu}} \cdot \varepsilon_{\mathrm{Ni}}} \approx 0.461\mathrm{eV} \quad \text{and} \quad \sigma_{\mathrm{Cu-Ni}} = \frac{\sigma_{\mathrm{Cu}} + \sigma_{\mathrm{Ni}}}{2} \approx 0.231\mathrm{nm}. \tag{12}$$

In the course of calculations it occured we obtain best results for Cu-Ni alloys assuming that the distance between first neighbours is equal to 0.257 nm. Hence we also assume that the lattice constant equals about $a = 0.363$ nm, and the layer thickness equals 0.157 nm. The 6-layer, 8-layer and 10-layer films have thickness of about 0.94 nm, 1.26 nm and 1.57 nm, respectively.

As both in the case of stoichiometric and non-stoichiometric case we define α sites as those occupied by Cu atoms and β sites as those occupied by Ni atoms and so the relative number of sites is equal to the relative number of corresponding atoms we can assume the classical long-range order parametres (4).

The results of the calculations of concentrations of Cu atoms in layers in a sample containing 6 layers of $Cu_{0.2}Ni_{0.8}$ alloy and also the long range order parametres are given in the Fig. 4. The horizontal axis in each case represents temperature in Kelvin degrees. It occurs that numerically there exist two possible schemes for the concentrations of atoms in the layers and the two constitute states of the same value of the free energy of the system – compare Figs. 4(a) and 4(b). At the temperature of 0 K a very strong segregation effect can be seen in the alloy. In the first scheme (Fig. 4(a)) at 0 K Cu atoms occupy fully one of the outer layers and partially the other outer layer while being absent in the interior of the sample. This effect is the strongest at very low temperatures. At about 200 K the concentrations of Cu atoms in the outer layers become nearly equal and continue being so at higher temperatures. The rise of the temperature makes the segregation effect weaker, though always visible. The second possible scheme (cf. Fig. 4(b)) is the symmetrical segregation through the whole range of temperatures – meaning that the concentrations of Cu atoms satisfy

$$z_1 = z_n, \quad z_2 = z_{n-1}, \quad \text{etc.}$$

throughout the whole range of temperatures.

As we have obtained in the calculations that the internal energy can be minimised in (at least) two different equivalent states, we may say it is confirmed by the various segregation schemes observed in the experiments [56].

As many researchers observed experimentally, copper segregates to the surface in the whole range of temperatures. In the first scheme, at low temperatures one of the external surfaces consist of Cu atoms exclusively, which is concordant with some results [11].

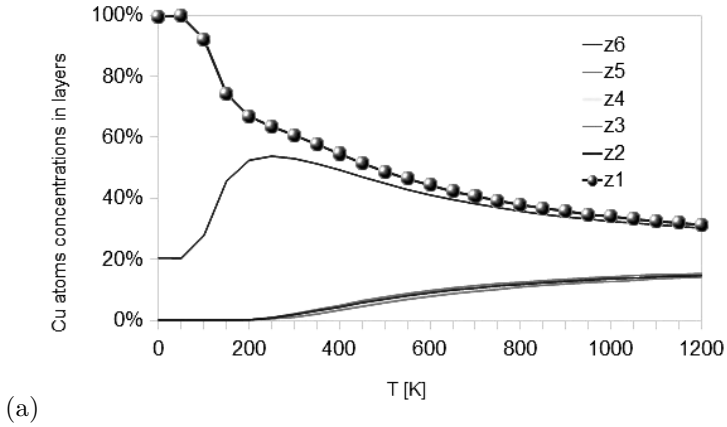

(a)

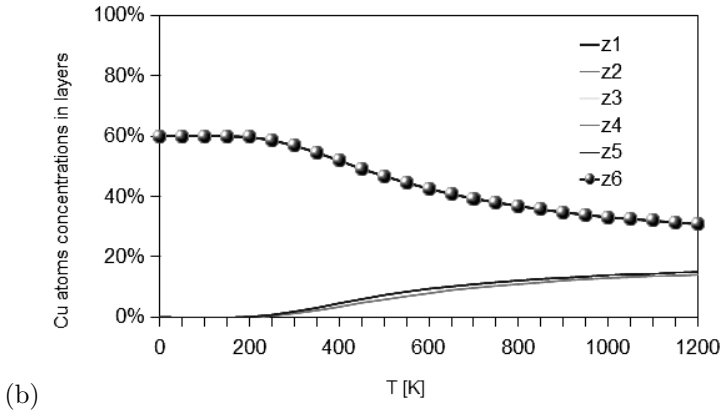

(b)

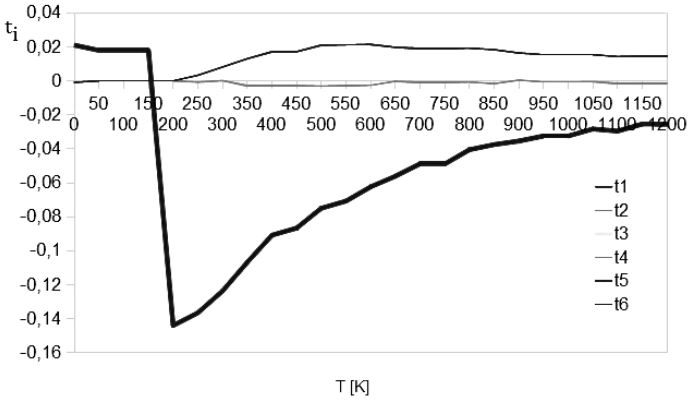

(c)

Fig. 2: (a) and (b): Concentrations of Cu atoms in layers 1–6 in a 6 layers sample of $Cu_{0.2}Ni_{0.8}$ alloy of orientation (111) in dependence of temperature. Graph (a) refers to non-symmetrical layers scheme, graph (b) refers to symmetrical layers scheme. Graph (c) shows the long range order parameters values for the sample in symmetrical layers scheme.

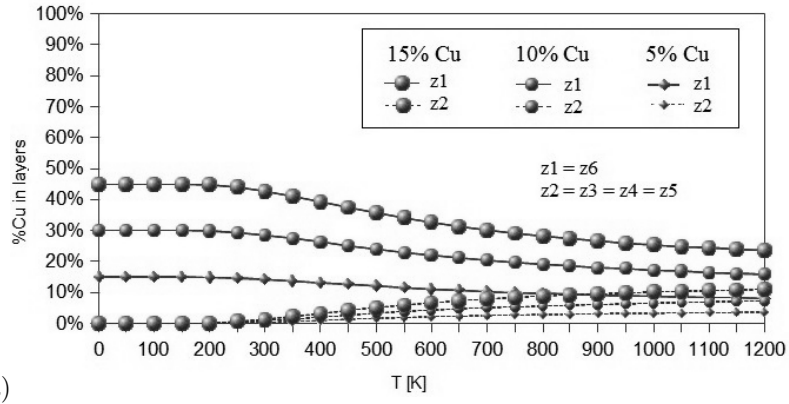

(a)

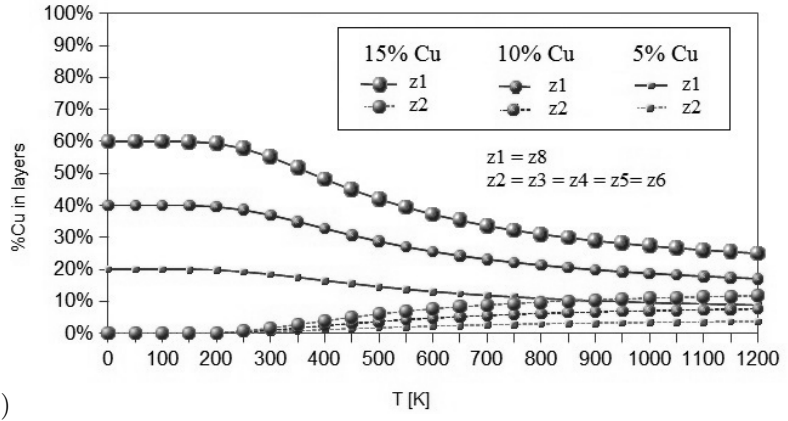

(b)

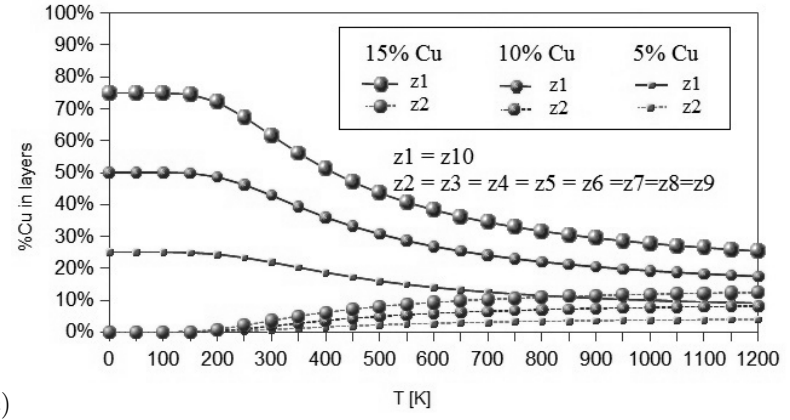

(c)

Fig. 3: Concentrations of Cu atoms in layers in a thin films of Cu_xNi_{1-x} alloy of orientation (111) in dependence of temperature, $x = 0.05, 0.1, 0.15$ and (a) the sample contains 6 layers, (b) the sample contains 8 layers, (c) the sample contains 10 layers. Symmetrical layers scheme is assumed.

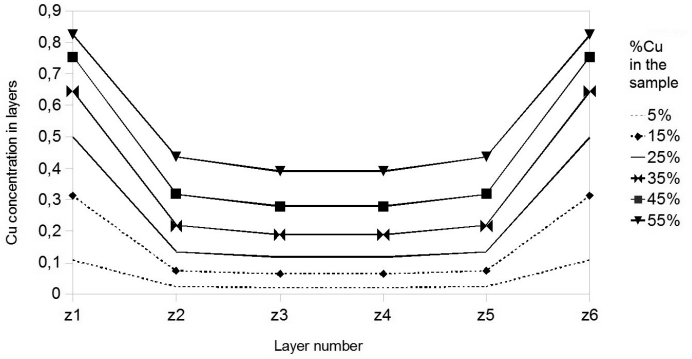

(a)

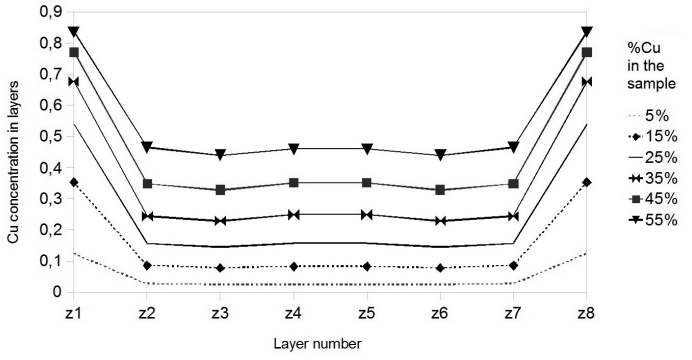

(b)

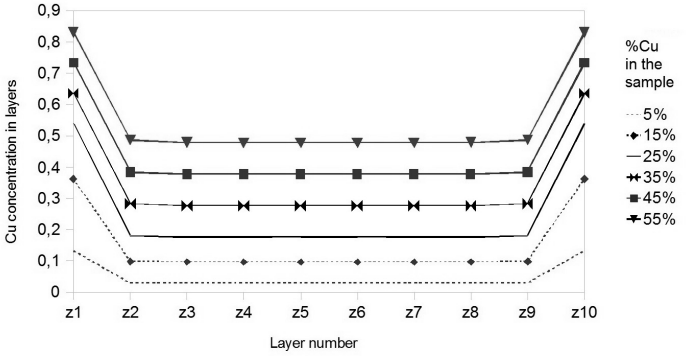

(c)

Fig. 4: Concentrations of Cu atoms in layers in a thin films of Cu_xNi_{1-x} alloy of orientation (111) temperature 650 K, $x = 0.05$, 0.15, 0.25, 0.35, 0.45, 0.55 and such that (a) the sample contains 6 layers, (b) the sample contains 8 layers, (c) the sample contains 10 layers. Symmetrical layers scheme is assumed.

The long range order parameters are practically zero throughout the whole range of temperatures and in all samples investigated, even in the stoichiometric ones. The graph in Fig. (c) makes a very good representation of all the long range order parameters in the sample, showing that the alloy is disordering for all Cu concentrations in the sample and so their graphs will not be presented further.

Let us consider thicker samples, namely of 8 and 10 layers and assume one of the two possible, the symmetrical segregation scheme.

As it can be seen in Fig. 3 throughout the whole range of temperatures the segregation profiles of the 8 and 10 layers' samples are similar to the one of 6 layers' sample (Fig. 4(b)). The difference, however is quatitative: the bigger the number of layers in the sample, the higher concentrations of Cu atoms are observed in the external layers. As before, in the cases of 8 and 10 layers' samples we also have two possible schemes of segregation: the non-symmetrical and symmetrical ones. This confirms the size effect obtained in the calculations of Yan *et al.* [67]. Obtaining the relevant experimental data for the samples of 6-10 layers is still an awaiting challenge. On the other hand, the large body of experimental data concerning the Cu-Ni alloys shall differ significantly from the data concerning very thin films, including up to several monoatomic layers.

Let us observe the Cu concentrations in layers for different Cu concentrations in the alloy and different number of layers in the sample but at a constant temperature of 650 K. The relevant graphs are shown in Fig. 4. It seems that for the segregation profiles vary: for the 6 and 10 layers' samples we might call them exponential while for the 8 layers' sample it is oscillatory.

References

[1] A. K. Al-Matar and D. A. Rockstraw, *A generating equation for mixing rules and two new mixing rules for interatomic potential energy parameters*, J. Comp. Chem. **25**, no. 5 (2004), 660–668.

[2] A. I. Anselm, *Osnovy Statisticheskoi Fiziki i Termodinamiki*, Nauka, Moscow 1973.

[3] T. Balcerzak, *Wykłady z Termodynamiki i Fizyki Statystycznej*, Wydawnictwo Uniwersytetu Łódzkiego, Łódź 2000.

[4] V. Blum, L. Hammer, Ch. Schmidt, W. Meier, O. Wieckhorst, S. Müller, and K. Heinz, *Segregation in Strongly Ordering Compounds: A Key Role of Constitutional Defects*, Phys. Rev. Let. **26**, no. 89 (2002).

[5] W. L. Bragg and E. J. Williams, *The effect of thermal agitation on atomic arrangement in alloys*, Proc. Roy. Soc. London **145A** (1934), 699–730.

[6] W. M. Bartczak, S. Romanowski, and M. Łandwijt, *Modelowanie oddziaływania wodoru z metalami przejściowymi za pomocą teorii funkcjonałów gęstości* (DFT). *Perspektywa kwantowych modeli katalizy heterogenicznej*, Wiadomości Chemiczne **55** (2001), 629–655.

[7] H. A. Bethe, *Statistical Theory of Superlattices*, Proc. Roy. Soc. London A **150** (1935), 552–575.

[8] A. Bienenstock and J. Lewis, *Order-Disorder of Nonstoichiometric Binary Alloys and Ising Antiferromagnets in Magnetic Fields*, Phys. Rev. **160** (1967), 393–403.

[9] L. Boltzmann, *Vorlesungen ber Gastheorie*, J. A. Barth, Leipzig 1896 and 1898.

[10] M. Brejnak and P. Modrak, *Electronic theory of surface segregation for dilute transition metal alloys: predictions based on rigid-band-like approach*, Surf. Sci. **247** (1991), 215-221.

[11] H. H. Brongersma, P. A. J. Ackermans, and A. D. van Langeveld, *Composition of* Cu-Ni *alloy surfaces*, Phys. Rev. B **34** (1986), 5974–5976.

[12] J. R. Chelikowsky, Surf. Sci. **139** (1984), L197.

[13] F. L. Castillo Alvarado, A. Sukiennicki, L. Wojtczak, and I. Zasada, *Order–disorder phenomena in binary alloy thin films*, Physica B **344** (2004), 477–488.

[14] F. L. Castillo Alvarado, Aneta Kazibudzka, and J. Ławrynowicz, *Trade turnover and binary alloys as chaotic dynamical systems*, Bull. Soc. Sci. Lettres Łódź **52** Sér. Rech. Déform. **36** (2002), 67–84.

[15] J. E. Frąckowiak, *Badania nadstruktur typu B2 i D03 metodą efektu Mössbauera*, Wydawnictwo Uniwersytetu Śląskiego, Katowice 1993.

[16] O. L. J. Gijzeman, Surf. Sci. **150** (1985), 1.

[17] A. I. Gusev, *Orderdisorder transformations and phase equilibria in strongly nonstoichiometric compounds,* Phys.-Usp. **43** (2000), 1–37.

[18] J. C. Hamilton, *Prediction of Surface Segregation in Binary Alloys Using Bulk Alloy Variables*, Phys. Rev. Lett. **42** (1979), 989-992.

[19] R. S. Ingarden, A. Jamiołkowski, and R. Mrugała, *Statistical Physics and Thermodynamics* (in Polish), PWN, Warszawa 1990.

[20] R. S. Ingarden and J. Ławrynowicz, *Physical and biophysical interpretations of a new model of open systems with superluminal velocities*, Acta Physicae Superficierum **6** (2004), 91–106.

[21] A. Kiejna, A. F. Wojciechowski, *Metal Surface Electron Physics*, Pergamon, Oxford 1996.

[22] R. Kikuchi, *A theory of cooperative phenomena*, Phys. Rev. **81** (1951), 988–1003.

[23] C. Kittel, *Introduction to Solid State Physics*, 3rd ed., Wiley, New York 1966.

[24] E. V. Kozlov, D. M. Shtern, N. M. Kormin, and O. A. Gudin, *Ordering of nonstoichiometric solid solutions*, J. Struc. Chem. **18** (1977), 64–69.

[25] L. D. Landau and E. M. Lifshitz, *The Classical Theory of Fields*, Pergamon Press Ltd, 1951.

[26] J. E. Lennard-Jones, *Cohesion*, Proc. Phys. Sci. 43 **5** (1931), 461.

[27] J. Ławrynowicz and O. Suzuki, *From order-disorder surface phenomena to graded fractal bundles related to complex and Pauli structures*, Bull. Soc. Sci. Lettres Łódź **51** Sér. Rech. Déform. **35** (2001), 67–98.

[28] J. Ławrynowicz, M. Nowak-Kępczyk, and O. Suzuki, *Fractals and chaos related to Ising-Onsager-Zhang lattices vs. the Jordan-von Neumann-Wigner procedures*, Internat. J. Bifurc. and Chaos, to appear.

[29] P. Matczak and S. Romanowski, *The effect of alloying on the H-atom adsorption on the* (100) *surfaces of* Pd-Ag, Pd-Pt, Pd-Au, Pt-Ag, *and* Pt-Au. *A theoretical study*, Cent. Eur. J. Chem, **9**, no. 3 (2011), 474–480 .

[30] A. Maidou and H. M. Polatoglou, *Monte Carlo study of the* [001] *surface of* Cu_3Au *for* $T \neq 0$ *K*, Phys. Rev. B **60** (1999), 9145–9156.

[31] C. Malinowska-Adamska, *Self-consistent calculations of the dynamic and thermodynamic properties of rare-gas solids*, Acta Phys. Hung. **59** (1986), 257–272.

[32] C. Malinowska-Adamska, P. Słoma, and J. Tomaszewski, J. Phys. Condensed Matter **18** (2006), 751.

[33] C. Malinowska-Adamska and P. Słoma, *Self-consistent calculations of the dynamic, thermodynamic and elastic properties of a lattice of atomic crystals*, Sci. Bull. Tech. Univ. Lodz, 1010 Physics, **28** (2007), 33–44.

[34] S. Mamica and H. Puszkarski, *Nearest and next-nearest neighbourhood surface mapping in thin cubic films. Properties of structural sums,* Acta Physicae Superficierum **9** (2006), 17–70.

[35] A. R. Miedema and Z. Metallkd, **69** (1978), 455.

[36] J.-L. Morán-López and K. H. Bennemann, *Surface effects on the order-disorder phase transition of A_3B alloys*, Phys. Rev. B **15** (1977), 4769–4780.

[37] J.-L. Morán-López and L. M. Falicov, *Theory of surface effects in binary alloys. I. Ordering alloys*, Phys. Rev. B **18** (1978), 2542–2548.

[38] P. M. Morse, *Diatomic molecules according to the wave mechanics*, II. *Vibrational levels*. Phys. Rev. **34** (1929), 57–64.

[39] M. Nowak-Kępczyk, *Binary alloy thin films. The concepts of entropy and nearest neighbours description*, Bull. Soc. Sci. Lettres Łódź **55** Sér. Rech. Déform. **48** (2005), 141–155.

[40] M. Nowak-Kępczyk, *On entropy and internal energy in alloy thin films*, Acta Physicae Superficierum **10** (2008), 25–44.

[41] M. Nowak-Kępczyk, *Binary alloy thin films with arbitrary atom concentrations and vacancies*, I. *Theory*, Bull. Soc. Sci. Lettres Łódź, Sér. Rech. Déform. **58** (2009), 87–99.

[42] M. Nowak-Kępczyk, *Binary alloy thin films with arbitrary atom concentrations and vacancies*, II. *Numerical results*, Bull. Soc. Sci. Lettres Łódź, Sér. Rech. Déform. **58** (2009), 101–110.

[43] M. Nowak-Kępczyk, *Binary and ternary alloy alloy thin films. Entropy and internal energy in dependence on surface orientation and nearest neighbours approximation*, in preparation

[44] M. Nowak-Kępczyk, *Binary and ternary alloy thin films vs. Lennard-Jones and Morse potentials*, in preparation.

[45] M. Ohya and D. Petz, *Quantum Entropy and Its Use* (Textloads and Monographs in Physics), Springer, Berlin-Heidelberg 1993.

[46] V. Ozolins, C. Wolverton, and A. Zunger, Cu-Au, Ag-Au, Cu-Ag, *and* Ni-Au *intermetallics: First-principles study of temperature-composition phase diagrams and structures*, Phys. Rev. B **57**, no. 11 (1998), 6427–6443.

[47] L. V. Pourovskii, A. V. Ruban, B. Johansson, and I. A. Abrikosov, *Antisite-defect-induced surface segregation in ordered* NiPt *alloy*, 2003.

[48] W. H. Press, S. A. Teukolsky, W. T. Vetterling, and B. P. Flannery, *Numerical recipes in C. The Art of Scientific Computing*, 2nd ed. Cambridge Univ. Press, Cambridge 1992.

[49] A. Rabenau (Ed.), Contributors: J. S. Anderson [and others], Problems of nonstoichiometry, North-Holland Pub. Co., Amsterdam 1970.

[50] S. Romanowski, W. M. Bartczak, and R. Wesołkowski, *Density Functional Calculations of the Hydrogen Adsorption on Transition Metals and Their Alloys. An Application to Catalysis*, Langmuir, **15** (18) (1999), 5773-5780.

[51] S. Romanowski, T. Pietrzak, and W. M. Bartczak, *Molecular dynamics calculations for a series of transition metals and their alloys*, Bulletin of the Polish Academy of Sciences. Chemistry **46**, no. 4 (1998), 397–410.

[52] S. J. Romanowski and J. A. N. F. Gomes, *Monte-Carlo Studies of the Chemisorption and Work Function-Temperature Effects on Noble-Metals,* Journal of Electroanalytical Chemistry (**1-2**) (1994), 133–140.

[53] A. V. Ruban and H. L. Skriver, *Calculated surface segregation in transition metal alloys*, Computational Materials Science **15** (1999), 119–143.

[54] A. V. Ruban, I. A. Abrikosov, D. Ya. Kats, D. Goreljikov, K. W. Jacobsen, and H. L. Skriver, *Self-consistent electronic structure and segregation profiles of the* Cu-Ni (001) *random-alloy surface*, Phys. Rev. B **49**, no. 16 (1994), 11383–11396.

[55] N. Sano and T. Sakurai, *Surface segregation of PtRh alloys*, J. Vacuum Science and Technology A: Vacuum, Surfaces, and Films, **8**, no. 4 (1990), 3421–3424.

[56] T. Sakurai, T. Hashizume, A. Kobayashi, A. Sakai, and S. Hyodo, *Surface segregation of* Ni-Cu *binary alloys studied by an atom-probe*, Phys. Rev. B **34**, no. 12 (1986), 8379–8390.

[57] T. Siklós, Acta Phys. Acad. Sci. Hung. **30** (1971), 181.

[58] J. Sokolov, F. Jona, and P. M. Marcus, *Multilayer relaxation of a clean* bcc Fe (111) *surface*, Phys. Rev. B **33** (1986), 1397–1400.

[59] A. Sukiennicki, L. Wojtczak, I. Zasada, and F. L. Castillo Alavarado, *Ferromagnetic thin films of binary alloys*, J. of Magnetism and Magnetic Materials **288** (2005), 137–145.

[60] P. Słoma, C. Malinowska-Adamska, and J. Tomaszewski, *Thermodynamic properties of solid Neon in the reduced all-neighbours approximation of the self-consistent phonon theory*, Sci. Bull. Phys., Technical University of Łódź **28** (2007), 69–77.

[61] U. Vahalia, P. A. Dowben, and A. Miller, *Surface segregation in binary alloys*, J. Vac. Sci. Technol. A **4**, no. 3 (1986), 1675–1679.

[62] L. Valenta and A. Sukiennicki, *Order-disorder phenomena at the surface of solids*, Phys. Stat. Sol. **17** (1966), 903–909.

[63] K. Watanabe, M. Hashiba, and T. Yamashina, Surf. Sci. **61** (1976), 483.

[64] L. Wojtczak, *Cienkie warstwy magnetyczne*, Wydawnictwo Uniwersytetu Łódzkiego, Łódź 2009.

[65] L. Wojtczak, I. Zasada, A. Sukiennicki, and F. L. Castillo Alavarado, *Order-disorder phenomena at the surfaces of alloy thin films*, Bull. Soc. Sci. Lettres Łódź **51** Sér. Rech. Déform. **35** (2001), 41–49.

[66] J. von Neumann, *Thermodynamik quantenmechanischer Gesamtheiten*, in Collected Works, vol. I, Pergamon Press, Oxford-London-New York-Paris 1961, pp. 236–254.

[67] X. L. Yan, J. Y. Wang, *Size effects on surface segregation in Ni-Cu alloy thin films*, Thin Solid Films, Available online 27 March 2012, ISSN 0040-6090, 10.1016/j.tsf.2012.03.061.
(http://www.sciencedirect.com/science/article/pii/S0040609012003471)

High School of Business
Kolejowa 22, PL-26-600 Radom
Poland

Presented by Julian Ławrynowicz at the Session of the Mathematical-Physical Commission of the Łódź Society of Sciences and Arts on November 24, 2011

SEGREGACJA POWIERZCHNIOWA W CIENKICH WARSTWACH STOPÓW W MODELU VALENTY-SUKIENNICKIEGO A DANE EKSPERYMENTALNE DLA STOPÓW $\mathbf{Cu}_x\mathbf{Ni}_{1-x}$

S t r e s z c z e n i e

Cienkie warstwy stopu Cu-Ni o orientacji (111) i koncentracji atomów Cu 5 %–55 % są opisane w modelu Valenty-Sukiennickiego. Przedstawiamy wyniki obliczeń dla warstw składających się z 6-, 8- i 10-ciu warstw monoatomowych o różnych koncentracjch Cu w próbce. Odnosimy się do istniejącego zbioru badań nad cienkimi warstwami stopu i wykazujemy, badając efekt rozmiaru, że dostępne dane eksperymentalne dla tzw. cienkich warstw mogą nie przystawać do obliczeń dla bardzo cienkich warstw.

PL ISSN 0459-6854

B U L L E T I N

DE LA SOCIÉTÉ DES SCIENCES ET DES LETTRES DE ŁÓDŹ

2012 Vol. LXII

Recherches sur les déformations no. 1

pp. 93–101

In memory of
Professor Hans Grauert

Agnieszka Niemczynowicz

A MODEL OF COUPLED HARMONIC OSCILLATOR IN ZWANZIG-TYPE CHAIN. PHONON APPROACH

Summary

This article is concerned with the review of the model of coupled harmonic oscillator in the theory of thin films. The theory of oscillators is a base for description of numerous phenomena because of its mathematical simplicity. In this paper we consider a model of coupled harmonic oscillator in a simple linear chain of atoms in ferromagnetic thin films under assumptions proposed in [5], but with respect to the conditions corresponding to the thin films theory, as well. The aim of our work is to study properties of Zwanzig's chain in context of theory of coupled harmonic oscillator. Finally, we examine numerically our results for a simple example of 5-atoms Zwanzig-type chain.

1. Preliminaries

Theory of harmonic oscillator plays a crucial role in many areas of physics. There are many physical problems which are described in the terms of coupled harmonic oscillators, e.g. the Lee model in quantum theory [1], the Bogolyubov transformation in superconductivity [2], the covariant oscillator model [3], and oscillator model formulated by Harris [4]. The problem of oscillations in a chain of coupled oscillators has been dealt many researches authors. One of the most illustrative example can be given in the paper [5], where the author study the interactions between an atom and a surface represented as a semi-infinite linear chain of oscillators, each of them coupled to its neighbours through harmonic forces.

Motivated by the mentioned references above and in particular [5, 6], in this paper, we undertake to develop a new approach to the theoretical study of interactions

between atoms in one-dimensional chains of coupled harmonic oscillators and processes occur during an initial impulse imparted to any one of the atoms of the chain. The literature contains many theoretical descriptions of accompanying processes occur in this model. A model of the collision of a gas atom with the surface of the crystal has been studied already many years ago e.g. by Jackson [16]. He considered the surface impurity as an independent oscillator, which exchanges energy with the gas atom. The computer simulations of this problem has been considered by McCarroll [17, 18]. The problem has been solved numerically [17, 18] for some different masses of the collision atom and for different force constants for the interaction of this with surface.

The first we formulate our problem by establishing the necessary materials to deal our task, it means we provide some preliminaries of Zwanzig's procedure and present the coupled harmonic oscillator model in thin films. In the second step we analyze the Zwanzig's method in the system of coupled harmonic oscillators. Finally, we examine numerical results for an example of 5-atoms Zwanzig-type chain.

2. Overview of classical coupled oscillators

Let us first consider the system of particles in the form of linear harmonic chain of atoms, where each of the oscillator is situated in a harmonic potential with frequency ω and each oscillator is coupled with its neighbour by a force $K_{\nu\nu'}$ (Fig. 1).

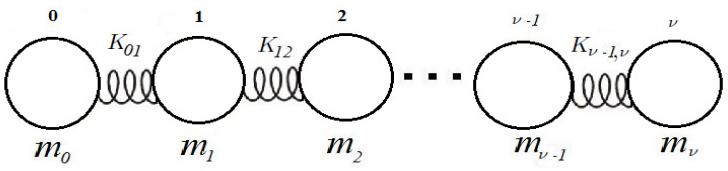

Fig. 1: Chain of coupled oscillators.

The equations of motion take the following form [7, 8]

$$m_\nu \frac{d^2}{dt^2} x_\nu + 2\gamma_\nu m_\nu \frac{d}{dt} x_\nu + \sum_{\nu' \in \nu} K_{\nu\nu'} (x_{\nu'} - x_\nu) = f_\nu, \tag{1}$$

where f_ν denote an external force, the mass m_ν stands for the mass of atom situated at the lattice side. Coefficients γ_ν localized at the point ν of the crystallographic lattice refers to the damping forces. Now, using the easy mathematical modification, we rewrite the equations (1) in the form

$$\frac{d^2}{dt^2} x_\nu + 2\gamma_\nu \frac{d}{dt} x_\nu + \sum_{\nu' \in \nu} \frac{K_{\nu\nu'}}{\sqrt{m_\nu m_{\nu'}}} x_{\nu'} - \sum_{\nu' \in \nu} \frac{K_{\nu\nu'}}{m_\nu} x_\nu = \frac{f_\nu}{\sqrt{m_\nu}}. \tag{2}$$

Let us introduce the following reduced notation for variables and forces, namely

$$u_\nu = \sqrt{m_\nu} x_\nu, \tag{3}$$

$$\kappa_{\nu\nu'} = \frac{K_{\nu\nu'}}{\sqrt{m_\nu m_{\nu'}}}. \tag{4}$$

With regard to the new notation, we can rewrite the equation (1) in the form a set of linear equations coupled by the interactions between the nearest neighbours

$$\frac{d^2}{dt^2}u_\nu + 2\gamma_\nu \frac{d}{dt}u_\nu + \sum_{\nu' \in \nu} \kappa_{\nu\nu'} u_\nu - \left(\sum_{\nu' \in \nu} \frac{K_{\nu\nu'}}{m_\nu} \right) u_\nu = F_\nu, \tag{5}$$

where $F_\nu = \dfrac{f_\nu}{\sqrt{m_\nu}}$. The solution of the considered equations ca be obtained by replace the variables (3) and (4) via linear transformation

$$u_\nu = \sum_q T_{q\nu} Q_q$$

with the orthogonality conditions

$$\sum_q T_{q\nu} T_{q\nu} = \delta_{\nu\nu'}, \quad \sum_\nu T_{q\nu} T_{q'\nu} = \delta_{qq'}.$$

Using these transformation, we now write eq. (5) as

$$\omega_{0\nu}^2 T_{q\nu} - \sum_{\nu' \in \nu} \kappa_{\nu\nu'} T_{q\nu'} = \omega_q^2 T_{q\nu}, \text{ with } \omega_{0\nu}^2 = \sum_{\nu' \in \nu} \frac{K_{\nu\nu'}}{m_\nu}, \tag{6}$$

and further

$$\frac{d^2}{dt^2}Q_q + 2\sum_{q'} \Lambda_{qq'} \frac{d}{dt} Q_q + \omega_q^2 Q_q = F_q \tag{7}$$

where $\Lambda_{qq'} = \sum_\nu T_{q\nu} \gamma_\nu T_{q'\nu}$ and $F_q = \sum_\nu T_{q\nu} F_\nu$. The equations (7) represent the behavior of the harmonic oscillator which is under the action of the external force.

3. Model of Zwanzig chain. Example for 5 atoms

Let us consider now the simple model of one-dimensional chain of atoms in the crystal lattice (Fig. 2).

The atoms of the model are identical and have mass M. We apply the Zwanzig's procedure [5] to the chain of coupled harmonic oscillations considered in the direction perpendicular to the chain axis [9]. In this case the Hamiltonian of the system takes the form [10]

$$\mathcal{H} = \frac{1}{2}\sum_\nu \frac{p_\nu^x}{M} + \frac{1}{2}\sum_{(\nu,\nu_\prime)} K_\nu \left(x_{\nu_\prime} - x_\nu \right)^2, \tag{8}$$

where K_ν denote the harmonic forces. We suppose that the chain of atoms is cutted from the sample of ferromagnetic thin films in the direction perpendicular to the sample plane. The sample is divided into N monoatomic, two-dimensional layers

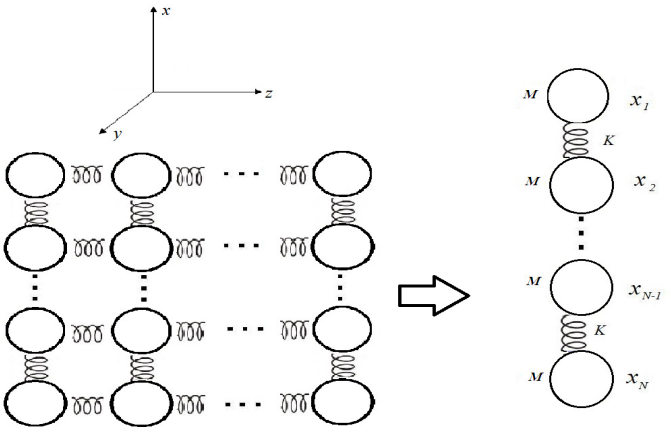

Fig. 2: The one-dimensional chain of atoms as a coupled oscillators in the meaning of Zwanzig, cutted from the sample of ferromagnetic thin films.

parallel to the surface planes labelled by $\nu = 1, ..., N$. In our approach we assume that $N = 5$. The equations of motions

$$\dot{p}^x_\nu = -\frac{\partial}{\partial x_\nu}\mathcal{H}, \qquad \dot{x}^x_\nu = -\frac{\partial}{\partial p^x_\nu}\mathcal{H} \tag{9}$$

read

$$\dot{p}^x_\nu = K_\nu \sum_{\nu\prime} \left(x_{\nu\prime} - x_\nu\right), \qquad \dot{x}_\nu = \frac{1}{M}\dot{p}^x_\nu \tag{10}$$

and, consequently

$$\ddot{x}_\nu = \frac{K_\nu}{M} \sum_{\nu\prime \in \nu} \left(x_{\nu\prime} - x_\nu\right). \tag{11}$$

Now, we can extended the Hamiltonian (8) by allowing the introduce boundary conditions and the effective external force κ_ν. The Hamiltonian (8) takes his generalized form, as follows [9]

$$\mathcal{H} = \frac{1}{2}\sum_\nu \frac{p^x_\nu}{M} + \frac{1}{2}\sum_{(\nu,\nu\prime)} K_\nu \left(x_{\nu\prime} - x_\nu\right)^2 + \sum_\nu \kappa_\nu x_\nu. \tag{12}$$

and the equations of motions

$$\ddot{x}_1 = (K/M)(x_2 - x_1) + \kappa_1, \tag{13}$$

$$\ddot{x}_\nu = (K/M)(x_{\nu+1} - 2x_\nu + x_{\nu-1}) + \kappa_\nu, \text{ for } \nu = 2, 3, 4, \tag{14}$$

$$\ddot{x}_N = -(K/M)(x_5 - x_4) + \kappa_5. \tag{15}$$

Here equations (13) and (15) form the boundary conditions. The system of equations (13)–(15) can be consider in more general case than it was presented in paper [5].

3.1. The role of third layer

The discussion given in earlier papers [9–14] motivates us to show the *specific* role of third layer in the considered model. We will study the model of the thin sample consist 5 monoatomic, two-dimensional layers parallel to the surface. Let us take into account the chain of atoms cutted from considered sample. According to the papers [12–14], we can write the system of differential – difference equations as (16)–(20)

$$x_1 = K\left(\omega_1^2\widetilde{u}_3 + \omega_2^2\widetilde{u}_5 + \omega_3^2\widetilde{u}_7 + \omega_4^2\widetilde{u}_9 + \omega_5^2\widetilde{u}_{11}\right) \text{ and } \quad \frac{d}{dt}x_1 = \frac{1}{2}\omega_1^2 K\widetilde{u}_2, \tag{16}$$

$$x_2 = K\left(\omega_2^2\widetilde{u}_5 + \omega_3^2\widetilde{u}_7 + \omega_4^2\widetilde{u}_9 + \omega_5^2\widetilde{u}_{11}\right) \quad \text{and} \quad \frac{d}{dt}x_2 = \frac{1}{2}\omega_2^2 K\widetilde{u}_4, \tag{17}$$

$$x_3 = K\left(\omega_3^2\widetilde{u}_7 + \omega_4^2\widetilde{u}_9 + \omega_5^2\widetilde{u}_{11}\right) \quad \text{and} \quad \frac{d}{dt}x_3 = \frac{1}{2}\omega_3^2 K\widetilde{u}_6, \tag{18}$$

$$x_4 = K\left(\omega_4^2\widetilde{u}_9 + \omega_5^2\widetilde{u}_{11}\right) \quad \text{and} \quad \frac{d}{dt}x_4 = \frac{1}{2}\omega_4^2 K\widetilde{u}_9, \tag{19}$$

$$x_5 = \omega_5^2 K\widetilde{u}_{11}. \tag{20}$$

We introduce the dimensionless functions [8]

$$x_\nu = \sum_q T_{q\nu}x_q, \quad \nu = 1, ..., 5, \tag{21}$$

with conditions given by the following system

$$\begin{gathered} T_{q2} - (1+\kappa)T_{q1} = \Omega\, T_{q1}, \\ T_{q,\nu} - 2T_{q,\nu+1} + T_{q,\nu+2} = \Omega\, T_{q,\nu+1}, \quad \text{for} \quad \nu = 2, 3, 4, \\ T_{q,4} - (1+\kappa)T_{q,5} = \Omega\, T_{q,5}, \end{gathered} \tag{22}$$

where $\Omega = \left(\omega_q/\omega_0\right)^2$.

An easy calculation shows that the substitutions (16)-(20) into (13)-(15) give the system

$$\frac{d}{dt}\widetilde{u}_2 = -\frac{1}{2}\left(\widetilde{u}_3 - \varepsilon_1\right), \tag{23}$$

$$\frac{d}{dt}\widetilde{u}_\nu = \frac{1}{2}\left(\widetilde{u}_{\nu-1} - \widetilde{u}_{\nu+1} + \varepsilon_{\frac{1}{2}\nu}\right), \quad \text{for} \quad \nu = 4, 6, 8, \tag{24}$$

$$\frac{d}{dt}\widetilde{u}_{10} = \frac{1}{2}\left(\widetilde{u}_9 - \varepsilon_{10}\right), \tag{25}$$

and

$$\frac{d}{dt}\widetilde{u}_\nu = \frac{1}{2}\left(\widetilde{u}_{\nu-1} - \widetilde{u}_{\nu+1}\right) \text{ for } \quad \nu = 1, 3, ..., 7, \tag{26}$$

where

$$\frac{d}{dt}\widetilde{u}_{2N-1}=\frac{1}{2}\widetilde{u}_{2N} \qquad \text{for} \qquad \omega_\nu^2 K\neq 0, \qquad \text{and} \qquad \varepsilon_\nu=\frac{1}{\omega_\nu}K\frac{\mu_B S}{\hbar}h_\nu^x(t),$$

along with

$$\omega_\nu^2 K\frac{d}{dt}\widetilde{u}_\nu=\frac{d}{dt}\left[x_{\frac{1}{2}(\nu-1)}-x_{\frac{1}{2}(\nu+1)}\right]=\frac{1}{2}\omega_\nu^2 K\Big(\widetilde{u}_{\nu-1}-\widetilde{u}_{\nu+1}\Big).$$

Now, we can rewrite the above system of equations to a more convenient form by replacing $u_\nu=\widetilde{u}_{\nu+2}$ for $\nu=0,1,...,9$:

$$\frac{d}{dt}u_0 = \frac{1}{2}\Big(u_1-\varepsilon_1\Big), \tag{27}$$

$$\frac{d}{dt}u_\nu = \frac{1}{2}\Big(u_{\nu-1}-u_{\nu+1}+\varepsilon_{\frac{1}{2}\nu+1}\Big) \text{ for } \nu=2,3,...,6, \tag{28}$$

$$\frac{d}{dt}u_{2N-2} = \frac{1}{2}\Big(u_{2N-3}+\varepsilon_N\Big), \tag{29}$$

$$\frac{d}{dt}u_\nu = \frac{1}{2}\Big(u_{\nu-1}-u_{\nu+1}\Big) \text{ for } \nu=1,3,...,7, \tag{30}$$

$$\frac{d}{dt}u_{2N-1} = \frac{1}{2}u_{2N-2} \quad \text{for} \quad \omega_\nu^2 K\neq 0. \tag{31}$$

As we can see, $u_1=\widetilde{u}_3$ *and* $u_3=\widetilde{u}_5$ *plays a specific role*, analogous to that of u_3 in [6, 9]. We can find the second order equation for $u_1(t)$ as a linear function u_3 by (25) for $r=1$, namely

$$\frac{d^2}{dt^2}u_1=\frac{1}{2}\left(\frac{d}{dt}u_0-\frac{d}{dt}u_2\right)=\frac{1}{4}(u_1-\varepsilon_1)-\frac{1}{4}(u_1-u_3+\varepsilon_2)=\frac{1}{4}(u_3-\varepsilon_1-\varepsilon_2).$$

3.2. Formulae for the first relative distances in the Zwanzig's chain. Example for 5 atoms

With respect the procedure applied by Zwanzig, described in [3] and its application presented in the papers [6, 12] we introduce the generating function in the form

$$\Theta(z,t)=\sum_{\substack{\nu=0,\\ \nu \text{ even}}}^{8}u_\nu(t)z^\nu+\sum_{\substack{\nu=1,\\ \nu \text{ odd}}}^{9}u_\nu(t)z^\nu, \quad \text{for } z\in\mathbb{C}, \quad \text{and } t\in[0,t^*]. \tag{32}$$

If we notice that

$$\Theta=\Theta_0\exp\left[\frac{1}{2}\left(z-\frac{1}{z}\right)t\right],$$

we can write the differential equation for the generating function

$$\frac{\partial}{\partial t}\Theta_0=\frac{1}{2}\left(-u_1+\sum_{\substack{\nu=0,\\ \nu \text{ even}}}^{8}\varepsilon_{\frac{1}{2}\nu+1}z^\nu\right)\exp\left[-\frac{1}{2}\left(z-\frac{1}{z}\right)t\right],$$

and taking into account

$$\exp\left[\frac{1}{2}\left(z-\frac{1}{z}\right)\tau\right]=\sum_{m=-\infty}^{+\infty}J_m(\tau)z^m \quad \text{for} \quad z\in\mathbb{C}\backslash\{0\},\ \ \tau\in\mathbb{R}\ \text{ or }\ \mathbb{C},$$

where $J_m(\tau)$ are the Bessel functions, next we obtain

$$\begin{aligned}\sum_{k=0}^{9}u_k(t)z^k &= \sum_{m=-\infty}^{+\infty}J_m(t)z^m\sum_{\nu=0}^{9}u_\nu(0)z^\nu \\ &+ \frac{1}{2}\sum_{m=-\infty}^{+\infty}\int_0^t J_m(t-s)z^m\left[-u_1(s)+\sum_{\substack{\nu=0,\\ \nu\ \text{even}}}^{8}\varepsilon_{\frac{1}{2}\nu+1}(s)z^\nu\right]ds.\end{aligned}$$

Further, follow in [6] and taking into account the recurrence relation for Bessel functions of the first kind $J_{n+1}(t)=\frac{2n}{t}J_n(t)-J_{n-1}(t)$ for $n\in\mathbb{Z}$, we receive the explicite formulae for the first relative displacement in the case of chain structured from 5 atoms (Fig. 3).

$$u_1(t)=-\sum_{\substack{\nu=0,\\ \nu\ \text{even}}}^{8}\int_0^t\frac{\nu}{t-s}J_\nu(t-s)\varepsilon_{\frac{1}{2}\nu+1}ds+2\sum_{\nu=0}^{9}(-1)^\nu\frac{\nu}{t}J_\nu(t)u_\nu(0). \tag{33}$$

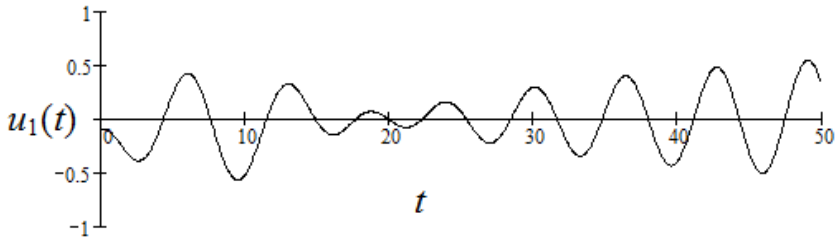

Fig. 3: Relative displacement between gas atom and surface atom $u_1(t)$ for $\varepsilon_1(s)=\varepsilon_5(s)=\sin(t)$, $\varepsilon_2(s)=...=\varepsilon_4(s)=\cos(t)$, and $u_0(0)=u_9(0)=10^{-2}$, $u_2(0)=u_3(0)=...=u_8(0)=10^{-1}$.

4. Conclusions

In our theoretical study of surface ferromagnetic excitations in thin films we develop theory of Zwanzig [5]. The solution of (27)–(31) is found as a sum of group of a series involving Bessel functions for given relative displacements, each of which is the mathematical image of the collision wave which has been reflected by the corresponding time distance from the film surface. Figure 3 shows the shape of curve of corresponding relative distances in the case when the initial conditions are the same at the end of the sample ($u_1(0)=u_{10}(0)$, $\varepsilon_1(t)=\varepsilon_5(t)$), but different from

the conditions inside the sample ($u_2(0) = ... = u_9(0),\ \varepsilon_2(t) = \varepsilon_3(t) = \varepsilon_4(t)$). The character of the shape of $u_1(t)$ evince a tendency to be periodic (up to $t \simeq 50$).

In many researches on the behaviour of atom condensation or processes (e.g. energy transfer or trapping) occurring during the external (constant) force colliding with a linear lattice, the problem and its solution is formulated in terms of the relative displacement $u_1(t)$. The oscillations of the first connection disperse after the collision. The disperse of the impulse initiated by a collision with the lattice can be observed for relative displacements of atom pairs down the chain [10, 12].

References

[1] S. S. Schweber, *An Introduction to Relativistic Quantum Field Theory*, Row-Peterson, Elmsford, New York 1961.

[2] A. L. Fetter and J. D. Walecka, *Quantum Theory of Many Particle Systems*, McGrow-Hill, New Yourk 1971.

[3] Y. S. Kim, *Observable gauge transformations in the parton picture,* Phys. Rev. Lett. **63** (1989), 348–351.

[4] E. G. Harris, *Quantum theory of the damped oscillator*, Phys. Rev. A **42** (1990), 3685-3694.

[5] R. W. Zwanzig, *Collision of a gas atom with a cold surface*, J. Chem. Phys. **32**, no. 4 (1960), 1173–1177.

[6] B. Gaveau, J. Ławrynowicz, and L. Wojtczak *Statistical mechanics of a body sliding on the surface trajectory*, Soc. Sci. Lettres Łódź **55** Sér. Rech. Déform. **48** (2005), 35–45.

[7] C. Surry, G. Wiatrowski, and L. Wojtczak, *Models of oscillators in physics of thin films*, Bull. Soc. Sci. Lettres Łódź **55** Sér. Rech. Déform. **46** (2005), 33–74.

[8] J. B. Stokoloff, *Theory of energy dissipation in sliding crystal surfaces*, Phys. Rev. B **42**, no. 1 (1990), 760–765.

[9] A. Corciovei, *Spin-Waves Theory of Ferromagnetic Thin Films*, Phys. Rev. **130** (1963), 2223–2229.

[10] J. Ławrynowicz and A. Niemczynowicz, *Harmonic oscillations in Zwanzig's chain*, to appear.

[11] A. Niemczynowicz, *The diagonal form of the Hamiltonian in a Zwanzig - type chain*, submitted to Bull. Soc. Sci. Lettres Łódź **61** Sér. Rech. Déform. **3** (2011)

[12] J. Ławrynowicz, L. Wojtczak, and —, *Zwanzig's trajectories use for the spin wave description*, to appear.

[13] A. Niemczynowicz, *On geometry of orbits and integral trajectories in the motion of a body sliding on the surface trajectory*, Bull. Soc. Sci. Lettres Łódź **55** Sér. Rech. Déform. **48** (2005), 125–142.

[14] —, *Spectral space modelling of orbits systems for lattice trajectory*, Bull. Soc. Sci. Lettres Łódź **55** Sér. Rech. Déform. **48** (2007), 113–125 .

[15] —, *On spin waves damping frequency eigenvalues*, Bull. Soc. Sci. Letters Łódź **59** Sér. Rech. Déform. **58** (2009) 111–115.

[16] J. Jackson, *A quantum mechanical theory of energy exchange between inert gas atoms and a solid surface,* Proc. Cambridge philos. Soc. **28** (1932), 136–164.

[17] B. McCarroll and G. Ehrlich *Trapping and energy transfer in atomic collisions with a crystal surface,* J. Chem. Phys. **38** (1963), 523–532.

[18] B. McCarroll, *Trapping and energy transfer in atomic collisions with a crystal surface, II, Impurities,* J. Chem. Phys. **39**, no. 5 (1963), 1317–1326.

Department of Relativity Physics
University of Warmia and Mazury in Olsztyn
Słoneczna 54, PL-10-710 Olsztyn,
Poland

Presented by Julian Ławrynowicz at the Session of the Mathematical-Physical Commission of the Łódź Society of Sciences and Arts on November 24, 2011

MODEL OSCYLATORA HARMONICZNEGO W ŁAŃCUCHU ATOMÓW TYPU ZWANZIGA. PODEJŚCIE FONONOWE

S t r e s z c z e n i e

Artykuł jest wprowadzeniem do rozważań nad modelem oscylatora harmonicznego w łańcuchu atomów typu Zwanziga. Rozważany jest prosty model oscylatora harmonicznego z uwzględnieniem założeń zaproponowanych w pracach [5, 6]. Otrzymane rozwiązanie zależności relatywnej odległości pomiędzy atomem kolidującym a atomem łańcucha (1) jest pierwszym krokiem do analizy ruchów oscylacyjnych i właściwości badanego modelu.

PL ISSN 0459-6854

B U L L E T I N

DE LA SOCIÉTÉ DES SCIENCES ET DES LETTRES DE ŁÓDŹ

2012 Vol. LXII

Recherches sur les déformations no. 1

pp. 103–115

In memory of
Professor Hans Grauert

Krzysztof Pomorski, Piotr Tempczyk, and Przemysław Prokopow

TRANSPORT PROPERTIES OF A MULTI-PENDULUM SYSTEM

Summary

We present numerical solutions of simple multi-pendulum system that is preliminary for modeling human or robotic movement in 2 dimensions. The model also takes into account friction. Various possible applications of the solutions presented are given.

1. Motivation

We develop universal 2-dimensional multi-pendulum model which shows the transport properties in one dimension. The model can be extended in a natural way to account more complex cases than given in [1–6] by means of the scheme depicted in Fig. 9. Applications can be found in medicine, robotics, sport, intelligent system design, biology including zoology, and many other areas.

2. Coupled pendulum system as a preliminary example

We analyze the system as depicted in Fig. 1 (2), which describes the system of 4 masses connected by 3 massless rods interconnected by 2 massless springs $|EF|$ and $|GF|$. All coordinates describing the position of the system (x_5, y_5), (x_4, y_4), (x_3, y_3), (x_2, y_2) can be parameterized by rods lengths L_1, L_2, L_3, x_5, y_5 and angles α_5, α_4, α_3 in the following way:

$$\begin{cases} x_4(t) = x_5(t) - L_4 \sin(\alpha_1(t)) \\ y_4(t) = y_5(t) - L_4 \cos(\alpha_1(t)) \end{cases}$$

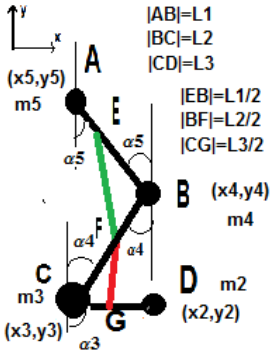

Fig. 1: Geometrical parametrization of reduced 2-dimensional model of humanoid robot as coupled 2-pendulum system driven by 2 active massless springs $|EF|$ and $|GF|$.4 masses are connected by stiff massless rods that can move without friction in combined effective gravitation-ground potential.

$$\begin{cases} x_3(t) = x_4(t) - L_3 \sin(\alpha_2(t)) \\ y_3(t) = y_4(t) - L_3 \cos(\alpha_2(t)) \end{cases}$$

$$\begin{cases} x_2(t) = x_3(t) - L_2 \sin(\alpha_3(t)) \\ y_2(t) = y_3(t) - L_2 \cos(\alpha_3(t)) \end{cases}$$

$$\begin{cases} x_1(t) = x_2(t) + L_1 \sin(\alpha_4(t)) \\ y_1(t) = y_2(t) - L_1 \cos(\alpha_4(t)) \end{cases}$$

We consider the Lagrangian of the system in the following form

$$L = \left[\frac{1}{2}(m_2 v_2^2 + m_3 v_3^2 + m_4 v_4^2 + m_5 v_5^2) - \frac{1}{2}k_{s1}(t)(L_{s1}(t) - L_{s10})^2 \right.$$
$$\left. -\frac{1}{2}k_{s2}(t)(L_{s2}(t) - L_{s20})^2 - U(y_5, m_5) - U(y_4, m_4) - U(y_3, m_3) - U(y_2, m_2)\right] \quad (1)$$

where $U(x) > -gx$, e.g. $U(x,y) = U_0 \exp(l_0 x)$ with $U_0 = \text{const} > 0$ and $l_0 = \text{const}_1 > 0$ as in the case of flat and very soft ground. The ground stiffness can be regulated by coefficients l_0 and U_0. Here $k(t)$ uses the fact that the spring constant is time dependent. In such case the active force(s) acting on the spring(s) is(are) introduced. Equations of motions are derived basing on the Lagrange equations as given by

$$\partial_{\alpha_i} L(t, \alpha_j, \dot{\alpha_j}, ...) = \frac{d}{dt}\partial_{\dot{\alpha_i}} L(t, \alpha_j, \dot{\alpha_1}, ...) \quad (2)$$

where α_i are general coordinates with $i = 5, 4, 3, 2, 1$ and with $\alpha_2 = x_5$, $\alpha_1 = y_5$. Providing that we have given initial values of $x_5(t_0)$, $y_5(t_0)$, $x_5'(t_0)$, $y_5'(t_0)$, $\alpha_1(t_0)$, $\alpha_2(t_0)$, $\alpha_3(t_0)$, $\alpha_4(t_0)$, $\alpha_5(t_0)$, $\alpha_1'(t_0)$, $\alpha_2'(t_0)$, $\alpha_3'(t_0)$, $\alpha_4'(t_0)$, $\alpha_5'(t_0)$, and parameters m_2, m_3, m_4, m_5, g, L_1, L_2, L_3 we can compute numerically or in the limited case analytically time evolution of all 4 masses coordinates for $t > t_0$ and thus determine

the time-dependent dynamics of the whole system. It should be underline that observing such system from outside as by camera by means of image processing we can derive all initial values except the masses and spring constants. They can be hidden variables that can be guessed (determined with certain accuracy) once the trajectories of all 4 masses are available. This is already another problem that will not be discussed in this work, but it is the subject of the future interest.

3. Accounting the passive and active spring presence

In the conduced computations for the system depicted in Fig. 2. we assume validity of the Hooke law. Spring 1 and 2 lengths can be obtained from preliminary geometrical analysis.

$$L_{s1}(t) = \sqrt{\frac{1}{4}(L_1^2 + L_2^2) - \frac{1}{2}L_1 L_2 \sin(\alpha_5(t) + \alpha_4(t))} \tag{3}$$

$$L_{s2}(t) = \sqrt{\frac{1}{4}(L_2^2 + L_3^2) - \frac{1}{2}L_2 L_3 \sin(\alpha_3(t) + \alpha_4(t))} \tag{4}$$

We define L_{s1}, L_{s2} the springs lengths when the spring tension is zero in the form

$$L_{s1} = \sqrt{\frac{1}{4}(L_1^2 + L_2^2) - \frac{1}{2}(L_1 L_2) \sin(\alpha_{s1})} \tag{5}$$

$$L_{s2} = \sqrt{\frac{1}{4}(L_2^2 + L_3^2) - \frac{1}{2}(L_2 L_3) \sin(\alpha_{s2})}. \tag{6}$$

In the passive case the α_{s1} and α_{s2} are time independent. In the case of active cases they are time dependent and they should be parameterized to account description of artificial or real muscle as given by Hill [9]. Another way of accounting for the presence of the active force in the spring is by assuming that spring 1 and 2 constants are time-dependent. Also one can consider that both spring constants and L_{s1}, L_{s2} are time dependent.

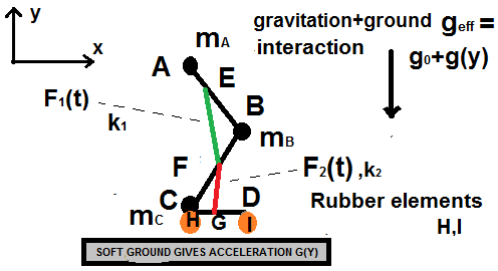

Fig. 2: Reduced two-dimensional model of humanoid robot as coupled two-pendulum system driven by two active springs. Such system shows the transport property in the x direction.

4. Inclusion of cognitive capabilities in studied case

It is possible to add eye (miniature camera) to the pendulum system to the mass m_5. If springs are active then the robot can avoid obstacles or jump over obstacles. The robot decision to jump can be made by signal coming out of neural network. 3 input signals of this network can provide the obstacle distance, its height and width. Two neural network output signals can be values of active forces that are needed to be applied to 2 springs. Before being operational and optimal the neural network has to be trained. It can be learned to be optimal by means of the genetic algorithm working in certain environment with mechanism rejecting bad performance and accepting good performance that is encoded in neural network weight coefficients. When genetic algorithm operates then neural network weights can evolve and finally be set to the most optimal values.

5. Accounting the realistic muscle presence in the agent model

The most common used model of human muscle was given by Hill [9]. It is depicted in Fig. 3. In the Hill model of human muscle the contractile element (CE) represents the active properties of the muscle fibers. A serial-elastic (T) element is representing the elasticity of the tendon. A parallel-elastic element (PE) models the passive stiffness of the muscle fibers. Muscles are viscoelastic and hence have a viscous damper. It is included in the model, when the dynamics of the second-order critically damped twitch is regarded. One common model for muscular viscosity is an exponential form damper, where the damping force F_d present in the muscle is of the form

$$F_d = k\left(\frac{d}{dt}L_d\right)^{\beta},$$

where β, k are the constants.

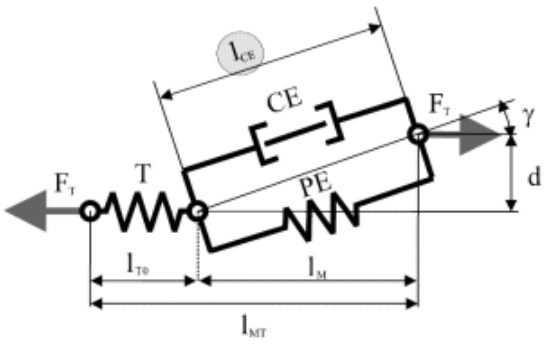

Fig. 3: Hill model of human muscle. We denote F_T-Force,T-tendon, CE-Contractile Element, SE-Series Element, PE-Parallel Element, L_t-tendon length, L_m-muscle length, L_{mt}-muscle-tendon length,L_{ce}-contractile-element length. Also γ and d coefficients parameterize the muscle properties.

6. Simulation results

Mathematica environment was used to conduct the numerical computations. Example of quasi knee movement (m_4 mass) in (x, y) plane with no friction and no active force is given in Fig. 10. The SI units were used. The ground impact was modeled by potential of the form $U(y) = \exp(-ay)$. The parameters used in the simulation are the following:

$$a = 10 \quad \text{(measure of floor stiffness)}, \quad m_1 = 2 = m_2,\ m_3 = 1,\ m_4 = 1,$$

$$g = 10 \text{ (gravitational constant)}, \quad l_1 = 2 = l_2 = l_3,$$

$$t_0 = 0,\ t_{\max} = 15,\ k_{1s} = 100 = k_{2s}.$$

As it is seen in Fig. 9. the constant propagation of multi-pendulum system (consisting 2 springs and 4 masses as depicted in Fig. 2.) in x direction is achieved.

It is possible to include the presence of friction in the studied model as in [10]. For the simplicity we can assume that friction forces are proportional to velocity (in cartesian coordinate system) or angular velocity. To obtain the equations of motion we first assume no presence of friction and get equations from Lagrange formalism. Having derived the equations of motion we can modify them by including friction force, which is always in the direction opposite to the direction of motion. The friction coefficients are assumed to be constants. However in more general case they can be functions of velocity and position of spring(s) in the space as it is in the case of human muscles or robotic artificial muscle. The presence of friction can cause robotic object to fall down and stop movement with certain frozen geometrical configuration as it is depicted in Fig. 12.

7. Future perspectives

The presented results can give some insight to biomechanics methodology. To consider the more realistic picture the special properties of human, animal or insect muscle have to be incorporated to the model. One of the important feature of muscles is given by Fig. 5 and 6. One should take into account that realistic muscles or springs can sustain certain maximum value of tension as given by Fig. 5. Also the speed of muscle contraction or expansion is dependent on the muscle tension. This means that in our reduced model k_{s1} and k_{s2} cannot longer be considered as constants, but to be the functions of the form $k_{s1}(t, \alpha_5 - \alpha_4, \dot{\alpha_5} - \dot{\alpha_4})$ and $k_{s2}(t, \alpha_4 - \alpha_3, \dot{\alpha_4} - \dot{\alpha_3})$. Also we should consider α_{s10} and α_{s20} to be the functions $\alpha_{s10}(t, \alpha_5 - \alpha_4, \dot{\alpha_5} - \dot{\alpha_4})$ and $\alpha_{s10}(t, \alpha_4 - \alpha_3, \dot{\alpha_4} - \dot{\alpha_3})$.

It should be underlined that the observation of human body by camera is deductive method. On another hand the building humanoid robots is inductive method that allows to reject certain class of hypothesis obtained by deductive observation. In the current work we have pointed certain very intuitive model and check its predictions. Such model can be relatively simple tested experimentally also with use of

external camera as the observator and it is the subject of current and future work. Then the results can be used in robotics or humanoid science and are combination of inductive and deductive view of the world.

Particularly interesting are the studies of the given structure in the presence of static non-uniform potential that is the superposition of the ground potential and gravitational potential. In such case the effective potential would be the function of x and y so $U(x, y)$. The translation symmetry of potential in x direction is broken. Nevertheless if non-uniformities of the ground are small than the pendulum system can still propagate with certain average velocity in x direction.

Another issue is the introduction of the small wind which is time dependent and uniform in x direction. This can be achieved by adding potential term to the Lagrangian of the form $U(x, t)$ for the case of uniform wind. The wind should last not too long and be small and vanish after certain short time. The wind can also to be considered non-uniform in y direction and to be in the form $U(x, y, t)$ form.

Another worth mentioning issue is the inclusion of the x dependent, but periodic potential modeling the periodic shape ground. For certain parameters the reduced 4 mass robotic object should exhibit the chaotic behavior. Even for the case of x translational invariant potential the quasi knee shows complex behavior in certain parameter regimes as it is depicted in Fig. 10. In future work in all pointed cases the harmonic analysis should be conducted.

Very particular example of the application of the studied system is the possibility to transport the rectangular shape mass of given dimensions over certain distance. The example of mass transport, which can be conducted by simple robotic agents on the hypothetical planet X, is given by Fig. 13. It is the simple generalization of the studied model. It is the subject of the future studies.

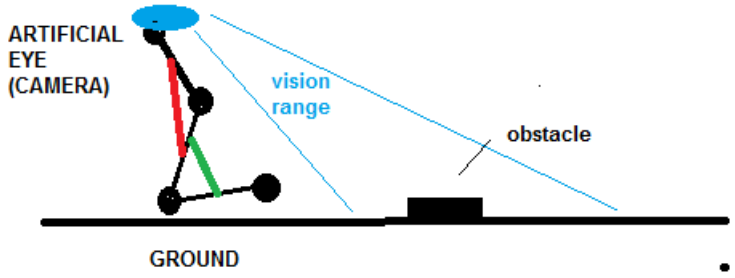

Fig. 4: The presence of the light and small camera on the top can allow for preparation to avoid or overcome obstacles. In such case the active springs have to be activated e.g. electrically as by signal coming from camera that has certain built-in pattern recognition and certain range area of obstacles. In order to succeed the distance to the obstacle and obstacle height has to be determined by camera.

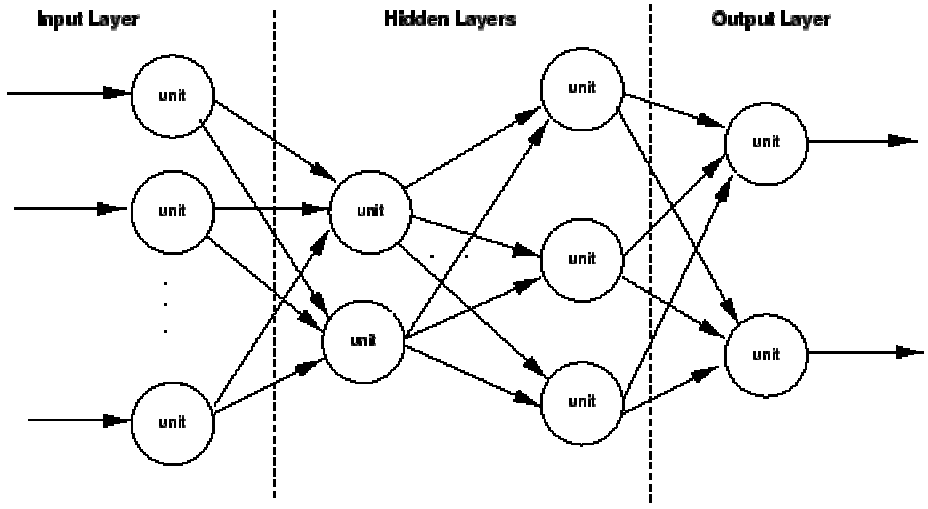

Fig. 5: Neural network can be used to make decisions about jump strategy over the obstacle. 3 inputs correspond to position of obstacle, height and width. 2 outputs correspond to the active force value that has to be applied to 2 springs. In order to make the recurrent neural network effective in give ensemble of obstacles it has to be trained by some genetic algorithm. The unit symbolizes non-linear or linear continuous function.

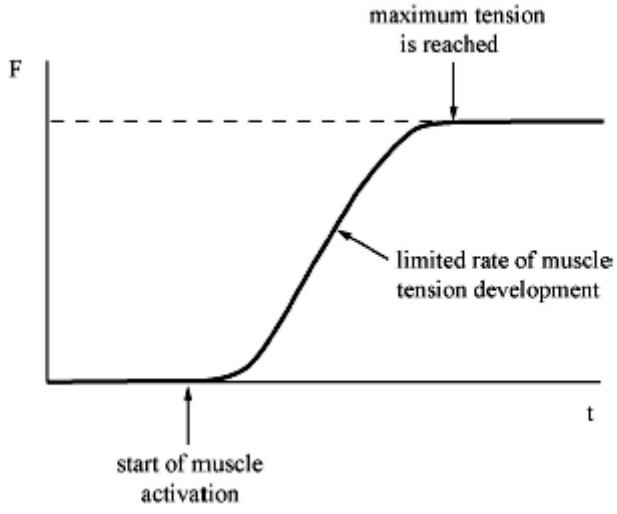

Fig. 6: Typical dynamics of human muscle operation.

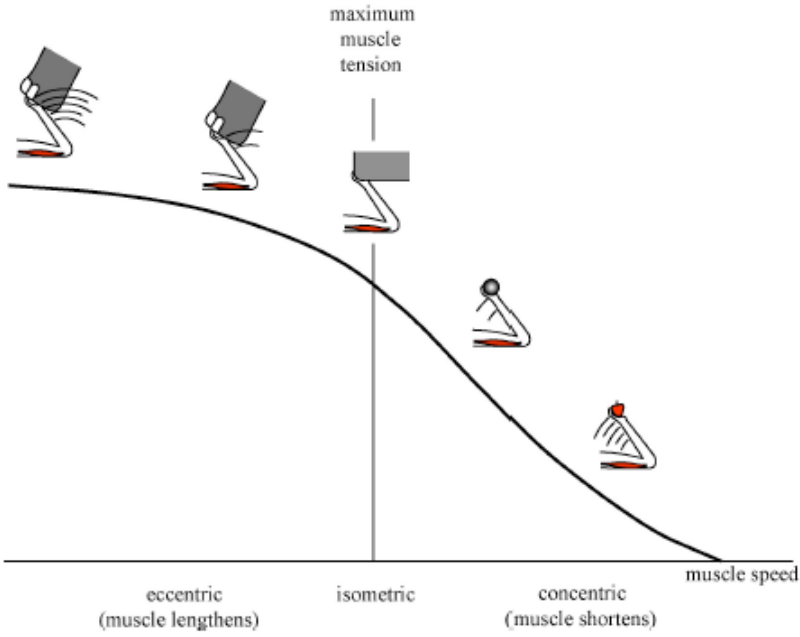

Fig. 7: Typical regimes of human muscle operation.

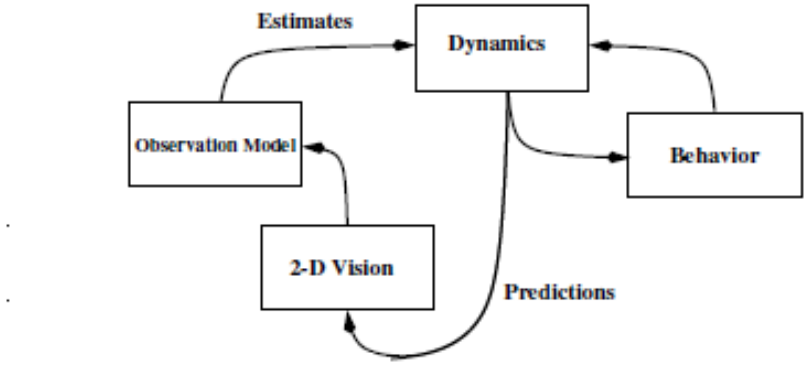

Fig. 8: The flow of information through the pendulum system with camera, on-line image recognition and neural network. Observation model is the on-line image processing system extracting the information on the object position and dimension. Estimation is the output of neural network and can incorporate certain level of intelligence.

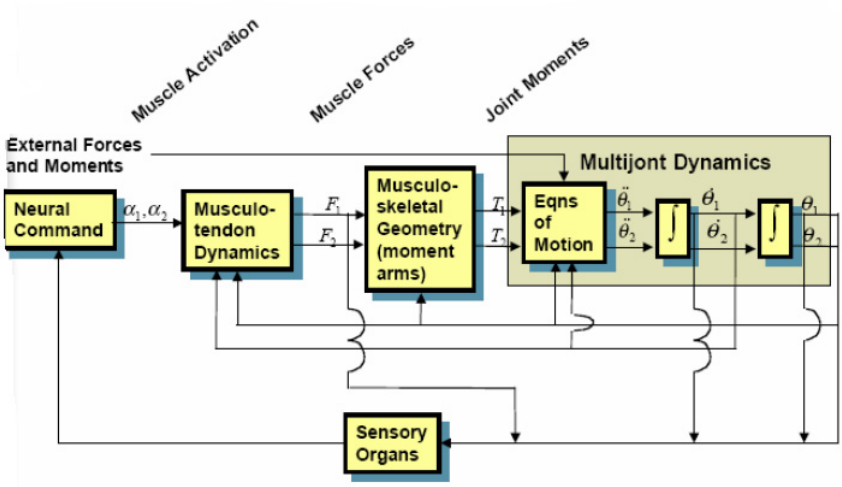

Fig. 9: Simulation scheme reproducing the movement of human body as used in [1, 2].

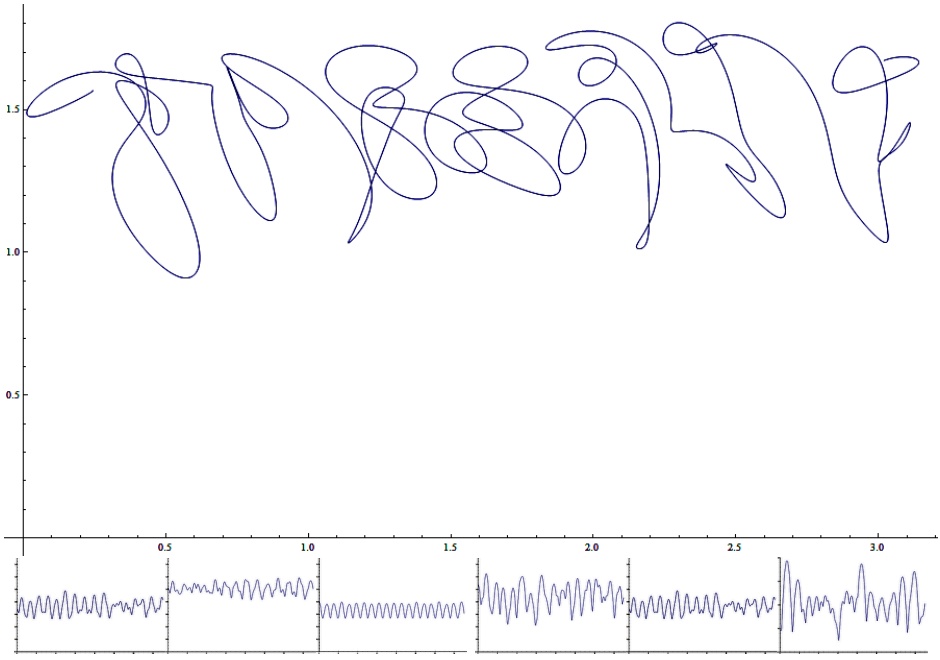

Fig. 10: Examples of vertical quasi knee movement (m_4 mass).Upper picture gives the case of movement in $(x(t), y(t))$ plane. Lower pictures describes different cases of movement of quasi knee with time in vertical direction. No friction and no active force occurs in the system.

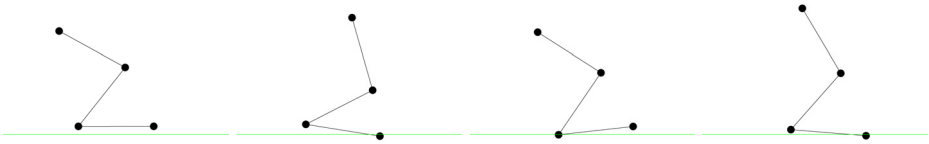

Fig. 11: 4 stages in times t, $t + \Delta t$, $t + 2\Delta t$, $t + 3\Delta t$ of reduced 4-mass robot-like object movement obtained by Mathematica simulations. No friction and no active force occurs in the system.

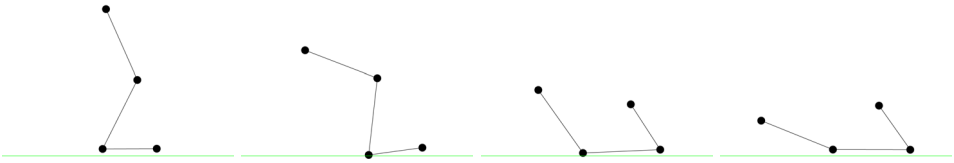

Fig. 12: 4 stages in times t_0, $t_0 + \Delta t'$, $t_0 + 2\Delta t'$, $t_0 + 3\Delta t'$ of reduced 4-mass robot-like object movement obtained by numerical computations conducted in Mathematica environment. Friction and no active force occurs in the system. The robotic object falls down and after certain time stops to move and mimics the dead creature.

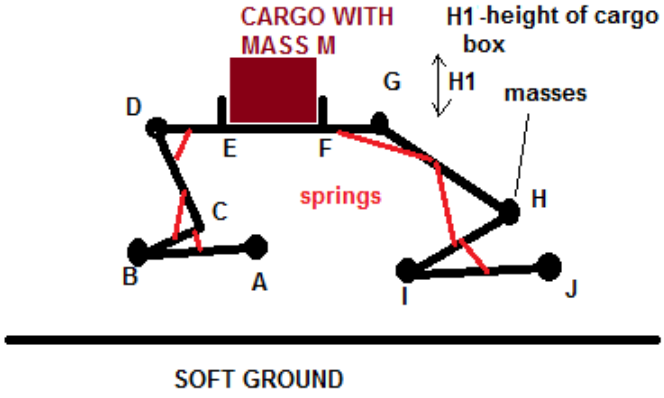

Fig. 13: Possible cargo transport implemented by 2 4-pendulum systems with active springs.

8. Conclusions

We have conducted the study of 4 mass system connected by 3 massless rods that can move with and without friction. The main formalism which was used is Lagrange formalism. We have proved the transport possibility of pendulum system representing reduced 4-mass robotic like object.

The same type of calculations can be done by usage of Hamiltonian formalism. Most obtained results are numerical. In the limited case some results can be obtained in analytical way. This is the case when angles α_5, α_4 are very small and value of α_3 is very close to 90 degrees. Then sine and cosine terms simplifies very much what makes possible analytical solution of equations in analogy to the 2 pendulum case with one mass fixed in space.

If rods have small but uniform mass distribution the obtained results should be similar to those presented in this work. Also in such case the analytic results are possible to be obtained for the limited range of angles as previously mentioned.

We hope that given work brings some insight to the development of simple robotic agents and studies of human motion. In order to obtain deeper analysis the presented model needs to be extended to the multi-pendulum system consisting N pendulums in 2-dimensions and 3-dimensions as the generalization of the system given in Fig. 1 (2).

It should be underlined that the studied system can also describe the molecule(s) colliding with certain surface. In certain cases such molecule can show transport properties along the surface as well. In some cases the dissipation can be pre-assumed to exist. Certain reference to real molecules and surfaces still need to be established in greater detail. Nevertheless by means of the usage of the quasi-classical approximation the quantum behavior of molecule can be simplified to the classical picture.

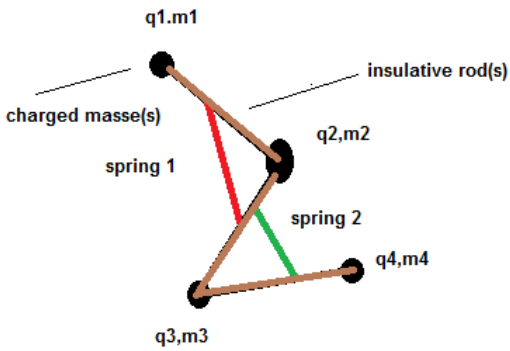

Fig. 14: The studied 4-masses robotic like object with no presence of friction and active forces is analogical to the case of 4 charged masses connected by massless rods in effective external electrostatic potential.

Hence given analogy is valid in certain regimes of molecule shapes, internal structure and type of the surfaces.

It is also worth mentioning that the studied 4-masses robotic like object with no presence of friction and active forces is analogical to the case of 4 charged masses connected by massless rods in effective external electrostatic potential what is depicted in Fig. 14.

References

[1] P. Prokopow and K. Pomorski, *Simulation study of the importance of biarticular muscles on human vertical jump performance*, Int. J. Experimental and Computational Biomechanics **1**, no. 4 (2011).

[2] P. Prokopow, S. Szyniszewski, and K. Pomorski, *The effects of changes in the timing of muscle activation on jump height: a simulation study*, Human movement **6** (2005).

[3] T. Zielińska, *Autonomous walking machines discussion of the prototyping problems*, Bulletin of the Polish Academy of Sciences Technical Sciences **58**, no. 3 (2010).

[4] W. Blajer, K. Dziewiecki, and Z. Mazur, *Multibody modeling of human body for the inverse dynamics analysis of sagittal plane movements*, Multibody Syst. Dyn. **18** (2007).

[5] R. Neptune, K. Sasaki, and S. Kautz, *The effect of walking speed on muscle function and mechanical energetics*, Gait and Posture **28** (2008).

[6] J. Aracewicz, G. Kudra, C. H. Lamarque, *Nonlinear dynamics of triple pendulum system with impacts*, Journal of Technial Physics **43** (2002).

[7] www.tokyolectures.org, www.shanghailectures.org.

[8] T. Ikegami, lectures on Artificial Life (University of Tokyo).

[9] A. Hill, *The heat of shortening and dynamics constants of muscles*, Proc. R. Soc. Lond. B **126** (1938).

[10] T. Mestdaga, W. Sarleta, and M. Crampin, *Second-order dynamical systems of Lagrangian type with dissipation.*

Krzysztof Pomorski
University of Warsaw
Institut of Phisics
Hoża 69, PL-00-681 Warszawa
and
University Jagiellonian
Faculty of Physics, Astronomy and Applied Computer Science
Reymonta 4, PL-30-059 Kraków
Poland

Piotr Tempczyk
University of Warsaw
Institut of Phisics
Hoża 69, PL-00-681 Warszawa
Poland

Przemysław Prokopow
Computational Biomechanics Unit
The Institute of Physical and Chemical Research (RIKEN)
2-1, Hirosawa, Wako, Saitama 351-0198
Japan

Presented by Julian Ławrynowicz at the Session of the Mathematical-Physical Commission of the Łódź Society of Sciences and Arts on July 5, 2012

WŁASNOŚCI TRANSPORTOWE UKŁADU WAHADEŁ SPRZĘŻONYCH

S t r e s z c z e n i e

W pracy zaprezentowano transport układu 4 punktów materialnych reprezentujących układ 2 sprzężonych nieliniowych wahadeł o 5 stopniach swobody, które mogą poruszać się w przestrzeni w potencjale efektywnym modelującym zachowanie pola grawitacyjnego i miękkiego podłoża. Uzyskane wyniki wskazują na możliwość prymitywnego naśladowania ludzkiego i robotycznego chodu przez uklad 4 punktow materialnych.

Rapporteurs – Referees

Richard A. Carhart (Chicago)
Fray de Landa Castillo Alvarado (México, D.F.)
Stancho Dimiev (Sofia)
Pierre Dolbeault (Paris)
Paweł Domański (Poznań)
Mohamed Saladin El Nashie (London)
Jerzy Grzybowski (Poznań)
Ryszard Jajte (Łódź)
Zbigniew Jakubowski (Łódź)
Tomasz Kapitaniak (Łódź)
Grzegorz Karwasz (Toruń)
Leopold Koczan (Lublin)
Dominique Lambert (Namur)
Andrzej Łuczak (Łódź)
Cecylia Malinowska-Adamska (Łódź)
Andrzej Michalski (Lublin)
Leon Mikołajczyk (Łódź)
Marek Moneta (Łódź)
Yuval Ne'eman (Haifa)
Adam Paszkiewicz (Łódź)
Krzysztof Podlaski (Łódź)
Yaroslav G. Prytula (Kyiv)
Henryk Puszkarski (Poznań)
Jakub Rembieliński (Łódź)
Carlos Rentería Marcos (México, D.F.)
Lino F. Reséndis Ocampo (México, D.F.)
Stanisław Romanowski (Łódź)
Monica Roşiu (Craiova)
Jerzy Rutkowski (Łódź)
Ken-Ichi Sakan (Osaka)
Hideo Shimada (Sapporo)
Józef Siciak (Kraków)
Józef Szudy (Toruń)
Luis Manuel Tovar Sánchez (México, D.F.)
Francesco Succi (Roma)
Massimo Vaccaro (Salerno)
Anna Urbaniak-Kucharczyk (Łódź)
Włodzimierz Waliszewski (Łódź)
Grzegorz Wiatrowski (Łódź)
Władysław Wilczyński (Łódź)
Hassan Zahouani (Font Romeu)
Lawrence Zalcman (Ramat-Gan)
Natalia Zorič (Kyiv)

CONTENU DU VOLUME LXII, no. 2